T.C. İSTANBUL KÜLTÜR UNİVERSİTY
INSTITUTE OF GRADUATE STUDIES

SIMPLIFIED MODELING OF ISOLATED BRIDGES WITH TRIPLE FRICTION PENDULUM BEARINGS USING OPENSEES

Masters of Applied Science Thesis

Rawan Ali NOUR

1900001122

Department: Civil Engineering

Programm: Structural Engineering

Supervisor: Assist. Prof Dr. Gökhan YAZICI

JUNE 2022

T.C. İSTANBUL KÜLTÜR UNİVERSİTY
INSTITUTE OF GRADUATE STUDIES

SIMPLIFIED MODELING OF ISOLATED BRIDGES WITH TRIPLE FRICTION PENDULUM BEARINGS USING OPENSEES

Master of Applied Science Thesis

Rawan Ali NOUR

1900001122

Date of Submission: 6 June 2022

Date of defence examination: 21 June 2022

Supervisor and Chairperson:
Assist. Prof Dr. Gökhan YAZICI
Members of Examining Committee:
Assist. Prof Dr. Erdal COŞKUN
Assist. Prof Dr. Abdullah Necmittin GÜNDÜZ

JUNE 2022

ACKNOWLEDGEMENT

First of all, I would like to express my sincere gratitude to Assist. Prof. Dr. Gökhan YAZICI gave me the opportunity to complete this work, through the motivation he gave me to work harder, for his patience throughout thesis meetings, and for the valuable information that I have earned thanks to his efforts.

Secondly, I would like to thank my university: ISTANBUL KULTUR UNIVERSITY, and all the academic staff, because they gave me the chance to be one of their students in order to improve my knowledge in structural engineering and be a better engineer.

Lastly, I would also like to thank my whole family and my friends for all the encouragement and support they gave me throughout my study and my whole life.

University	**:**	**İstanbul Kültür University**
Institute	**:**	**Institute of Graduate Studies**
Department	**:**	**Civil Engineering**
Programme	**:**	**Structural Engineering**
Supervisor	**:**	**Assist. Prof. Dr. Gökhan YAZICI**
Degree Awarded and Date	**:**	**MSc Thesis - June 2022**

ABSTRACT

SEISMIC RESPONSE OF SEISMICALLY ISOLATED BRIDGES WITH TRIPLE FRICTION PENDULUM BEARINGS

Rawan Ali Nour

Many recent studies and research have been concerned with the issue of seismic isolation and its importance for our buildings, but very few of them have concentrated on this issue regarding bridges even though bridges are important as residential buildings or even more. Therefore, further studies of seismic isolation for highway bridges will lead to a better understanding of this concept. Especially the seismic response of these isolated bridges should be studied to learn the importance of this issue and discover its gaps and weaknesses to improve this concept and apply it on a larger scale. In this paper, we are going to study the seismic response of an existing bridge that is isolated seismically by using a special type of sliding components isolator which is: "The Triple Friction Pendulum Bearings". The seismic behavior of the bridge will be examined in two conditions: fixed and isolated base structure simultaneously through time history analysis using the OpenSees software. Furthermore, Nodal displacement of the selected bridge, the base shear and the force-displacement hysteresis loops of the isolation system are presented graphically under three earthquake ground motion records. The findings of the study are summarized in the conclusion section.

Keywords: Seismic Isolation, Triple friction pendulum bearings, OpenSEES, Seismic Response, Ground Motion

Science Code: 624.03.01

Üniversite	**:**	**İstanbul Kültür Üniversitesi**
Enstitüsü	**:**	**Lisansüstü Eğitim Enstitüsü**
Anabilim Dalı	**:**	**İnşaat Mühendisliği**
Programı	**:**	**Yapı Mühendisliği (İngilizce)**
Tez Danışmanı	**:**	**Assist. Prof. Dr. Gökhan YAZICI**
Tez Türü ve Tarihi	**:**	**Yüksek Lisans – Haziran 2022**

KISA ÖZET

ÜÇLÜ SÜRTÜNMELİ SARKAÇ MESNETLİ SİSMİK YALITIMLI KÖPRÜLER DEPREM YÜKLERİ ALTINDA DAVRANIŞI

Rawan Ali Nour

Son zamanlarda yapılan birçok çalışma ve araştırma, sismik izolasyon konusu ve bunun binalar için önemi ile ilgilenmiştir, ancak bunların çok azı köprülerle ilgili bu konuya odaklanmıştır. Bu nedenle, karayolu köprüleri için sismik izolasyonla ilgili daha ileri çalışmalar, bu kavramın daha iyi anlaşılmasını sağlayacaktır. Özellikle bu izole köprülerin sismik tepkisi. Bu çalışma kapsamında, "Üçlü Sürtünmeli Sarkaç Mesnetleri" ile sismik olarak yalıtılmış mevcut bir köprünün sismik davranışı araştırılmıştır. Köprünün sismik davranışı OpenSees yazılımı kullanılarak zaman tanım alanında analiz yoluyla sabit ve sismik yalıtımlı koşullar için incelenmiştir. Seçilen köprünün düğüm noktası yer değiştirmeleri, taban kesmesi ve izolasyon sistemi için kuvvet- yer değiştirme histeretik çevrimleri üç deprem yer hareketi kaydı altında grafikler aracılığıyla sunulmuştur. Çalışmanın bulguları sonuç bölümünde özetlenmiştir.

Anahtar Kelimeler: Sismik İzolasyon, Üçlü Sürtünmeli Sarkaç Sistemi, OpenSEES, Deprem Yükleri Altında Davranış, Köprüler

Bilim Dalı Sayısal Kodu: 624.03.01

TABLE OF CONTENTS

LIST OF FIGURES

LIST OF TABLES

LIST OF ABBREVIATIONS

B.C :	Before Christ
USA :	United States of America
FPS :	Friction Pendulum bearings
EQS :	Eradiquake bearings
ERB :	Elastomeric Rubber Bearings
LDRB :	Low Damping Rubber Bearing
HDRB :	High Damping Rubber Bearing
LRB :	Lead Rubber Bearing
SFP :	Single Friction Pendulum
DCFP :	Double Concave Friction Pendulum bearing
DFP :	Double Friction Pendulum bearing
TFPS :	Triple Friction Pendulum bearings
FE :	Frequent Earthquake (Event)
DBE :	Design Based Earthquake (Event)
MCE :	Maximum Considered Earthquake (Event)
RC :	Reinforced Concrete
FEMA :	Federal Emergency Management Agency
OPENSEES :	Open System for Earthquake Engineering Simulation
PEER :	Pacific Earthquake Engineering Research Centre
3D :	Three-Dimensional
TCL :	Tool Command Language

C++ : Object-Oriented Programming Language

DOF : Degree Of Freedom

NDM : Spatial Dimension of the Model

THA : Time History Analysis

PGA : Peak Ground Acceleration

NPTS : Number of Data Points

DT : Time Step

LIST OF SYMBOLS

$\boldsymbol{\xi}$ **:** Damping ratio

$\boldsymbol{G}$ **:** Shear modulus (MPa)

$\boldsymbol{S_1}, \boldsymbol{S_2}$**:** Double friction pendulum bearing sliding plate surfaces 1 and 2

$\boldsymbol{R_1}, \boldsymbol{R_2}$**:** Double friction pendulum bearing radius 1 and 2 (m)

$\boldsymbol{\mu_1}, \boldsymbol{\mu_2}$**:** Friction coefficients of double friction pendulum bearing surfaces 1 and 2

$\boldsymbol{h_1}, \boldsymbol{h_2}$**:** Double friction pendulum bearing slider heights 1 and 2 (m)

$\boldsymbol{d_1}, \boldsymbol{d_2}$**:** Double friction pendulum bearing displacement capacities 1 and 2 (m)

$\boldsymbol{R_1}, \boldsymbol{R_2}, \boldsymbol{R_3}, \boldsymbol{R_4}$**:** Triple friction pendulum displacement radius 1, 2, 3 and 4 (m)

$\boldsymbol{d_1}, \boldsymbol{d_2}, \boldsymbol{d_3}, \boldsymbol{d_4}$**:** Triple friction pendulum bearing displacement capacities 1, 2, 3 and 4 (m)

$\boldsymbol{\mu_1}, \boldsymbol{\mu_2}, \boldsymbol{\mu_3}, \boldsymbol{\mu_4}$**:** Triple friction pendulum bearing friction coefficients 1, 2, 3 and 4

$\boldsymbol{h_1}, \boldsymbol{h_2}, \boldsymbol{h_3}, \boldsymbol{h_4}$**:** Triple friction pendulum bearing slider heights 1, 2, 3 and 4 (m)

$\boldsymbol{D_1}, \boldsymbol{D_2}, \boldsymbol{D_3}, \boldsymbol{D_4}$**:** Triple friction pendulum bearing Diameters 1, 2, 3 and 4 (m)

$\boldsymbol{u_i}$ **:** Slider's relative displacement (m)

$\boldsymbol{W}$ **:** Vertical load applied on the bearing (kN)

$\boldsymbol{F_{fi}}$ **:** Frictional force of the surface (kN)

$\boldsymbol{F_{dri}}$**:** Lateral force at the moment when the slider begins to bear (kN)

$\boldsymbol{R_{eff1}}, \boldsymbol{R_{eff2}}, \boldsymbol{R_{eff3}}, \boldsymbol{R_{eff4}}$**:** Effective radius of triple friction pendulum 1, 2, 3 and 4 (m)

F: Lateral force (kN)

$\boldsymbol{u_{dr1}}$**:** Total displacement at regime III (m)

$\boldsymbol{u_{dr4}}$**:** Total displacement at regime IV (m)

$\boldsymbol{u^{**}}$**:** Total displacement at regime II (m)

$\boldsymbol{u^{*}}$**:** Total displacement at regime I (m)

$\boldsymbol{F_f}$**:** Frictional force (kN)

$\boldsymbol{D_C}$**:** The preliminary diameter of the concave plates (m)

$\boldsymbol{D_S}$, $\boldsymbol{D_R}$: Diameter of the sliders (m)

$\boldsymbol{U_X}$**:** Nodal displacement (m)

CHAPTER 1

INTRODUCTION

1.1 Background

Bridges are very important structures that have been constructed since the 9th century (around 850 BC) and evolved over the years in terms of structure and building materials. Various types of bridge structures have been widely applied such as Beam bridges, Cantilever bridges, Tied arch bridges, Suspension bridges and, Cable-stayed bridges, depending on the location and the purpose of the constructed bridge [1]. Also, a great number of bridges were built to serve the increased traffic, using sustainable and more resistant materials.

While bridge structures are enormous and costly, it is important to protect them from different factors that may cause damage to these structures, the most important factor that should be taken into consideration during the design process is the seismic load, which is “the external force applied on the surface of the bridge as a result of the earthquake generated agitation”, it refers to the amount of seismic energy transferred into the structure through the earth [2]. In spite of the fact that refers to minor probabilities for destructive earthquakes anywhere in the world in short periods, the statistics assess that a large number of earthquakes take place each year and 20% of them can be actually felt. That number might reach 500 thousand earthquakes per year [3]. For this reason and as a result of the increasing number of earthquakes that have been recorded in the past years, many countries around the world tend recently to take precautionary procedures to protect their facilities against such catastrophic events. These procedures can be taken during the design phase or even after construction and using the facility (then it is called retrofit), and the most effective action that could be taken is “Seismic Isolation”.

1.2 Seismic Isolation Overview

"Isolation" can be defined as; the action of separating two objects or individuals or more and decreasing the interaction between them.
"Seismic Isolation" holds the same concept with regard to the structures, as it works on decoupling the structure from the earth’s base using an elastic surface in order to dissipate the impacts of the destructive earthquakes that may occur [4][5].

Studies refer that the base isolation system was applied before to the structures of the ancient ages around 550 B.C, and some of these constructions are still existing until the time such as the Tomb of Cyrus the Great that was built in Pasargadae, Iran according to this system, in order to protect it from the effects of the numerous earthquakes [6]. After thousands of years during the 1970s, the base isolation system that contains rubber and steel was discovered by Dr. Bill Robinson, and it was proved that the mechanism of this system and the base-isolated Cyrus tomb perform identically [7].

The Tomb of Cyrus the Great in Figure 1.1 was constructed in the 6th century BC, in the province of Fars in the South-West of Iran. The structure of this sepulcher that was built of limestone is considered to be the most ancient existing base-isolated construction in the world, and an important historical instance for earthquake engineering for its flexibility against seismic ground motions throughout the years [6][8][9].

Figure 1.1: Tomb of Cyrus the Great [8]

The Foothill Community Law and Justice Centre shown in Figure 1.2 were built in 1985 in the city of Rancho Cucamonga in the East of downtown Los Angeles in the United States of America. This building was constructed with an area of 15.794 m^2 (170,000 ft^2) and four floors in addition to a full basement, in order to afford legal services for the inhabitants of San Bernardino County. The center is considered the first seismically isolated construction in the

USA and the first in the world to be supported by elastomeric rubber bearings of high damping with a total number of 98 isolators giving the building the ability to resist earthquakes with a magnitude reaching 8.3 [4].

Figure 1.2: Foothill Community Law and Justice Centre [4]

1.3 General

When a ground motion takes place, the construction drifts under the effect of the vibrations transmitted from this earthquake, which caused shaking of the soil beforehand as a result of the movement of the underground layers, which in turn leads to a displacement at the substructure base of this construction, transferring the effects of the earthquake to the other floors as the vibration continues. As a result, the construction will swing strongly causing its structure to fail in the case of a severe ground motion with a natural frequency corresponding to the natural frequency of the construction. The construction won't be stable against the seismic hazards unless this value is modified to be Incompatible with the value of the natural frequency of ground motion [4].

The mechanism of seismic isolation systems is mainly based on adjusting the natural period of the structure by incrementing the total vibration interval of the structure beyond the essential period of earthquake ground motion, thus minimizing the inertial loads' amplification as an effect of the resonance, and consequently gaining a more resilient construction [4][5]. In this case, the substructure base of the construction will respond separately to the vibrations of ground motion preventing the effects of these vibrations from reaching the superstructure with the same intensity [4]. Figures 1.3 and 1.4 show the demeanor of buildings and bridges under the effect of ground motions with and without having an isolation system against the seismic hazards respectively.

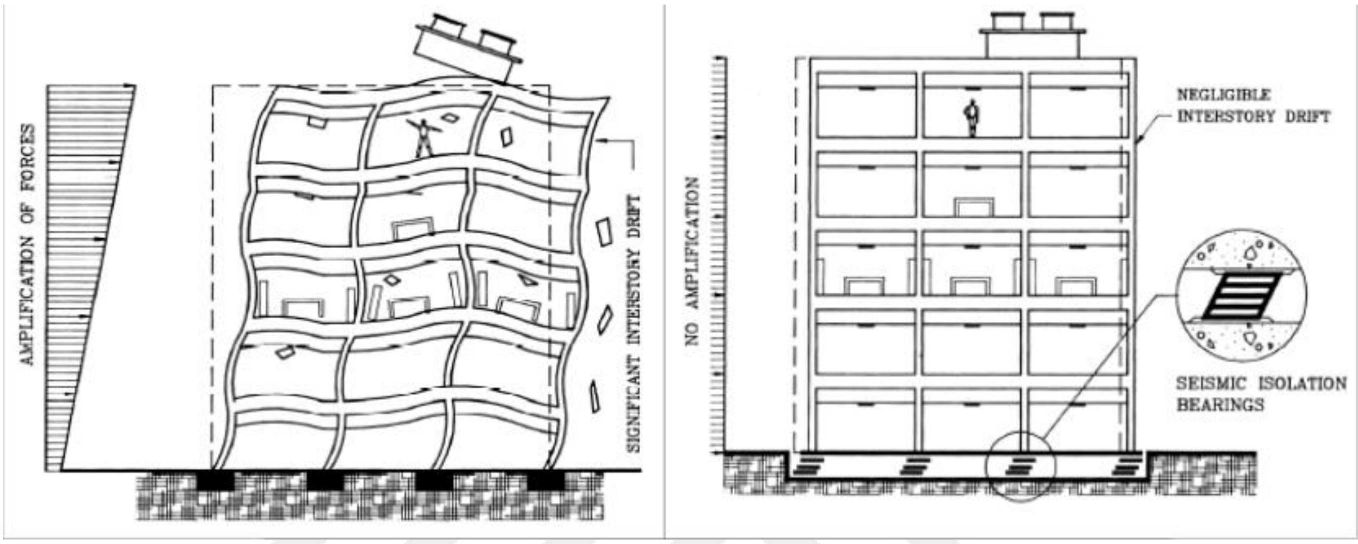

Figure 1.3: Behaviour of Seismically Isolated and Non-Isolated Buildings [17]

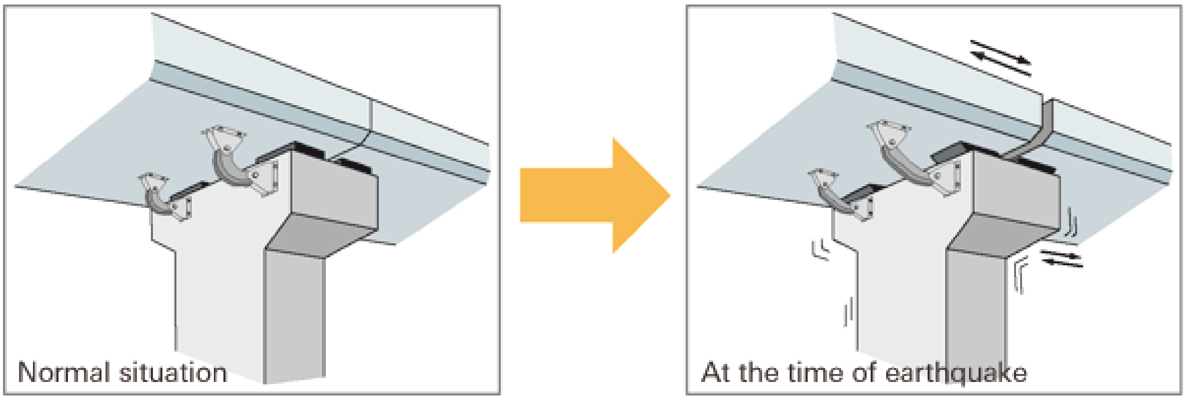

Figure 1.4: Behaviour of Seismically Isolated Bridges

The impact of the seismic isolation system on the constructions can be described as illustrated in figure 1.5; By increasing the natural period of the structure the damping due to earthquake vibrations will be reduced which, in turn, reduces the acceleration and story-drift of the building, thereby causing minimal harm to the construction and its contents. Although this increase has a good impact on the behavior of the structure during the earthquake, however, it increases the displacement of the isolation system causing contrary results to it which in return reflects on the structure. Therefore, choosing the right type of isolation system for the construction also has a direct effect on the behavior of the construction during earthquakes [4][10].

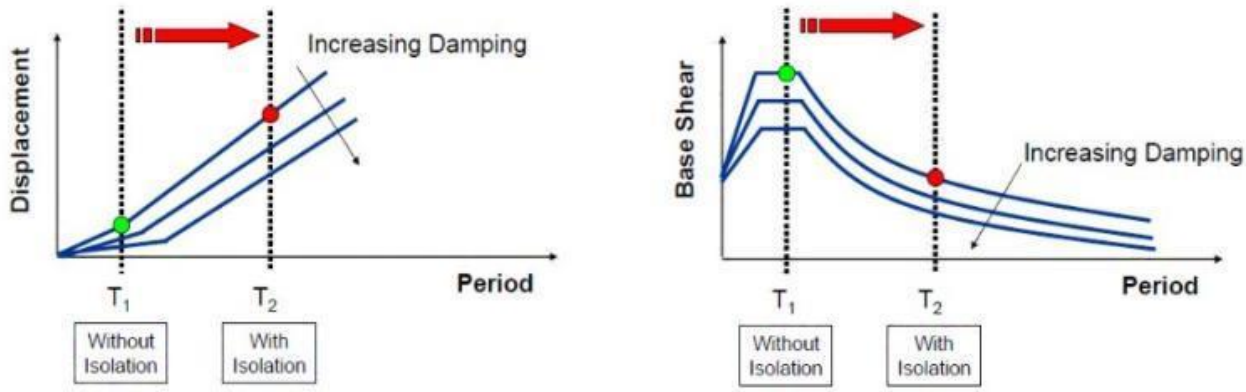

Figure 1.5: Behaviour of Seismically Isolated Structures [4]

1.4 Literature Review

The objective of this review is to present an evaluation of the literature investigations made by researchers on the influence of seismic isolation systems on bridges.

Fenz and Constantinou (2008a, 2008c) [19][35]: The 2008a research investigates the precepts of process, in addition to theoretical studies of the dynamic features of the frictional sliding bearings in which the damping and rigidity values can be expected and modified, in order to obtain adjustable displacement capacities, as the sliding happens on several sliding surfaces with different characteristics. This shows the employment ability of these sliding isolation systems for numerous purposes at any level of seismic hazards credited to their adaptive functional demeanor. The research also presents the model of force-displacement mathematical formulations of these adaptive bearings with a methodology for defining the interface on which the sliding occurs at any timing, depending on the values of displacement amplitude, friction coefficient, and the effective radii of every sliding interface.
While The 2008c research proposed a numerical model that discusses the demeanor of the three

types of sliding spherical isolators (single, double, and triple frictional bearings) that were demonstrated in the previous 2008a research, through applying experiments that test the two preliminary configurations for these bearings, which are force and displacement. The test was based on depending on several values for friction coefficients and displacement amplitudes for the tested type of bearing and checking the force-displacement hysteresis demeanor. Regarding the dynamic part of the experiments, the highest velocity value applied for the conducted tests reached nearly (400 mm/sec); however, most of these experiments were performed at low-velocity values.

Research outcomes demonstrated a large resemblance with the theoretical research results and both types of research proved that the values of force and displacement can be adjusted during the design phase, as the transformation where the rigidity happens can be predicted. Moreover, the process of beginning or ceasing the sliding on a particular surface in the experimental research was identical to the predictable sliding of the theoretical research, the thing that affirms the underlying precepts of the process.

Malekzadeh, Masoud, and Touraj Taghikhani (2012) [20]: This research discusses the effects of the triple friction pendulum isolation systems on the bridges isolated by this type of isolator under various scales of seismic hazards and examines the dynamic response of these bridges. Therefore, an isolated bridge model was studied and analyzed utilizing OpenSees platform software in accordance with the defined equations related to the dynamic nonlinear analysis (THA) applied to this seismically isolated bridge. The structure of the bridge was subjected to a number of 20 earthquake records for each level of ground motion levels; 20 records of service Level Earthquake that may occur every 72 years (SLE), 20 records of the design-based earthquake that may occur every 475 years (DBE), and 20 records of maximum considered earthquake that may occur every 2475 years (MCE), with a total of 60 records. Also, a parametric study for the seismic demeanor of the isolated bridge was executed in order to examine the influence of triple friction pendulum isolator parameters (radii, coefficients of friction, and displacement amplitudes) on this behavior by applying different values for these parameters with the analyses implemented for the considered bridge.

Research outcomes demonstrated that the TFPs with the elevated friction value is normally accompanied by a notable reduction in the structure's displacement under the MCE level of ground motions. Also, showed that the dynamic response of the bridge isolated with TFP bearings can be basically influenced by the values of coefficient of friction and radii, while the displacement amplitude wouldn't have any notable effect on the behavior of the bridge.

Jianian Wen, and Qiang Han & Xiuli Du (2019) [34]: In this research, the force-Displacement mathematical formulations of both single and triple types of frictional sliding bearings were examined by applying the experiments of displacement-controlled, for the purpose of investigating the efficiency of these isolation systems and the seismic response of the isolated bridges simultaneously. Furthermore, the experiments of shaking-table were also conducted on a typical bridge example 1/10 scaled and isolated by FPBs and TFPs isolators, under four two-directional seismic excitations. The comprehensive empirical results were used as well, in order to test the influence of triple friction pendulum bearing parameters (Radii and coefficients of friction) on the seismic performance (acceleration of the superstructure and displacement) of the considered bridge model.

Research outcomes confirmed the functional efficiency of the triple friction pendulum bearings in controlling the seismic performance of the bridges at the high-seismicity zones, the thing that fulfills design requirements dependent on performance in these regions, this consequence was approved depending on the numerical results and the empirical information. In addition, the outcomes of the research also clarified that the dynamic performance of the bridge is directly affected by the response of the triple friction pendulum bearings under the two-directional excitation, however, if this interaction is neglected then the displacement of the bridge's superstructure will be decreased.

1.5 Thesis Structure

Chapter 2 illustrates basic information about seismic isolators' types, components, and characteristics. Also, the mechanism and mathematical equations of single and triple friction pendulum isolators (TFPs) are summarized according to the proposal in Fenz and Constantinou 2008a. In conclusion, a table that contains a number of major isolated bridges around the world, which use friction pendulum bearings FP or triple friction pendulum bearings TFP as seismic isolators are presented.

Chapter 3 presents the materials' geometry and sections' characteristics of the considered bridge. It also demonstrates the steps of modeling and analyzing the bridge structure through OpenSees software for two different cases which are fixed and isolated bridge structures. Lastly, the steps of time history analysis (THA) for both cases (fixed and TFP isolated structure) are presented.

In chapter 4, the outcomes of the analyses applied in the previous chapter 3 are debated and presented with the aid of the graphs conducted with Excel software. The comparisons of nodal displacement and base shear reaction for the time history analysis of the OpenSees modeled bridge structure in two modeling conditions isolated and non-isolated bridge structures are illustrated. In addition, force-displacement hysteresis loops for the TFP isolators under the three types of seismic events applied in the THA are assessed.

Chapter 5 presents concluding notes regarding the thesis results and recommendations for further research.

Appendix A presents the calculations of the effective radius of the triple friction pendulum bearings.

Appendix B presents the displacement and base shear outcomes of the applied analyses through excel graphical charts in two conditions of structure model fixed and isolated.

CHAPTER 2

SEISMIC ISOLATORS

2.1 Ideology of Seismic Isolators

Seismic Isolators are special designed structural elements in addition to devices that dissipate the energy absorbed from the earth through the substructure due to seismic events, they work on separating the superstructure of the bridge and its infrastructure as they are usually installed between the girders and abutments of the bridge as shown in figure 2.1, and over the footing pads for the buildings that do not have basement while for the buildings containing basement the isolators will be placed either at the top, middle or the undermost part of the pillars and walls as shown in figures 2.2a and 2.2b respectively. Seismic isolation systems achieve a reduction in base shear, acceleration, and forces applied to the superstructure of the construction by increasing the vibration period of the structure, which in turn increases the displacement that is limited to the substructure [11]. (Qt. in Constantinou et al, 2011. 3).

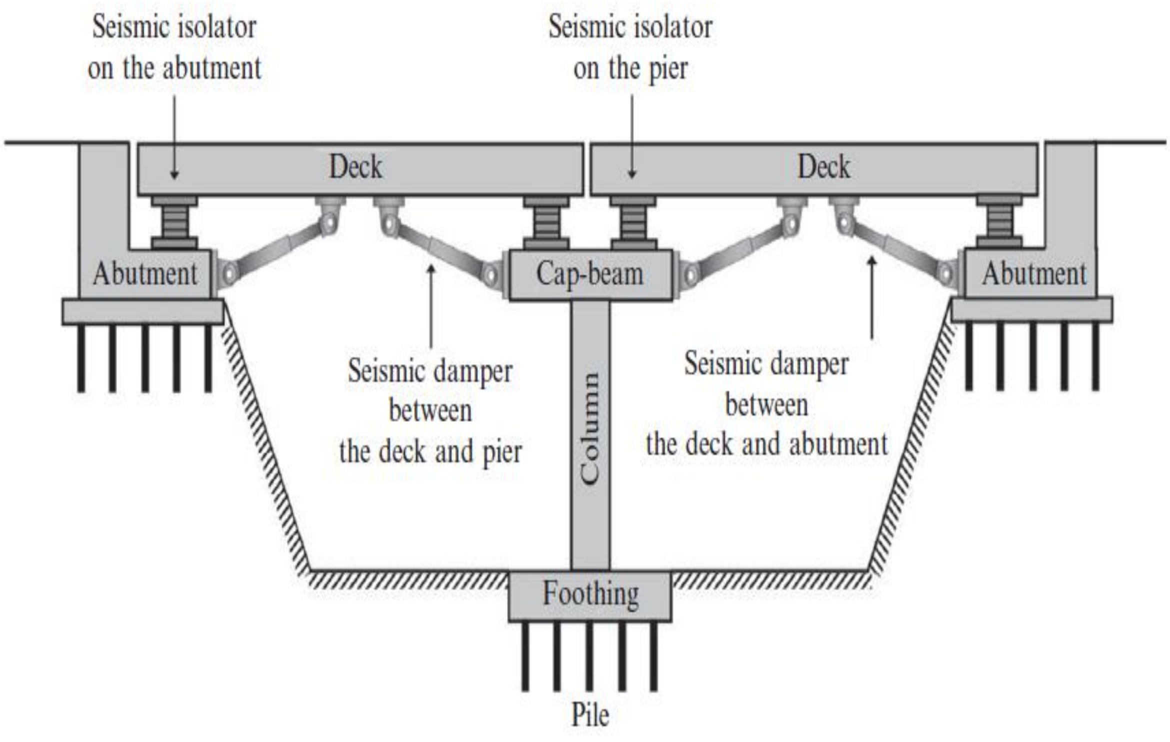

Figure 2.1: Bridge Model Shows Installation Position for Seismic Isolators [16]

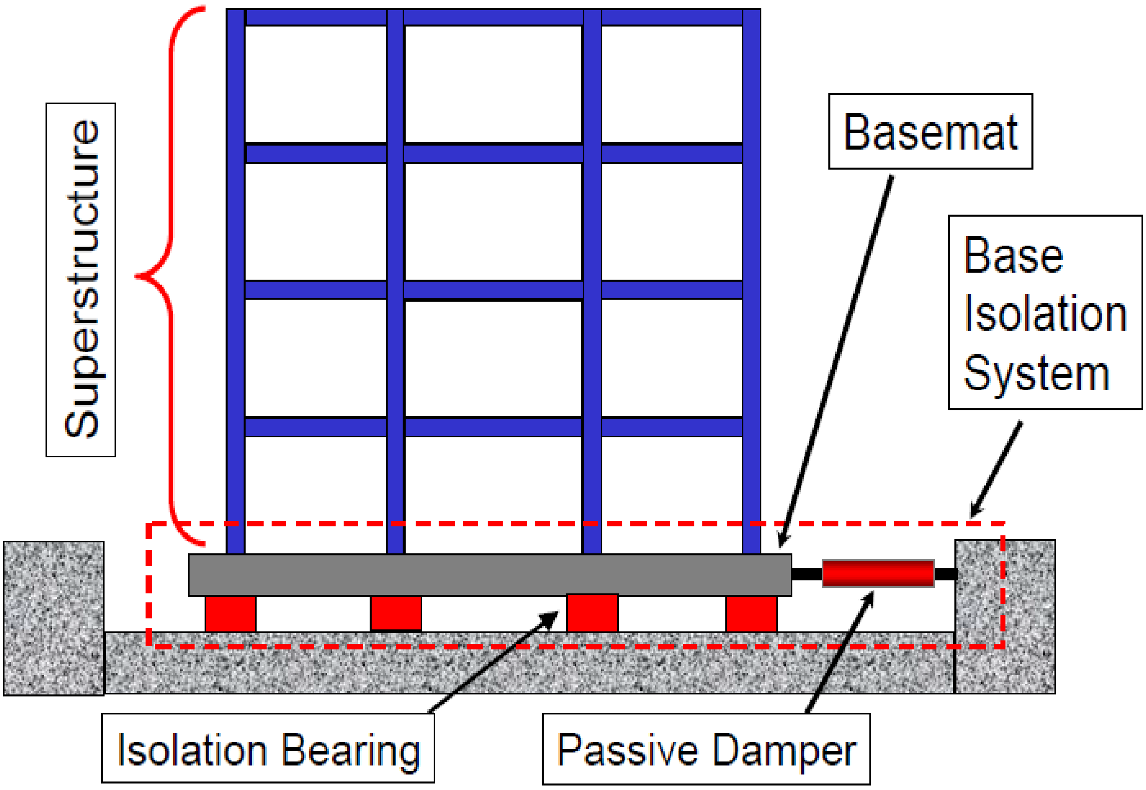

Figure 2.2a: Model Shows Installation Position of Seismic Isolators for Buildings without Basement [12]

Figure 2.2b: Model Shows Installation Position of Seismic Isolators for Buildings with Basement [12]

2.2 Seismic Isolators Types

In general, seismic isolators are divided into two categories; isolators that use elastomeric components such as (lead rubber isolator, high-damping isolators, and low-damping isolators) are all made from natural rubber, and they are characterized by a high damping ratio especially lead rubber isolators. The other category of isolators are the isolators that use sliding components (spherical or flat) such as (Friction Pendulum bearing FPS which are normally spherical stainless-steel sliding plates and EradiQuake bearing EQS that are normally flat stainless-steel sliding plates), and they are characterized by a high amplitude for axial loads [11][13][14].

2.3 Required Specifications of Seismic Isolators

Regardless of the type of isolator used for the structure, it is more important that it meets the requirements that it was already designed for. A good isolation system that improves seismic performance and reduces deformations and construction costs should enclose the following specifications:

- Flexibility that allows increasing the vibration period to reduce the forces applied on the upper and lower parts of the bridge.
- Dissipating the energy of earthquakes as much as possible to give the system the ability to dominate the structure's displacement.
- Stiffness against low loads (car braking, wind load, low-intensity seismic events).
- Stability of characteristics for extended periods, to endure the environmental changes that would occur in the bridge's superstructure without affecting the substructure [13]. (Qt. in buckle El at. 2-7)

The efficiency of seismic isolators can be influenced by many factors including the elasticity of the substructure, type of superstructure, and soil condition of the construction location [12][13]. (Qt. in buckle El at, 2006. 31)

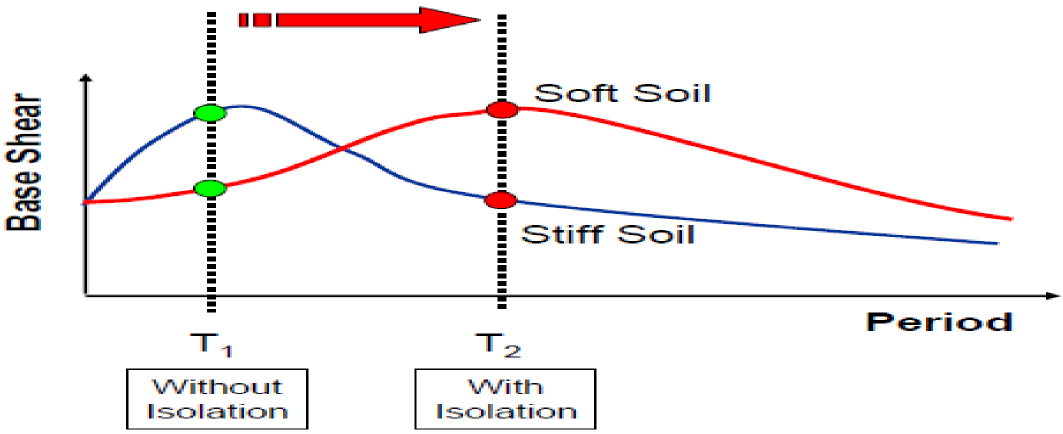

Figure 2.3: The Impact of Soil Type on the efficiency of Seismic Isolators [12]

2.4 Elastomeric Rubber Bearings (ERB)

Elastomeric bearings have been employed further than 50 years ago, in order to adapt to the dilation arising at bridges due to temperature changes and permit rotations at girder braces. Subsequently, this use expanded to involve seismic isolation taking advantage of their high stability under movements and overload and minimal maintenance demands [13]. The bearings are manufactured by applying an industrialization procedure called vulcanization, they are normally formed of middle steel sheets that fasten a number of rubber layers that overlay alternately, these layers might be produced either of natural or artificial rubber materials. Also, a lid of rubber is fitted to the bearing to conserve the inner components of rubber and steel from erosion and ecological degeneracy [13][23]. The function of the steel sheets is to prohibit the isolator from inflating under the compressive strength as illustrated in figure 2.4.

Three kinds of elastomeric rubber bearings have developed through time so they can comfort the diverse demands of isolating applications [13].

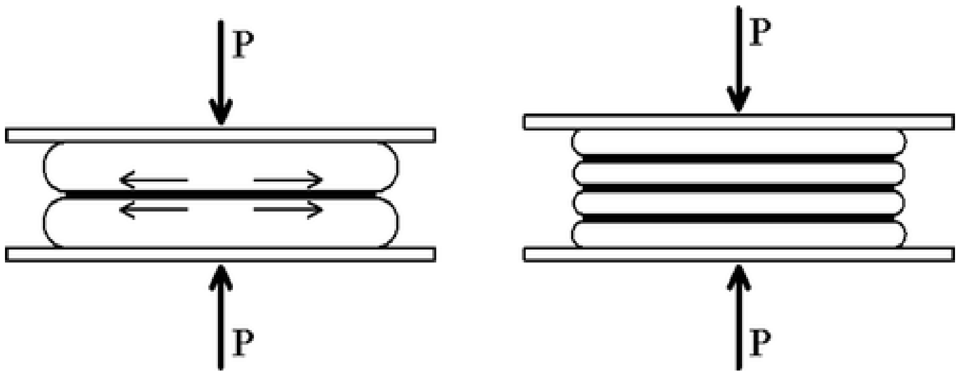

Figure 2.4: Elastomeric Bearing inflating effect [25]

2.4.1 Low Damping Rubber Bearing (LDRB)

This type of bearing is usually manufactured of natural raw rubber material and used in addition to, separate devices (dampers, elastic steel sheets, or bars) that work on dissipating the energy and dominating the displacement within the isolation system, as the raw rubber exhibits small damping values. The damping proportion (ξ) for this type of rubber isolator normally rates between 2% and 3% at a shear stress of 100%, and the shear modulus (G) varies between 0.65 MPa and 0.9 MPa (in this case the natural rubber used for the seismicity implementations is with an endurance rigidity value of 50) [19][23].

The Low-damping rubber bearings show a demeanor of roughly linear shear stress-strain reaches around 150% shear strain before they solidify [19][23].

2.4.2 High Damping Rubber Bearings (HDRB)

This type of bearing is usually fabricated by mingling the materials of natural rubber with fillers and carbon black and supplied with a core of lead in order to obtain the damping at high levels for dissipating the energy. The damping proportion (ξ) for this type of rubber isolator normally rates between 10% to 20% at a shear stress of 100%, and the shear modulus (G) varies between 0.35 MPa (50 psi) and 1.4 MPa (200 psi) [19][23].

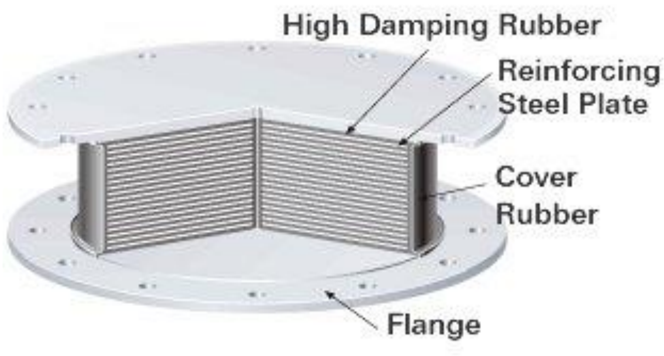

Figure 2.5: High-Damping Rubber Bearing [24]

2.4.3 Lead Rubber Bearings (LRB)

Lead-Rubber isolators are distinguished from other types of elastomeric bearings, by the lead core set in the middle of the bearing which works on incrementing energy dissipation capacity during lateral displacements, in addition to reducing the motion of the construction due to the stiffness acquired from this lead-core against wind and braking forces [23].

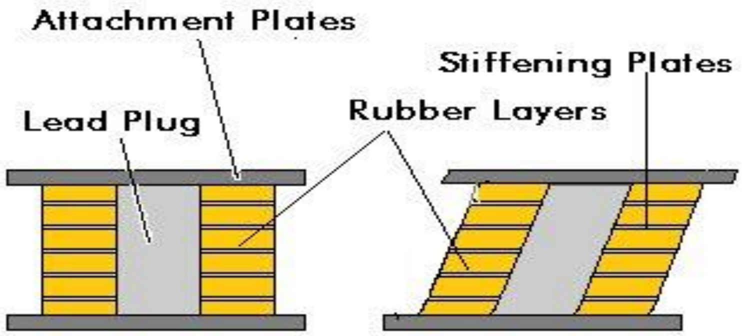

Figure 2.6: Lead Rubber Bearing [24]

2.5 Frictional Bearings

2.5.1 Single Friction Pendulum Bearings (FPS)

Frictional bearings normally consist of a stainless-steel spherical-shaped concave lamina which is usually faced downward, a hinged slider, and a housing plate. These isolators can be manufactured in different formations single, double or triple, and are characterized by their ability to carry high values of axial loads. Also, they can be modeled to have great lateral amplitudes of displacement with prolonged durations for vibration reach to more than 5 seconds [13]. (Qt. in buckle El at, 2006. 76-78). Single friction pendulum bearings (FPS) achieve the basic requirements of seismic isolators systems through the following:

- The isolation is accomplished when the hinged slider slips on the concave plate.
- Damping (Dissipating the energy) is achieved due to rubbing between the layer of stainless steel and composite bearing material.
- The performance of an FP isolator is greatly influenced by the sliding surface.
- Surface's friction resistance is controlled by; the diameter of the slider, Temperature, Sliding velocity, corrosion, and compression of contact.
- The strength of the FPS is commanded by the friction coefficient of the slider, and its rigidity is commanded by the curvature radius.
- The required value of displacement amplitude can be obtained by choosing the concave plate's and slider's diameter, considering that this value should be less than 20% of the effective curvature radius to achieve more economy [11][14][15]. (Qt. in Constantinou et al,2011. 35; Constantinou et al,2007. 13; Ryan and Richins. 5)

Figure 2.7 is a cross-section of the friction pendulum bearings (FPS) that illustrates the main components of the FPS isolator.

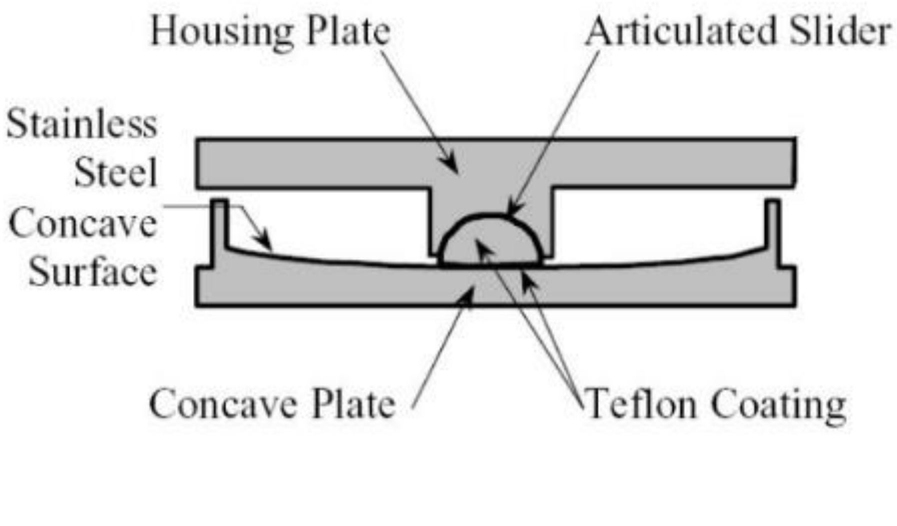

Figure 2.7: Single Friction Pendulum Isolator Cross-Section [11]

2.5.2 Double Friction Pendulum

Double Frictional bearings (DCFP) are normally formed of two stainless-steel spherical-shape concave laminas (S_1 , S_2) faced to each other and separated with a hinged slider that is coated with a non-metallic sledding substance. The main function of the hinged slider is conciliating the differential motions along the sliding interfaces located above and under it, in addition to appropriately distributing the pressure transmitted on the sliding surfaces [14]. (Qt. in Constantinou et al,2007. 156). The Dimensions of DFP for each surface consist of two radii R_1 , R_2 with heights h_1 , h_2 , and friction coefficients of μ_1 and μ_2 respectively, also displacement amplitudes d_1, d_2. These dimensions could be different and unequal which gives this type of isolator the ability to bear two different levels of ground motions at the same time.

Double friction pendulum isolators are considered to be higher in efficiency than the triple type of pendulum isolators during earthquakes with high peak acceleration rates [21][22].

Figure 2.8 is a cross-section of the double friction pendulum bearings (DFPS) that illustrates the main components of the DFPS isolator.

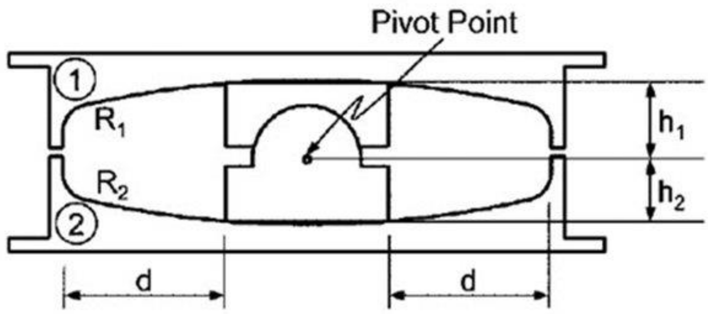

Figure 2.8: Double Friction Pendulum Bearing Cross-Section [11]

2.5.3 Triple Friction Pendulum Bearings (TFPS)

Triple friction pendulum isolators are an advanced generation of isolators that can provide perfect preservation for structures located in seismically unstable regions, by controlling the seismic response of these structures under the different levels of the seismic events, due to the sliding friction coefficient and radius of curvature. This type of isolator has different stages that can perform perfectly during any possible earthquake; whether it was a low, moderate, or even destructive intensity event, without affecting the continuity of the isolated facility's function, this is accomplished by progressively transmitting the force to bridge's superstructure at the definitive displacement. Triple friction pendulum bearings (TFP) are produced with lid film for the inner parts to provide more protection for these parts of the isolators, unlike the single pendulum bearings that are designed with bare working parts [15]. (Qt. in Ryan and Richins. 106).

Figure 2.9, is a cross-section diagram of triple friction pendulum bearing (TFP), showing the basic parameters of the TFP isolator.

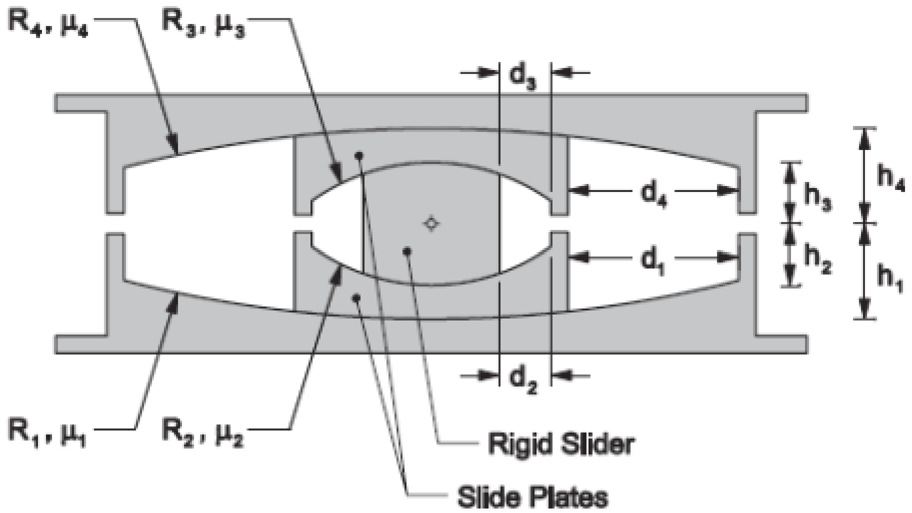

Figure 2.9: Triple Friction Pendulum Isolator Cross-Section [11]

Where.

R_1, μ_1 : refers to the lower sliding surface.

R_2, R_3, μ_2, μ_3 : refer to the inner sliders of curvature.

R_4, μ_4 : refers to the upper sliding surface.

D_1, D_4 : refers to the outer diameters.

D_2, D_3 : refers to the inner diameters.

h_1, h_2, h_3, h_4 : refers to the radial distance between the pivot point and the number referred surface (height of the slider).

Each one of the surfaces has its own radius R, coefficient of friction at the sliding surface μ , and diameter D.

There are some essential principles must be observed during the design process of the triple friction pendulum isolators (TFP) for bridges:

- The upper and lower outer sliders radii R_1 , R_4 should be equal, also the friction coefficients μ_1 , μ_4 are usually presumed to be equal.
- The inner slider of the isolator should be designed with a low value of the friction coefficient, while the value of friction coefficient of the outer slider should be higher than the value of the inner one. The reason is that the slider of the small friction coefficient works during low-intensity seismic events, and it should be decreased to prohibit the isolation system from being overly damped and thus being inefficient in such events. Likewise, the large value friction coefficient slider works during moderate and destructive intensity seismic events and should be increased to try to restrict the displacement of the isolation system when the energy of the extreme seismic event is transmitted to the bridge's structure.
- The effective curvature radius R is defined when simultaneously fulfilling the following:

1. $R =$ the actual radius of curvature $\pm$ a fragment of the height (h) of the hinged slider for single friction pendulum bearings FP.
2. $R =$ the sum of the actual radii of curvature of the two concave plates $-$ the height (h) of the slider for double friction pendulum bearings FP [15]. (Qt. in Ryan and Richins. 93).

2.6 Working Mechanism of Friction Pendulum Bearings (FPS)

The mechanism of friction pendulum bearings (FPS) is very familiar to classical pendulum movement, as the radius of the spherical concave interface equals the radius of pendulum movement. When seismic action occurs the friction slider shifts upper the concave interface as the isolated bridge begins to move due to earthquake agitation, and both of them acquire energy, which increases the amount of potential energy, and this energy including the weight of the bridge acts as a retrieving force for the bearings that help the bridge return back to its steady balanced state.

The displacement of the bridge under major seismic events or minor loads such as (vehicles and wind loads), is managed or restrained by the isolator when the movement takes place, thanks to friction coefficient μ between the slider and the concave interface, where the sliding interface has a restriction edge around the rim to control the definitive displacement when displaced in one direction [18]. (Qt. in Becker. 3).

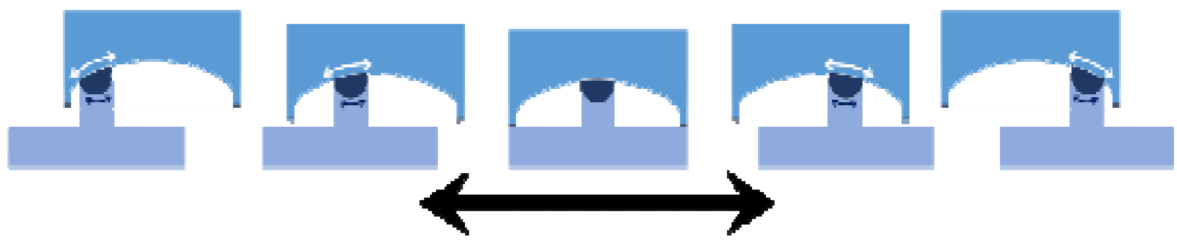

Figure 2.10: Behaviour of FPS during an Earthquake [43]

2.7 Working Mechanism of Triple Friction Pendulum Bearings (TFPS)

Recently the structures and isolators are being designed according to all types of earthquakes; frequent events (FE), design basis events (DBE), and maximum considered events (MCE) in order to exhibit enough displacement amplitude and withstand the forces transferred to bridge's structure under any seismic event that might occur.
As the typical triple friction isolators (TFP) are composed of four spherical sliding surfaces with restriction edges, work as a chain, where two of these surfaces (usually the internal surfaces)

are conformed in friction coefficient and radius of curvature, then this gives such type of isolators three different mechanisms to control the displacements under any motion occurs to the bridge, While the external surfaces are not identical with each other (sometimes they may also be identical). Thus when an earthquake take place and the motion starts on the inner surfaces of the isolator, this phase reflects the mechanism of single pendulum and determines the characteristics of isolator during frequent events FE, then the displacement of the bearing increases gradually causing changing to the sliding surface on which the motion happens so the movement pauses on one of the inner surfaces (2) and starts on one of the outer sliding surfaces (1) and continues also on the surface (3), defining the fundamental characteristics of the isolator during design basis events DBE, this change leads to an extra ductility demeanour, therefore the sliders reach its own displacement constraints and the bearing almost reach its maximum capacity when this bearing moves farther, at that point the slider alters the sliding surface once again; where the movement stops on the inner surfaces 2 and 3 and starts on the outer surfaces 1 and 4, on which the value of friction coefficient is sufficient enough to limit the sliding until the maximum considered event MCE take place, which in turn cause an extra rigidity demeanour until the bearing reaches its definitive displacement amplitude consequently the movement persist paused on the inner surface (3) and the slider on the outer surface (1) touches the constraining rim, while the sliding resumes on surfaces 2 and 4 determining the characteristics of the isolation system later than the maximum event MCE, In the end the sliding returns back on the inner surfaces 2 and 3 whilst the slider contacts the constraining edges on the outer surfaces 1 and 4 [18][19]. (Qt. in Becker. 4; Fenz and Constantinou theory).

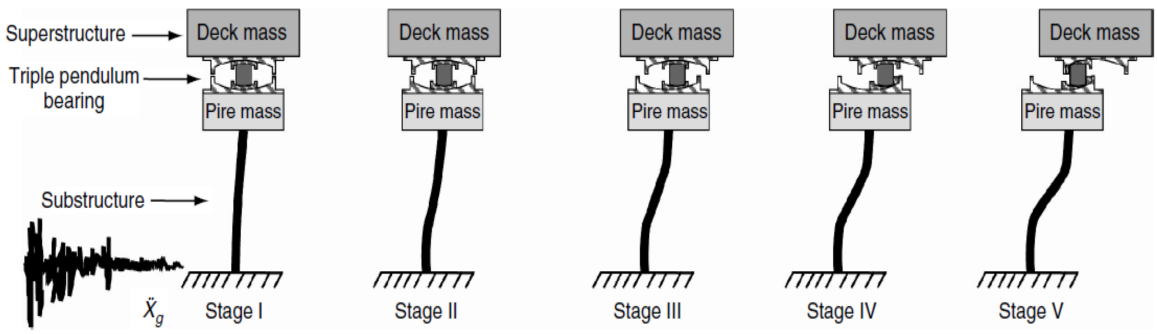

Figure 2.11: Behaviour of TFP during an Earthquake for a Seismically Isolated Bridge [20]

2.8 Mathematical Formulations of Triple Friction Pendulum Bearings (TFP)

Motion's behavior of triple friction pendulum isolators resembles the hysteretic monotonous loops, so depending on this behavior the motion can be categorized into five different sliding phases, where the motion occurs alternately on two different surfaces during each phase. For this reason, the relationship between force and displacement should be determined for each phase separately. Depending on the equilibrium equations for the bearing in each phase independently, the equation of motion at that phase can be defined by implementing a similar procedure to that utilized for the single friction pendulum bearing, also the force-displacement relation can be deduced from the free body diagram for each phase.

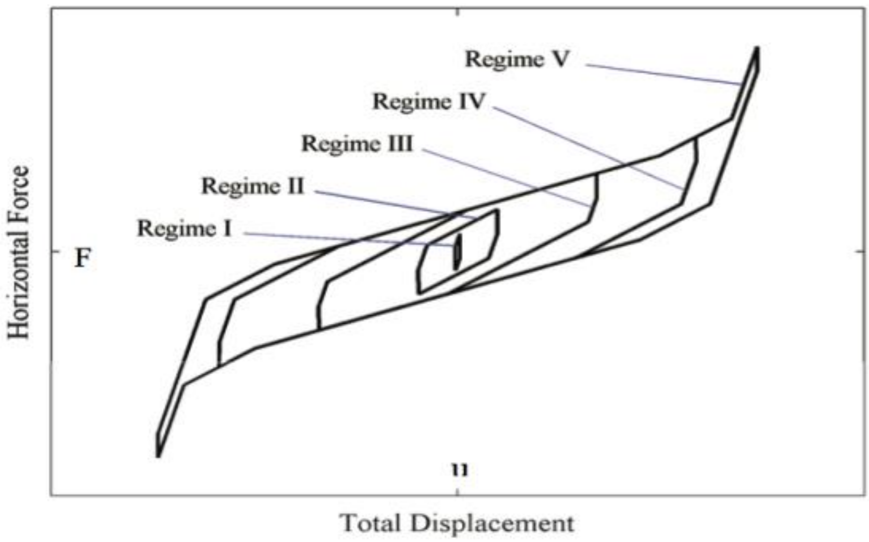

Figure 2.12: Force-Displacement Hysteresis Loops of TFP Bearings [11]

As explained in detail in (Fenz and Constantinou 2008a) the relations of force-displacement related to TFP's different phases can be illustrated; by referring that the motion starts on one of the surfaces when the horizontal force transferred by the bearing (F) becomes higher than surface's friction force, $F_{fi} = \mu_i * W$, where; W: is the vertical load applied on the bearing. Similarly, the sliding on the surface is halted when the relative displacement of the slider on this surface u_i is equal to the displacement amplitude d_i . The process of beginning or pausing the sliding on a particular surface can be defined by comparing the value of the surface's friction force F_{fi} with the value of lateral force at the moment when the slider begins to bear upon the displacement restrainer of this surface F_{dri}:

$$F_{dri} = \frac{W}{R_{eff}} d_i + F_{fi} \tag{2.1}$$

Phase I

The sliding occurs on the inner surfaces 2 and 3, then the force–displacement relationship for this phase will be:

$$F = \frac{W}{R_{eff\,2}+R_{eff\,3}} u + \frac{F_{f\,2}R_{eff\,2} + F_{f\,3}R_{eff\,3}}{R_{eff\,2}+R_{eff\,3}} \tag{2.2}$$

The motion on these surfaces will continue until:

$$F = F_{f1} = \mu_1 W \tag{2.3a}$$

and when displacement (u^*) is reached:

$$u = u^* = (\mu_1 - \mu_2)R_{eff\,2} + (\mu_1 - \mu_3)R_{eff\,3} \tag{2.3b}$$

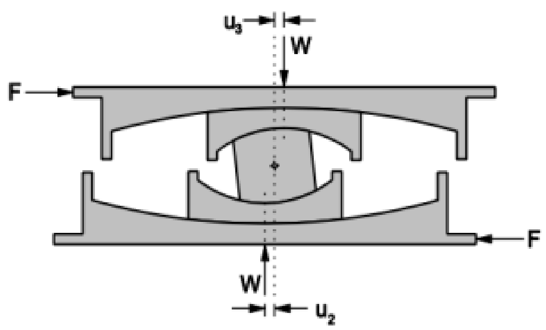

Figure 2.13: Triple Friction Pendulum First Regime I [19]

Phase II

The sliding occurs on the surfaces 1 and 3, then the force–displacement relationship for this phase will be:

$$F = \frac{W}{R_{eff\,1}+R_{eff\,3}}u + \frac{F_{f\,1}(R_{eff\,1}-R_{eff\,2})+F_{f\,2}R_{eff\,2} + F_{f\,3}R_{eff\,3}}{R_{eff\,1}+R_{eff\,3}} \qquad (2.4)$$

The motion on these surfaces will continue until:

$$F = F_{f4} = \mu_4 W \qquad (2.5a)$$

and when displacement (u^{**}) is reached:

$$u = u^{**} = u^{*} + (\mu_4 - \mu_1)(R_{eff\,1} + R_{eff\,3}) \qquad (2.5b)$$

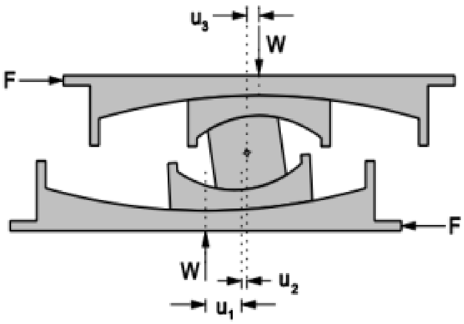

Figure 2.14: Triple Friction Pendulum Second Regime II [19]

Phase III

The sliding occurs on the outer surfaces 1 and 4, then the force–displacement relationship for this phase will be:

$$F = \frac{W}{R_{eff\,1}+R_{eff\,4}}u + \frac{F_{f\,1}(R_{eff\,1}-R_{eff\,2})+F_{f\,2}R_{eff\,2} + F_{f\,3}R_{eff\,3}+F_{f\,4}(R_{eff\,4}-R_{eff\,3})}{R_{eff\,1}+R_{eff\,4}} \qquad (2.6)$$

The motion on these surfaces will continue until:

$$F = F_{dr1} = \frac{W}{R_{eff\,1}}d_1 + F_{f1} \qquad (2.7a)$$

and when displacement (u_{dr1}) is reached:

$$u = u_{dr1} = u^{**} + d_1\left(1+\frac{R_{eff\,4}}{R_{eff\,1}}\right) - (\mu_4 - \mu_1)(R_{eff\,1} + R_{eff\,4}) \qquad (2.7b)$$

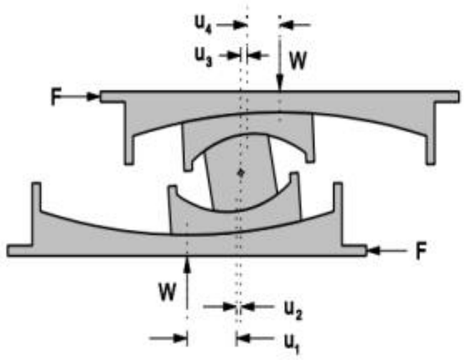

Figure 2.15: Triple Friction Pendulum Third Regime III [19]

Phase IV

The sliding occurs on surfaces 2 and 4, then the force–displacement relationship for this phase will be:

$$F = \frac{W}{R_{eff\,2}+R_{eff\,4}}(u - u_{dr1}) + \frac{W}{R_{eff\,1}} d_1 + F_{f1} \tag{2.8}$$

The motion on these surfaces will continue until:

$$F = F_{dr4} = \frac{W}{R_{eff\,4}} d_4 + F_{f4} \tag{2.9a}$$

and when displacement (u_{dr4}) is reached:

$$u = u_{d4} = u_{dr1} + \left[\left(\frac{d_4}{R_{eff\,4}} + \mu_4\right) - \left(\frac{d_1}{R_{eff\,1}} + \mu_1\right)\right](R_{eff\,2} + R_{eff\,4}) \tag{2.9b}$$

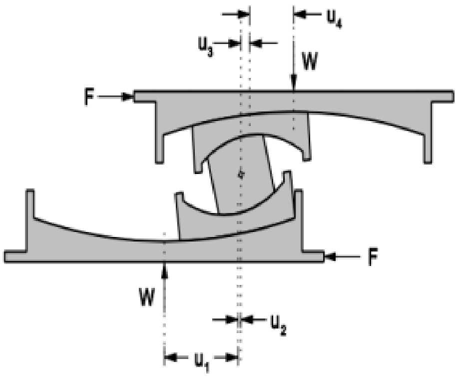

Figure 2.16: Triple Friction Pendulum Fourth Regime IV [19]

Phase V

Slider bears on restrainer of surfaces 1 and 4 and the sliding occur on surfaces 2 and 3, then the force–displacement relationship for this phase will be:

$$F = \frac{W}{R_{eff\,2}+R_{eff\,3}}(u - u_{dr4}) + \frac{W}{R_{eff\,4}} d_4 + F_{f4} \qquad (2.10)$$

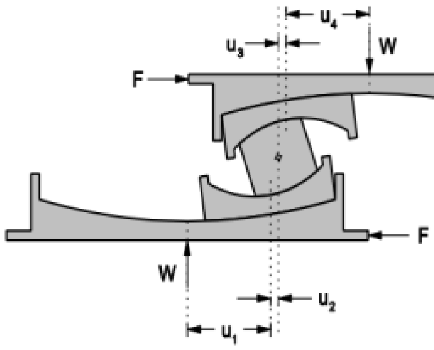

Figure 2.17: Triple Friction Pendulum Fifth Regime V [19]

All the equations of the different stages of triple friction pendulum bearings that were listed previously are related to the following assumptions:

1. friction coefficient ($\mu_2 = \mu_3 < \mu_1 < \mu_4$),
2. surface radius (R_{eff1}= R_{eff4}>> R_{eff2}= R_{eff3})
3. Displacement capacities d_1 > $(\mu_4 - \mu_1)R_{eff1}$
4. d_2 > $(\mu_1 - \mu_2)R_{eff2}$
5. $d_3 > (\mu_4 - \mu_3)R_{eff\,3}$

where.

R_{eff} : is the effective radii and is calculated from the equation: $R_{eff} = R_i - h_i$.

As proposed in Fenz and Constantinou 2008a each section of the motion loop of the triple friction pendulum isolator can be simulated by a series of three single pendulum isolators that are connected in parallel where the single elements are restrained to own the same force of the

TFP, while the relative displacements of each are distinct and spring's stiffness is specified by $1/R_{eff}$.

Figure 2.18 shows a model of three triple friction pendulum isolators that are connected in parallel and utilized to simulate the triple friction isolator demeanor.

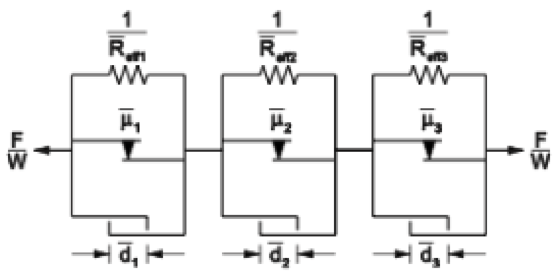

Figure 2.18: Model of Three single FP Isolators used to simulate TFP Isolator Demeanor[19]

Table 2.1 illustrated below, includes examples of a number of major isolated bridges around the world, which use friction pendulum bearings FP or triple friction pendulum bearings TFP as seismic isolators to protect these structures from seismic hazards either during the construction phase or as a retrofitting solution to fix the damages that had already caused harms to parts of these bridges due to major earthquakes.

Table 1.1: Bridges with Friction Pendulum Bearings

Bridge	Location (Country, City)	Length	Type	Materials	Number of Isolators
Tappan Zee bridge	United States, New York	5 Km (4989 m)	Dual-span Cable-stayed twin bridge	Precast concrete, steel girder	584 EPS Triple Pendulum isolators
Los Caras Bridge	Ecuador, Manabi	2 Km (1980 m)	Deck - Construction Type Chess		152 TFP
Lake Natoma Crossing bridge	United States, Folsom, California	2.264 ft (690 m)	Post - tensioned box girder bridge, with false deck arches	Concrete box girder	48 FPS
Antioch bridge	United States, California	2.897 Km	Steel plate twin girder	Steel girder, lightweight Concrete slab composite	86 FPS
Dumbarton bridge (Buffalo bridge)	United States, California	2.6 Km (2621 m)	Box twin girder bridge	Steel box girder and pre-stressed concrete spans	6 FPS
Benicia – Martinez bridge	United States, California	2.72 Km	Truss (southbound span) + Box girder segmental bridge (northbound span)	Pre-stressed lightweight concrete and reinforced concrete	22 FPS
Helicoidal dosquebradas bridge	Columbia – Coffee Highway connects Pereira and Manizales with Santa Rosa	500 m (part of a 3.5 Km highway road)	Helical Viaduct	Concrete	TFP

Tappan Zee Bridge:

The bridge is constructed across the Hudson River. The structure of this bridge was renewed in 2013 due to the worries of breaking down after the increase in traffic capacity together with the maintenance expenses.

Figure 2.19: New Tappan Zee Bridge [33]

Los-Caras Bridge:

The bridge is constructed on the Chone River estuary and experienced a severe earthquake in 2016 with forces reaching 7.8 magnitudes (Muisine Earthquake) and remained fully functional thanks to the triple friction pendulum bearings that were installed to the bridge's structure during the design and construction phase [27].

Figure 2.20: Los Caras Bridge [26]

Lake Natoma Crossing Bridge:

The bridge is located across the American river, and the use of Single Frictional isolators has Saved approximately one million dollars (1$) of construction expenses. Figure 2.21 shows the structure of the Lake Natoma Crossing Bridge [27].

Figure 2.21: Lake Natoma Crossing Bridge (American River) [28]

Antioch Bridge:

The bridge crosses the San Joaquin river and uses a number of 86 friction pendulum bearings. Figure 2.22, shows the structure of the Antioch bridge.

Figure 2.22: Antioch Bridge [29]

Dumbarton Bridge (Buffalo bridge):

The bridge crosses San Francisco Bay and is equipped with 6 friction pendulum bearings that were installed to prohibit damage to bridges' pillars during the seismic motions and accommodate a predicted displacement capacity reaching 42 inches [27].

Figure 2.23: Dumbarton Bridge (Buffalo bridge) [31]

Benicia – Martinez bridge:

The bridge crosses Carquinez Strait and it was one of the largest bridges to use the largest seismic isolation bearings ever manufactured for retrofit [30].

Figure 2.24: Benicia – Martinez Bridge [30]

Helicoidal Dosquebradas Bridge:

The bridge connects Pereira and Manizales with Santa Rosa, as it is a part of the 3.5 Km Columbia coffee highway road that contains viaducts and a 125 m tunnel. Using triple friction pendulum isolators in the construction of the bridge was a great solution to the instability of the slope and the difference in height in the area, with 35m in height [27][32].
Figure 2.25 shows a part of the Columbia-Coffee highway road that contains the helicoidal dosquebradas bridge and the tunnel.

Figure 2.25: Helicoidal Dosquebradas Bridge [32]

CHAPTER 3

MS BRIDGE MODELING

3.1 Introduction

In order to illustrate the application of analysis and bearing design procedures for seismic isolation, an example of an existing bridge was chosen. All the properties of the bridge's section and geometry are presumed to be the same as in the original bridge in the MS bridge example. Figures 3.1 and 3.2 illustrate respectively, a 3D view and a finite element mesh for the studied MS Bridge.

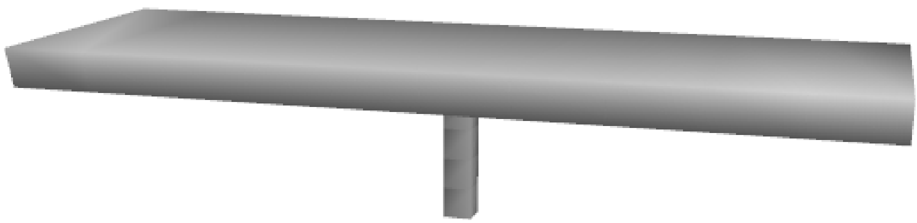

Figure 3.1: 3D View of the MS Bridge [38]

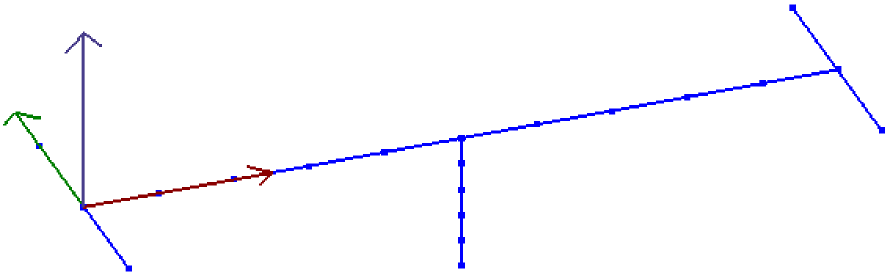

Figure 3.2: Finite Element Mesh of the MS Bridge [38]

3.2 Description of the Bridge

3.2.1 General

The selected structure is a continuous, two-span bridge with a deck of reinforced concrete (RC) cast-in-place box girder. The bridge has a single bent in the middle which is composed of a reinforced concrete cap beam laid on two RC circular columns. The bridge structure is isolated by TFP bearings that are located under the box girder and carried on the top of the bent cap with a total of 8 bearings for the bridge, whereas each abutment and bent has a number of two bearings.

3.2.2 Superstructure

The superstructure box girder is composed of a top slab with a thickness of 8 inches and a 6 inches thickness bottom slab, its depth is around 6 inches with a total width of about 39 ft. The weight per unit length of the bridge's deck is 10.216667 kip/ft. Figure 3.3, shows an X-Y plane of MS Bridge’s box girder.

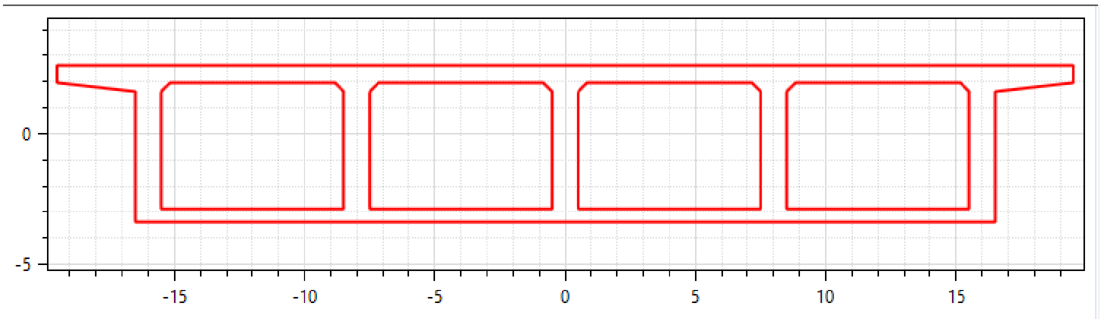

Figure 3.3: MS Bridge Box Girder's plane [38]

3.2.3 Piers

The substructure of the considered bridge consists of a single bent cap with RC columns supported from the bottom by footings at the foundation level. The detailed information about the bridge's column reinforcement contains a number of 30 longitudinal reinforcement bars with a size of 10 and a diameter of 48 inches distributed over the longer direction. Whilst, in the shorter direction a transverse bar of size 7 is distributed with a spacing of 3.4 inches. Figure 3.4 shows a section at the middle bent.

The modeling of the bridge was conducted by using OpenSees Simulation Software Framework. In order to simplify the modeling process, only the intermediate bent of the bridge was modeled by three dimensions (3D) with restriction of movement on the Y - Z plane.

All the properties of the bridge's bent materials and geometry are illustrated in Tables 3.1 and 3.2. Also, Table 3.3, shows the geometry and material properties of the selected Triple Friction Pendulum isolator.

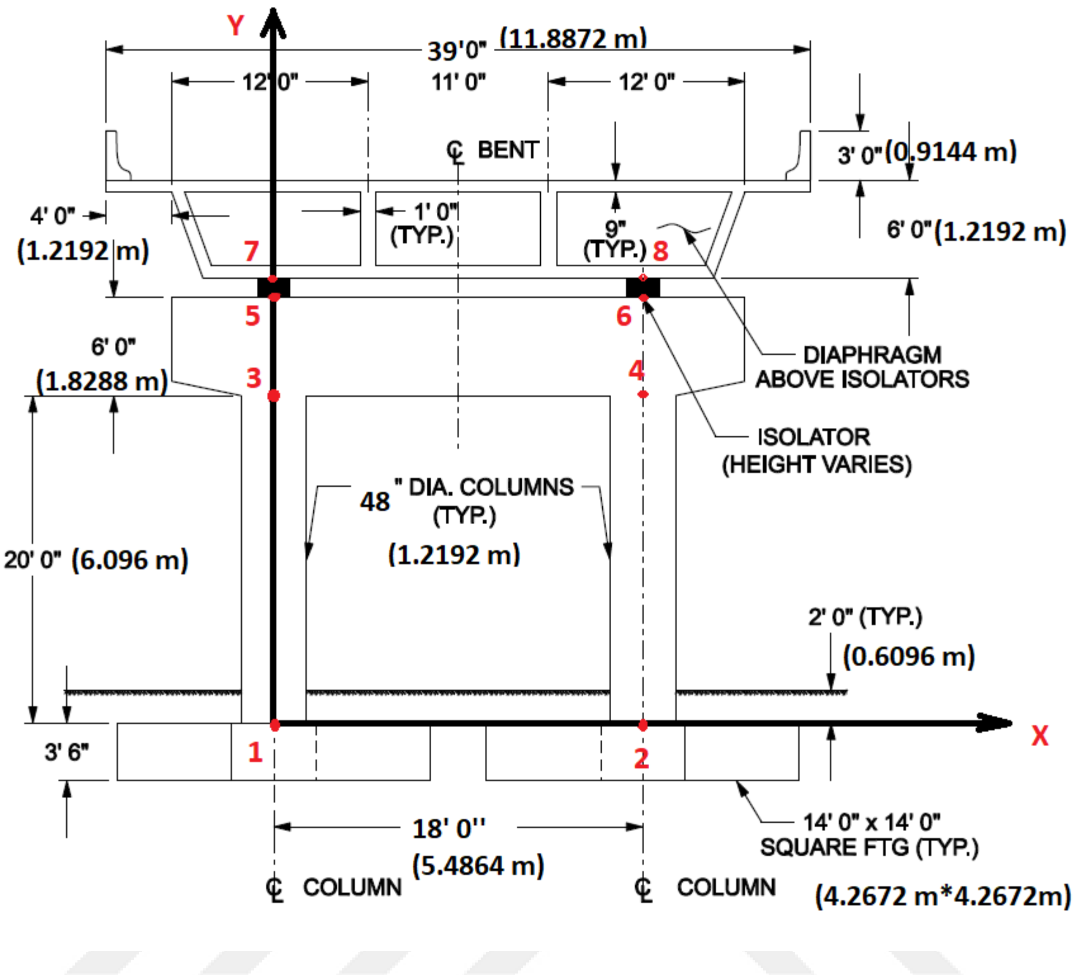

Figure 3.4: Section at the Middle Bent of MS Bridge [11]

Table 3.1: Geometric and Material Properties of Bridge’s bent-cap

Properties	Specifications	Units	Specifications	Units
Area of Cross Section	6.0 * 4.0	ft^2	1.83 * 1.22	m^2
Height of Bent-Cap	6.0	ft	1.8288	m
Moment of Inertia about Horizontal Axis	32.0	ft^4	0.2762	m^4
Moment of Inertia about Vertical Axis	72.0	ft^4	0.6214	m^4
Torsion Constant	75.125	ft^4	0.6484	m^4
Concrete Compressive Strength	4061	ksi	27999.61	MPa
Shear Modulus	1667.94	ksi	11500.0415	MPa

Table 3.2: Geometric and Material Properties of Bridge's bent-body

Properties	Specifications	Units	Specifications	
Column Diameter	48.0	$inch$	1.2192	m
Column Height	22.0	ft	6.096	m
Column Spacing	18.0	ft	5.4864	m
Moment of Inertia about Horizontal Axis	12.566371	ft^4	0.10846	m^4
Moment of Inertia about Vertical Axis	12.566371	ft^4	0.10846	m^4
Torsion Constant	25.132741	ft^4	0.2169	m^4
Concrete Compressive Strength	4350	ksi	29992.19	MPa
Shear Modulus	1677	ksi	11562.51	MPa

Table 3.3: Geometric and Material Properties of Triple Friction Pendulum Bearing

Dimension	Value	Unit	Value	Unit
Bearing's Cross-Section	1000 * 1000	mm^2	-	-
Thickness of the bearing	500	mm	-	-
Radius of the bearing: $R_1 = R_4$	88	$inch$	2.2352	m
Radius of the bearing: $R_2 = R_3$	16	$inch$	0.4064	m
Nominal Displacement Capacity: $d_1 = d_4$	14	$inch$	0.3556	m
Nominal Displacement Capacity: $d_2 = d_3$	2	$inch$	0.0508	m
Slider height: $h_1 = h_4$	4	$inch$	0.1016	m

Slider height: $h_2 = h_3$	3	$inch$	0.0762	m
Lower bound Velocity Dependent Friction coefficient: $\mu_1 = \mu_4$	0.06	-	-	-
Upper bound Velocity Dependent Friction coefficient: $\mu_1 = \mu_4$	0.1	-	-	-
Lower bound Velocity Dependent Friction coefficient: $\mu_2 = \mu_3$	0.035	-	-	-
Upper bound Velocity Dependent Friction coefficient: $\mu_2 = \mu_3$	0.058	-	-	-

The numerical values of bearing parameters that are listed in the previous table No.3 were taken from the study of the bridge example that was used in Constantinou et al,2011. For more detailed information about the utilized TFP bearing Constantinou et al,2011. Appendix C can be reviewed.

3.3 Opensees Overview

OpenSees is an open programming system that was developed by the University of California during the 2000s. The program uses TCL or Python programming language to help provide simple and easy emulation of the seismic action records for the constructions, by generating finite element computer implementations in both types parallel and sequent, in order to come up with better improvements against earthquakes in the structures that will be designed afterward. The program also uses different sources of numerical libraries to solve the various types of equations and introduce the used elements and materials, such as Fortran and C libraries, whereas the OpenSees software was originally written in C++ programming language. The program permits using either complex or simple coding language for analysis depending on the dexterity of the user, consequently, the analysis could seem like a complicated application or may look like an ordinary text file. OpenSees license allows users and programmers to utilize, adjust, clone, and distribute the program for uncommercialized objectives and academic research only, therefore it has two separate sections according to the information included:

- Opensees User section

- Opensees Developer section

3.4 OpenSees Bridge Structure Modeling

In this study, the bridge was modeled using OpenSees Software depending on TCL scripting language in two stages: first without using the Isolation system during the modeling phase, and the second after considering the triple friction seismic isolation system in the modeling. Bridge's structure model can be formed by following specific steps:

I. Starting with defining (DOF) “the number of degrees of freedom” and (NDM) “the locative dimension” at the nodes of the model; this can be fulfilled by applying the Model Builder command.

   For our study first, a directory file called “Data” was allocated for the purpose of storing the results that will be obtained from the analysis later, then the output units were defined in order to clarify to the program which units we want to deal with for our analysis (N, m, ton, sec). After that, a three-dimensional (3D) model with 6 degrees-of-freedom (6-DOF) was selected for the analysis by using the command "model BasicBuilder". Subsequently, the geometry and parameters of each element of the bridge model such as (Length, Weight, Cross-sectional area, Moment of Inertia, etc.....) were determined based on the information stated in tables 3.1 and 3.2. Figures 3.5 and 3.6, show the first step of MS bridge modelling.

```
#unites: N, m, sec, ton

wipe;
file mkdir Data;
set N 1.0;
set m 1.0;
set ton 1.0;
set sec 1.0;
set LunitTXT "m";
set FunitTXT "N";
set TunitTXT "sec";
set MunitTXT "ton";
set mm [expr 0.001*$m]
set cm [expr 0.01*$m];
set m2 [expr $m*$m];
set m4 [expr $m*$m*$m*$m];
set mm2 [expr $mm*$mm];
set ft [expr 0.3048*$m];
set ft2 [expr $ft*$ft];
set ft4 [expr $ft*$ft*$ft*$ft];
set in [expr 2.54*$cm];
set kip [expr 0.45359*$ton]
set kN [expr 1000.*$N];
set MPa [expr 1.*$N/$mm2];
set ksi [expr 6.89476*$MPa]
set g [expr 9.81*$m/pow($sec,2)];
set PI [expr 2.0*asin(1.0)];
model BasicBuilder -ndm 3 -ndf 6;
set Ubig 1.e10;
set Usmall [expr 1/$Ubig];
```

Figure 3.5: First Step of The Fixed MS Bridge Modelling (Defining Units)

```
#Define geometry:

set LBbody [expr 22.0*$ft];             #Bent body height
set LBcap [expr 6.0*$ft];               #Bent cap height
set HBcap [expr 4.0*$ft];               #Bent cap length
set BBcap [expr 6.0*$ft];               #Bent cap Width
set LI [expr 0.5*$m];                   #Isolator length
set D [expr 48*$in];                    #Bent body diameter
set W [expr (10.216667*39)/2*$kip];     #Weight of superstructure

#Calculated parameters:

set Mass [expr ($W/$g)*$kip];            #Mass of superstructure
set ABcap [expr $HBcap*$BBcap*$ft2];     #Bent cap cross sectional area
set ABbody [expr $PI*pow($D,2)/4*$ft2];  #Bent body cross sectional area
set IyBcap [expr 32.0*$ft4];
set IzBcap [expr 72.0*$ft4];
set JBcap [expr 75.125*$ft4];
set IBbody [expr $PI*pow($D,4)/64*$ft4];
set Jbody [expr 25.1327*$ft4];
```

Figure 3.6: First Step of The Fixed MS Bridge Modeling (Defining Parameters)

II. The second step of modeling steps is determining the nodal coordinates; this can be obtained by using the command “Node” with a labeled sequence for the selected nodes. In our model, the nodal coordinates were defined depending on the preferable axes that were assumed to pass from the center of the left column of our bridge, and a number of 6 nodes was defined along the bridge; where the first two nodes are located in the bottom of bridge's columns and the last two nodes located on the top of bridge's cap. Figure 3.7, shows the second step of MS bridge modeling.

```
#Nodal coordinates:

node  1   0.0                 0.0     0.0;
node  2   [expr 18.0*$ft]     0.0     0.0;
node  3   0.0                 0.0     $LBbody;
node  4   [expr 18.0*$ft]     0.0     $LBbody;
node  5   0.0                 0.0     [expr $LBbody+$LBcap];
node  6   [expr 18.0*$ft]     0.0     [expr $LBbody+$LBcap];
```

Figure 3.7: Second Step of The Fixed MS Bridge Modeling (Defining Nodal Coordinates)

III. The third step of modeling includes assigning the boundary conditions for the previously defined nodes; this can be determined by utilizing the command of single-point restriction "fix". This determination depends on the stability state of the considered node; while some nodes are fully fixed, other nodes are considered to be semi-fixed. Thus, the restriction has to be determined at each degree of freedom; whereas the number 1 is used in the state of fixity and the number 0 is used in the state of no restriction, and for the fully free-of-restriction nodes there won't be any need to be mentioned while defining the boundary conditions. In this step also masses should be assigned to the nodes using the "mass" command, to allow the dynamic analysis to be applicable later. For our bridge model, the movement on the Y - Z plane was restricted in order to simplify the analysis. Regarding the stability status of the nodes; the nodes at the top and bottom of the bridge's columns (1, 2, 3, 4) were assumed to be fully fixed, while the other nodes (5 and 6) were assumed to be semi-fixed. As for the nodal masses, it is obvious that the bridge's superstructure lies over the top of the bent, and its weight is being transferred to the bent's body through nodes 5 and 6 that are located on the top of the bent. Therefore, half of the calculated mass is assigned to each of these two nodes equally. Figure 3.8 shows the third step of MS bridge modeling.

```
#Nodal constraints:
#converting the model from 3D to 2D by restricting the movements in Y-Z
direction:

fix 1 1 1 1 1 1 1;
fix 2 1 1 1 1 1 1;
fix 3 1 1 1 1 1 1;
fix 4 1 1 1 1 1 1;
fix 5 0 1 1 1 0 1;
fix 6 0 1 1 1 0 1;
mass 5 [expr $Mass/2] 1e-9 0.0 0.0 0.0 0.0;
mass 6 [expr $Mass/2] 1e-9 0.0 0.0 0.0 0.0;
```

Figure 3.8: Third Step of The Fixed MS Bridge Modeling (Defining Nodal Constraints)

IV. The last step of modeling in OpenSees software is defining the elements of the structure. But before that, the force of resistance and rigidity of a beam-column should be switched from the primary coordinate into the global system coordinate by using the element geometric transformation “geomTransf" command; OpenSees has three types of geometric transformation Linear Transformation, PDelta Transformation, and Corotational Transformation. Withdrawing attention that this transformation is only needed for 3D cases as the geometric transformation can be identical for all the elements in a 2D case study. After a convenient geometric transformation is chosen for the elements, then model elements can be determined from one of the commands of the various element types available in the OpenSees library as suits the case we are working on.

In this study, a "Linear" geometric transformation type was determined for the beams and "PDelta" type for the columns. Regarding defining the elements of the model; firstly, the material properties for beams and columns were determined using the information stated in Tables 3.1 and 3.2, then the columns of the bent body were defined using the "ElasticBeamColumn" command to connect nodes from (1 to 5) using element tag 1 for the left column and nodes from (2 to 6) using element tag 3 for the right column utilizing the same command, while for the bent cap; it was defined as a beam section by using element tag 2 and utilizing the same command "ElasticBeamColumn" to connect between nodes from (5 to 6) that forms this beam. Figure 3.9 shows the fourth step of MS bridge modeling.

```
#Define elements & sections :

geomTransf Linear 1 1 1 0;            #Beams
geomTransf PDelta 2 1 0 0;            #Columns
set EcBcap [expr 4061*$ksi];          #BentCap Concrete Compressive Strength
set GBcap [expr 1667.94*$ksi];        #BentCap Body Shear Modulus
set Ecbody [expr 4350*$ksi];          #Body Concrete Compressive Strength
set Gbody [expr 1677*$ksi];           #Body Shear Modulus

uniaxialMaterial Elastic 1 100000000000;
uniaxialMaterial Elastic 2 0.1 ;

element elasticBeamColumn  1  1  5 $ABbody $Ecbody $Gbody $Jbody $IBbody $IBbody 2;
element elasticBeamColumn  2  5  6 $ABcap $EcBcap $GBcap $JBcap $IyBcap $IzBcap 1;
element elasticBeamColumn  3  2  6 $ABbody $Ecbody $Gbody $Jbody $IBbody $IBbody 2;
```

Figure 3.9: Fourth Step of MS Bridge Modeling (Defining Elements and Sections)

3.5 OpenSees Gravity Analysis

In order to execute any type of analysis for the model, first, a gravity analysis should be applied under the structure's self-weight. For this to be applied the output recorders of the analysis should be defined first to determine the type of response we are interested in observing through this analysis. So, before defining loads of gravity analysis output recorders should be determined using the "recorder" command. For our considered bridge model, two recorders were defined as following: A displacement recorder for the nodes (5 and 6) located on the top of the bent cap to create an output file for the displacements of these semi-fixed nodes at DOF 1 with the name of Data/Displacement. Out, and a Base Shear recorder for the nodes (1 and 2) located on the bottom of bent columns' to create an output file for the reactions of these restrained nodes at DOF 1 with the name of Data/BaseShear.out.

After defining the recorders of gravity analysis that will be applied, then the components of this static analysis can be determined. The first step of the analysis is to apply the nodal loads using a specific time series from the OpenSees time series library; for our model, the gravity load is the weight of the superstructure which equals (199,225 kips) and lies over the top of the bent-cap. Therefore, the load of gravity will be assigned at nodes 5 and 6 equally in the negative Y direction using Linear time series with identification tag 1. In order to create this load and insert it into the framework, a convenient pattern should be used corresponding to the utilized type of timeSeries using the "pattern" command; For our bridge, a **Plain pattern** was determined to construct the gravity load.

Later, analysis objects should be determined, the first object can be determined utilizing the "Constraints" command, and this object defines how to apply restraint equations throughout the analysis. Regarding our model, **Plain constraints** were used due to the full restriction at nodes (1 and 2) at all DOFs.

The next step is, determining the object that defines digits of the degrees of freedom (numbering of equilibrium equations of the model); which is the DOF numberer that can be defined using the "numberer" command. A **Plain numberer** was chosen for our considered case as the model is quite small and uncomplicated.

After that, a solver should be defined using the "system" command, in order to store and resolve the equations of the analysis; A **BandGeneral** system was used for our case.

The following object to be determined of analysis objects is the one that defines paces concatenation for solving the equilibrium equations of our analysis, and this can be achieved by creating a SolutionAlgorithm object using the "algorithm" command. Regarding our bridge since all model elements are elastic then the **Linear algorithm** was used for solving the equations.

In the analysis being applied, the calculated gravity load will be assigned gradually to nodes 5 and 6 using an integrator object which defines the load control according to the analysis' time step increment. For our case using the "integrator" command, a **0.1 load control** with 10 equal analyzing steps was set.

The subsequent step to be performed is choosing the type of analysis. Concerning our model, a **Static** analysis was set using the "analysis" command, since gravity analysis is a static type of analysis.

The last step is executing the analysis after all of our analysis components were defined, by determining the number of steps that will be applied for this analysis and calling the "analyze" command. For our model a number of 10 steps was set previously thus, the scripting will be; **analyze 10**.

An additional step can be applied to the analysis if a transient analysis will be applied later on, this step is; restarting the time to (0.0) in order to allow the following analysis to begin with a new time history, and preserve the gravity load constant by using the "loadConst" command.

Figure 3.10 shows the recorders and steps of Gravity analysis for the MS bridge.

```
#Define recorder :

recorder Node -file Data/Displacement.out -time -node 5 6 -dof 1 disp;
recorder Node -file Data/BaseShear.out -time -node 1 2 -dof 1 reaction;

#Define gravity analysis :

timeSeries Linear 1
pattern Plain 1 1 {
 load 5 0.0 [expr -$W/2] 0.0 0.0 0.0 0.0;
 load 6 0.0 [expr -$W/2] 0.0 0.0 0.0 0.0;
}
constraints Plain;
numberer Plain;
system BandGeneral;
test NormDispIncr 1.0e-6 10;
algorithm Linear;
integrator LoadControl 0.1;
analysis Static;
analyze 10;
loadConst -time 0.0;
setTime 0.0;
```

Figure 3.10: Steps of the Gravity Analysis of The Fixed MS Bridge

3.6 OpenSees Time History Analysis

The steps of transient type analysis are similar to the steps followed in the static type of analysis with a slight difference in defining the pattern object.

For the time history analysis, an acceleration record of an earthquake motion will be determined at nodes 5 and 6 as a load pattern instead of a numerical value. The acceleration records of several ground motions were obtained from the PEER NGA database and used to perform the analysis for our model; The 1999 Duzce, Turkey earthquake (PGA of 0.739 g) that was recorded at Bolu station component **BOL090** with a number of data points (nPts) 5590, and a **0.01**-time step (dt) between data points. And the 1995 Kobe, Japan earthquake (PGA of 0.474 g) that was recorded at Nishi-Akashi station component **NIS090** with a number of data points (nPts) 4096, and a **0.01**-time step (dt) between data points. Also, the 1978 Tabas, Iran earthquake (PGA of 0.8 g) that was recorded at Tabas station component **TAB-L1** was used with a number of data points (nPts) 1650, and a **0.02**-time step (dt) between data points. Before defining the pattern type, a TimeSeries of identification tag 2 with the selected ground motion file path needs to be determined. Since the values of acceleration records of the earthquakes are in G units, then a **g** factor needs to be used with the TimeSeries to convert these values into the units of m^2/sec.

A **uniform excitation** pattern was the suitable pattern to be used for the time history analysis of our bridge model in the X-axis direction (direction 1) with an identification tag 2 using the "pattern" command.

Before defining other analysis objects, the proportional values of mass and rigidity should be allocated to the model; these values are recognized as damping components and can be set utilizing the "Rayleigh" command. The value of stiffness proportional can be calculated using the formula:

[2*(damping ratio/frequency)]; the damping ratio is adjusted to **0.05** for our case, and the frequency value can be computed from the first eigenvalue for all the applied ground motions.

After allocating the damping components, the other analysis' objects can be set accordingly; (Restriction handler, Degrees-of-freedom numberer, Numerical solver, Algorithm, and integrator). For this to be achieved, the objects determined earlier for the previous static analysis need to be cleared using the "wipeAnalysis" command, to allow the objects of the dynamic (transient) analysis to be determined. Analysis objects for our bridge model can now be determined, as the Constraint handler and DOF numberer were set to be **Plain** type; the same as the type defined for the gravity analysis, while the numerical solver, the algorithm, and integrator were defined differently as **ProfileSPD** and **KrylovNewton** and **Newmark** respectively.

Consequently, all the needed objects for the analysis were set. Thus, the **Transient** analysis type is defined for our model, and the last step to be applied is determining the number of steps (nPts) and the value of analysis increments (dt) that should be executed during the analysis process. Concerning our model, the number of steps for the Duzce earthquake was defined as **5590** steps and the increment **0.01**, while the number of steps for the Kobe earthquake was defined as **4096** steps with the same value of **0.01** for the analysis' increment, and the number of steps for Tabas earthquake was defined as **1650** steps with the value of **0.02** increment. Figures 3.11, 3.12, and 3.13 show the steps of the Dynamic analysis of the modeled MS bridge for both applied ground motions; Duzce, Turkey, Kobe, Japan, and Tabas, Iran earthquakes.

```
#Define DYNAMIC analysis :

set accelSeries "Series -dt 0.02 -filePath RSN1602_DUZCE_BOL090.AT2 -factor $g";
pattern UniformExcitation 2 1 -accel $accelSeries;
set freq [expr pow([eigen 1],0.5)];
set dampRatio 0.05;
rayleigh 0.0 0.0 0.0 [expr 2*$dampRatio/$freq];
wipeAnalysis;
constraints Plain;
numberer Plain;
test NormDispIncr 1.0e-6  10;
system ProfileSPD;
algorithm KrylovNewton;
integrator Newmark 0.6 0.3025;
analysis Transient;
analyze 5590 0.01;


puts "Done";
```

Figure 3.11: Dynamic Analysis Steps of The Fixed MS Bridge for Duzce, Turkey Earthquake

```
#Define DYNAMIC analysis :

set accelSeries "Series -dt 0.02 -filePath RSN1111_KOBE_NIS000.AT2 -factor $g";
pattern UniformExcitation 2 1 -accel $accelSeries;
set freq [expr pow([eigen 1],0.5)];
set dampRatio 0.05;
rayleigh 0.0 0.0 0.0 [expr 2*$dampRatio/$freq];
wipeAnalysis;
constraints Plain;
numberer Plain;
test NormDispIncr 1.0e-6  10;
system ProfileSPD;
algorithm KrylovNewton;
integrator Newmark 0.6 0.3025;
analysis Transient;
analyze 4096 0.01;


puts "Done";
```

Figure 3.12: Dynamic Analysis Steps of The Fixed MS Bridge for Kobe, Japan Earthquake

```
#Define DYNAMIC analysis :

set accelSeries "Series -dt 0.02 -filePath RSN143_TABAS_TAB-L1.AT2 -factor $g";
pattern UniformExcitation 2 1 -accel $accelSeries;
set freq [expr pow([eigen 1],0.5)];
set dampRatio 0.05;
rayleigh 0.0 0.0 0.0 [expr 2*$dampRatio/$freq];
wipeAnalysis;
constraints Plain;
numberer Plain;
test NormDispIncr 1.0e-6  10;
system ProfileSPD;
algorithm KrylovNewton;
integrator Newmark 0.6 0.3025;
analysis Transient;
analyze 1650 0.02;


puts "Done";
```

Figure 3.13: Dynamic Analysis Steps of The Fixed MS Bridge for Tabas, Iran Earthquake

3.7 OpenSees Seismically Isolated Bridge Structure Modeling

The process of modeling the structure of the seismically isolated bridge involves the same steps of modelling the fixed (non-isolated) structure, in addition to some addings related to the isolation system that should be taken into consideration during each modeling step of the steps that form the whole structure of this isolated bridge:

I. For the addition of the first step; after defining the number of degrees-of-freedom (6-DOF) and the locative dimension at the nodes of the model (3D) by applying the command of model BasicBuilder, and determining the geometry and parameters of each element of the bridge model based on the information stated in tables 3.1 and 3.2 in the same way they were determined for the non-isolated model, then the geometry of used the triple friction isolators can be determined depending on the information stated in table 3.3. Figures 3.14 and 3.15, show the first step of modeling the structure of the isolated MS bridge.

```
#unites: N, m, sec, ton

wipe;
file mkdir Data;
set N 1.0;
set m 1.0;
set ton 1.0;
set sec 1.0;
set LunitTXT "m";
set FunitTXT "N";
set TunitTXT "sec";
set MunitTXT "ton";
set mm [expr 0.001*$m]
set cm [expr 0.01*$m];
set m2 [expr $m*$m];
set m4 [expr $m*$m*$m*$m];
set mm2 [expr $mm*$mm];
set ft [expr 0.3048*$m];
set ft2 [expr $ft*$ft];
set ft4 [expr $ft*$ft*$ft*$ft];
set in [expr 2.54*$cm];
set kip [expr 0.45359*$ton]
set kN [expr 1000.*$N];
set MPa [expr 1.*$N/$mm2];
set ksi [expr 6.89476*$MPa]
set g [expr 9.81*$m/pow($sec,2)];
set PI [expr 2.0*asin(1.0)];
model BasicBuilder -ndm 3 -ndf 6;
set Ubig 1.e10;
set Usmall [expr 1/$Ubig];
```

Figure 3.14: First Step of The Isolated MS Bridge Modeling (Defining Units)

```
#Define geometry:

set LBbody [expr 22.0*$ft];                   #Bent body height
set LBcap [expr 6.0*$ft];                     #Bent cap height
set HBcap [expr 4.0*$ft];                     #Bent cap length
set BBcap [expr 6.0*$ft];                     #Bent cap Width
set LI [expr 0.5*$m];                         #Isolator length
set D [expr 48*$in];                          #Bent body diameter
set W [expr (10.216667*39)/2*$kip];           #Weight of superstructure

#Calculated parameters:

set Mass [expr ($W/$g)*$kip];                  #Mass of superstructure
set ABcap [expr $HBcap*$BBcap*$ft2];           #Bent cap cross sectional area
set ABbody [expr $PI*pow($D,2)/4*$ft2];        #Bent body cross sectional area
set IyBcap [expr 32.0*$ft4];
set IzBcap [expr 72.0*$ft4];
set JBcap [expr 75.125*$ft4];
set IBbody [expr $PI*pow($D,4)/64*$ft4];
set Jbody [expr 25.1327*$ft4];
```

Figure 3.15: First Step of The Isolated MS Bridge Modeling (Defining Parameters)

```
#Define elements & sections :

set L1 [expr 13*$in];
set L2 [expr 84*$in];
set L3 [expr 84*$in];
set d1 [expr 2*$in];
set d2 [expr 14*$in];
set d3 [expr 14*$in];
set uy 0.0025;
set kvt 0.1;
set minFv 0.1;
set tol 1.E-5;

frictionModel VelDependent 1 0.035 0.058 100;
frictionModel VelDependent 2 0.06 0.1 100;
frictionModel VelDependent 3 0.06 0.1 100;
```

Figure 3.16: First Step of The Isolated MS Bridge Modeling (Defining Isolator's Geometry)

II. For determining the nodal coordinates using the node command in the Second step of modeling, two additional nodes (7 and 8) will be added in addition to the nodes that were defined for the non-isolated structure. Thus, after depending on the preferable axes that are assumed to pass from the center of the left column of our bridge, and determining the 6 nodes along the bridge, the additional nodes (7 and 8) will be set to be located on the upper top of the triple friction isolators that will be settled between the nodes (5 and 6) on the top of bridge's bent cap and the newly defined nodes. Figure 3.17 shows the second step of modeling the structure of the isolated MS bridge.

```
#Nodal coordinates:

node  1   0.0               0.0     0.0;
node  2   [expr 18.0*$ft]   0.0     0.0;
node  3   0.0               0.0     $LBbody;
node  4   [expr 18.0*$ft]   0.0     $LBbody;
node  5   0.0               0.0     [expr $LBbody+$LBcap];
node  6   [expr 18.0*$ft]   0.0     [expr $LBbody+$LBcap];
node  7   0.0               0.0     [expr $LBbody+$LBcap+$LI];
node  8   [expr 18.0*$ft]   0.0     [expr $LBbody+$LBcap+$LI];
```

Figure 3.17: Second Step of The Isolated MS Bridge Modeling (Defining Nodal Coordinates)

III. Similarly, the third step of modeling that includes assigning the boundary conditions and masses for the defined nodes using the commands "fix" and "mass" relatively. After defining the nodes at the top and bottom of the bridge's columns (1, 2, 3, 4) that were assumed to be fully fixed, and the nodes (5 and 6) that were assumed to be semi-fixed, two additional boundary conditions should be assigned for the newly added nodes 7 and 8 which also are assumed to be semi-fixed. As for the nodal masses, after inserting the triple friction pendulum isolators the bridge's superstructure now lies over the isolators, and its weight is being transferred to the isolator's body through nodes 7 and 8 located on the top of the isolators, and a part of this weight will be transferred to bridge's bent cap. Therefore, half of the calculated mass is assigned to the nodes located on the top of the isolators equally, and a quarter of this mass is assigned to nodes 5 and 6 on the top of the bent cap.
Figure 3.18, shows the third step of modeling the structure of the isolated MS bridge.

```
#Nodal constraints:
#converting the model from 3D to 2D by restricting the movements in Y-Z direction:

fix 1 1 1 1 1 1 1;
fix 2 1 1 1 1 1 1;
fix 3 1 1 1 1 1 1;
fix 4 1 1 1 1 1 1;
fix 5 0 1 1 1 0 1;
fix 6 0 1 1 1 0 1;
fix 7 0 1 1 1 0 1;
fix 8 0 1 1 1 0 1;
mass 5 [expr $Mass/4] 1e-9 0.0 0.0 0.0 0.0;
mass 6 [expr $Mass/4] 1e-9 0.0 0.0 0.0 0.0;
mass 7 [expr $Mass/2] 1e-9 0.0 0.0 0.0 0.0;
mass 8 [expr $Mass/2] 1e-9 0.0 0.0 0.0 0.0;
```

Figure 3.18: Third Step of The Isolated MS Bridge Modeling (Defining Nodal Constraints)

IV. In the last step of modeling through OpenSees software which includes defining the elements of the structure, after determining the geometric transformation type for the bridge’s beams and columns and allocating them to the elements of the considered structure depending on the information stated in tables 3.1 and 3.2, afterward the isolation system elements could be defined depending on the data stated in table 3.3

using tag elements 4 and 5 to connect the nodes (5 to 7) and (6 to 8) of the triple friction elements and tag element 6 for the nodes (7 to 8) that forms the beam of superstructure above the isolators. Figure 3.19 shows the fourth step of modeling the isolated MS bridge structure.

```
geomTransf Linear 1 1 1 0;          #Beams
geomTransf PDelta 2 1 0 0;          #Columns
set EcBcap [expr 4061*$ksi];        #BentCap Concrete Compressive Strength
set GBcap [expr 1667.94*$ksi];      #BentCap Body Shear Modulus
set Ecbody [expr 4350*$ksi];        #Body Concrete Compressive Strength
set Gbody [expr 1677*$ksi];         #Body Shear Modulus

uniaxialMaterial Elastic 1 100000000000;
uniaxialMaterial Elastic 2 0.1 ;

#Columns
element elasticBeamColumn  1  1  5 $ABbody $Ecbody $Gbody $Jbody $IBbody $IBbody 2;
element elasticBeamColumn  2  2  6 $ABbody $Ecbody $Gbody $Jbody $IBbody $IBbody 2;
#BentCap
element elasticBeamColumn  3  5  6 $ABcap $EcBcap $GBcap $JBcap $IyBcap $IzBcap 1;
#Isolator
element TripleFrictionPendulum 4 5 7 1 2 3 1 2 2 2 $L1 $L2 $L3 $d1 $d2 $d3 [expr -
$W/2] $uy $kvt $minFv $tol
element TripleFrictionPendulum 5 6 8 1 2 3 1 2 2 2 $L1 $L2 $L3 $d1 $d2 $d3 [expr -
$W/2] $uy $kvt $minFv $tol
#Bridge Deck
element elasticBeamColumn  6  7  8 $ABcap $EcBcap $GBcap $JBcap $IyBcap $IzBcap 1;
```

Figure 3.19: Fourth Step of Modeling the Isolated MS Bridge (Defining Elements and Sections)

3.8 OpenSees Seismically Isolated Structure Gravity Analysis

Gravity analysis for the isolated structure includes the same steps as the fixed (non-isolated) one. Regarding the gravity load (weight of the superstructure) that should be applied to the nodes, will be assigned at nodes 7 and 8 in the negative Y direction using Linear time series with identification tag 1, as these two nodes are now located under the superstructure of the bridge instead of the nodes 5 and 6 due to the existence of triple friction pendulum isolators. Also, an additional two recorders were added in addition to the previously defined output recorders, in order to extract the force-displacement relationship for the isolation system used; the first recorder is a displacement recorder for the nodes (7 and 8) that are located on the top of the Isolators to create an output file for the displacements of these semi-fixed nodes at DOF 1 with the name of Data/Displacement. Out, and the second recorder is an element force recorder for the triple friction pendulum isolator elements (4 and 5) located under the bridge's superstructure to create an output file for the force of these elements at DOF 1 with the name of Data/eleForce.out. Figure 3.20 shows the recorders and steps of Gravity analysis for the isolated MS bridge.

```
#Define recorder :

recorder Node -file Data/NodeForce.out -time -node 5 6 -dof 1 reaction;
recorder Element -file Data/eleForce.out -time -ele 4 5 force;
recorder Node -file Data/Displacement.out -time -node 5 6 7 8 -dof 1 disp;
recorder Node -file Data/BaseShear.out -time -node 1 2 -dof 1 reaction;


#Define gravity analysis :

timeSeries Linear 1
pattern Plain 1 1 {
 load 7 0.0 [expr -$W/2] 0.0 0.0 0.0 0.0;
 load 8 0.0 [expr -$W/2] 0.0 0.0 0.0 0.0;
}
constraints Plain;
numberer Plain;
system BandGeneral;
test NormDispIncr 1.0e-6 10;
algorithm Linear;
integrator LoadControl 0.1;
analysis Static;
analyze 10;
loadConst -time 0.0;
setTime 0.0;
```

Figure 3.20: Steps of the Gravity Analysis of isolated the MS Bridge

3.9 OpenSees Seismically Isolated Structure Time History Analysis

The steps of the transient time history analysis (THA) for the seismically isolated structure with the triple friction pendulum bearings type of seismic isolation systems are the same as the steps followed in the THA for the fixed (non-isolated) structure modeling process. As it was also obtained for three ground motions (Duzce, Turkey, Kobe, Japan, and Tabas, Iran earthquakes) as applied in the previously conducted analysis for the fixed structure, to observe the difference in analysis's results between the isolated and non-isolated structures.

CHAPTER 4

ANALYSIS RESULTS

4.1 General

This chapter investigates the time history analysis (THA) outcomes, for both fixed and TFP isolated models of the considered MS bridge structure under three different horizontal earthquakes, in order to observe the seismic response of the bridge in both cases and compare the values differences after applying the seismic isolation. The results will be presented in this section are as follows:

1. Nodal Displacement (for isolated and non-isolated bridge model)
2. Base Shear Reaction (for isolated and non-isolated bridge model)
3. Force-Displacement Hysteresis Loops of the TFP Isolators

The properties of the earthquakes used in the analyses are as shown in the following table:

Table 4.1: Earthquakes Properties

Earthquake and Station Name	Peak Ground Acceleration (PGA-g)	Peak Ground Velocity (PGV-cm/sec)	Peak Ground Displacement (PGD-cm)	Number of Points (nPts)	Time step (dt)
Duzce, Turkey – Bolu (1999)	0.80568	65.88261	13.0985	5590	0.01
Kobe, Japan – Nishi Akashi (1995)	0.48323	46.82464	8.40581	4096	0.01
Tabas, Iran– Tabas(1978)	0.85398	98.84753	37.53233	1650	0.02

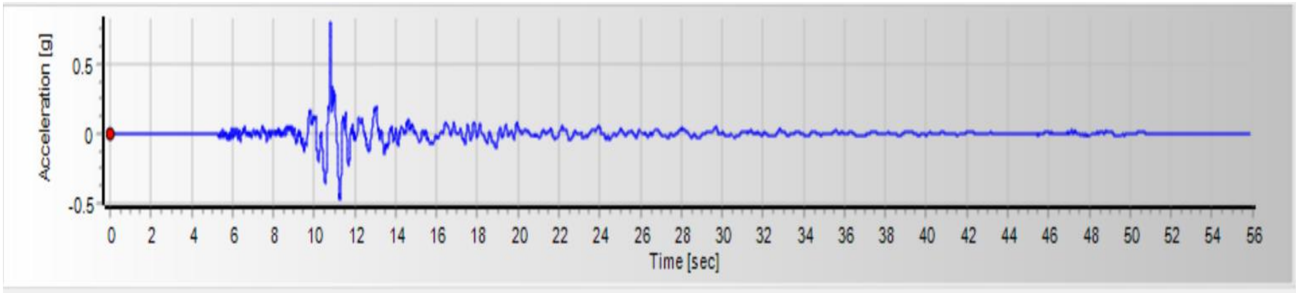

Figure 4.1: Bolu Ground Acceleration

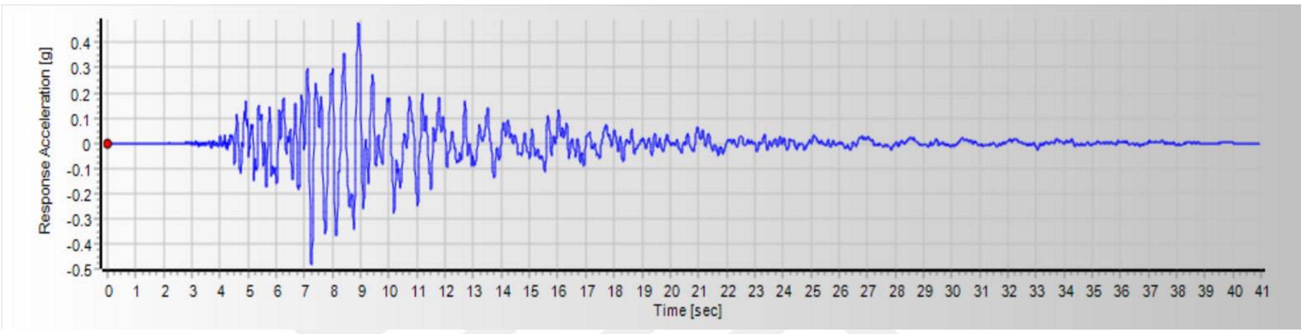

Figure 4.2: Nishi-Akashi Ground Acceleration

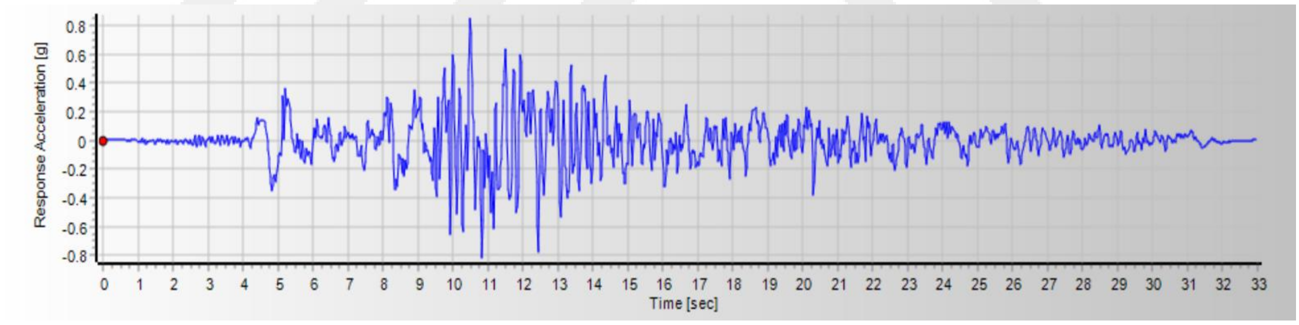

Figure 4.3: Tabas Ground Acceleration

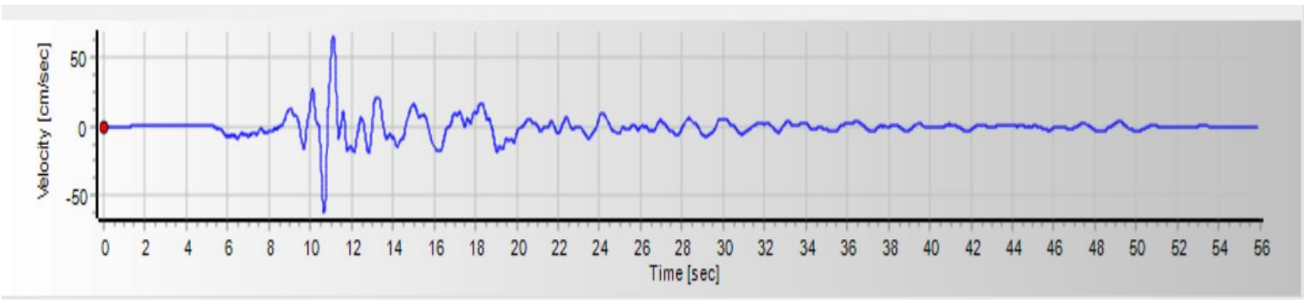

Figure 4.4: Bolu Ground Velocity

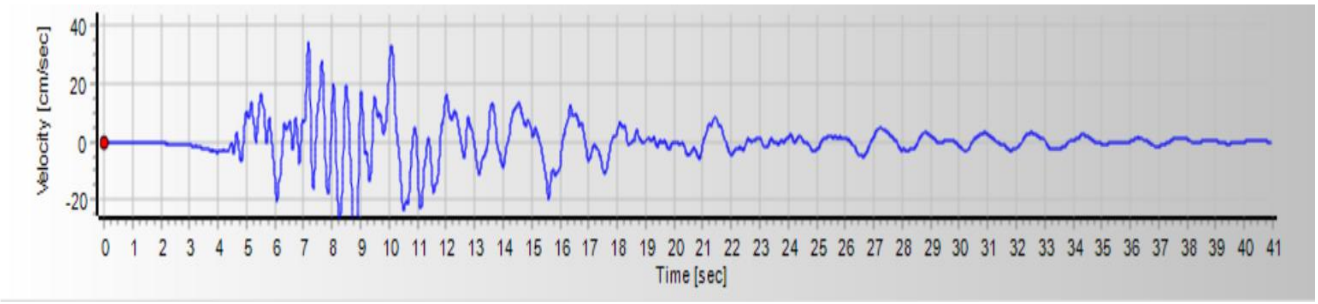

Figure 4.5: Nishi-Akashi Ground Velocity

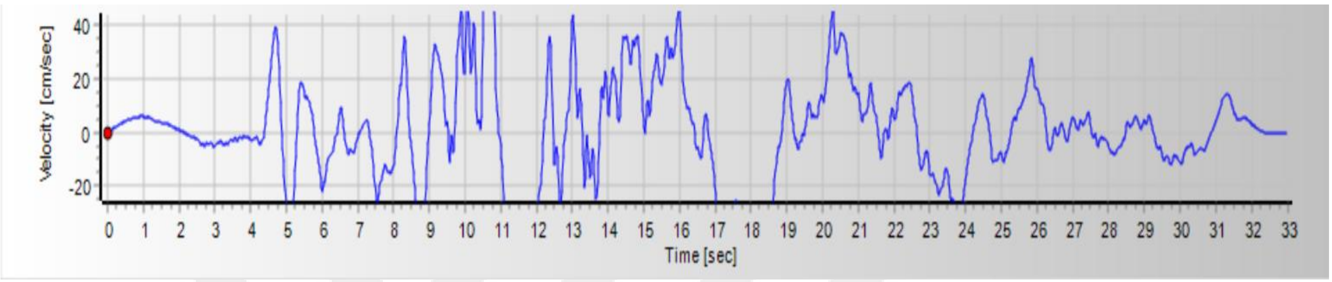

Figure 4.6: Tabas Ground Velocity

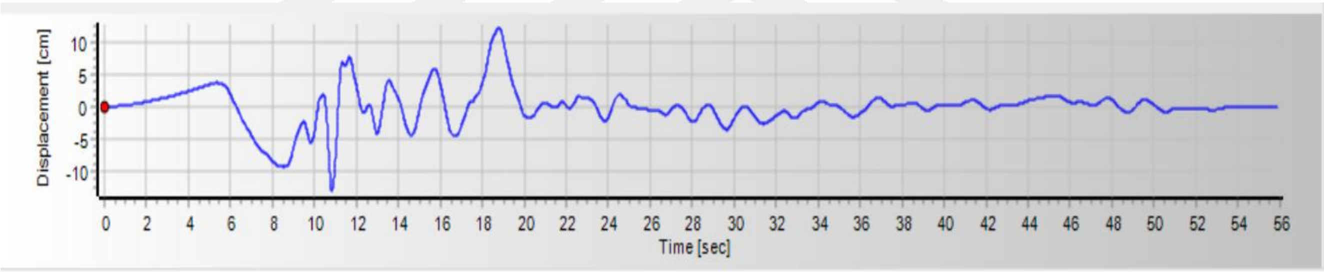

Figure 4.7: Bolu Ground Displacement

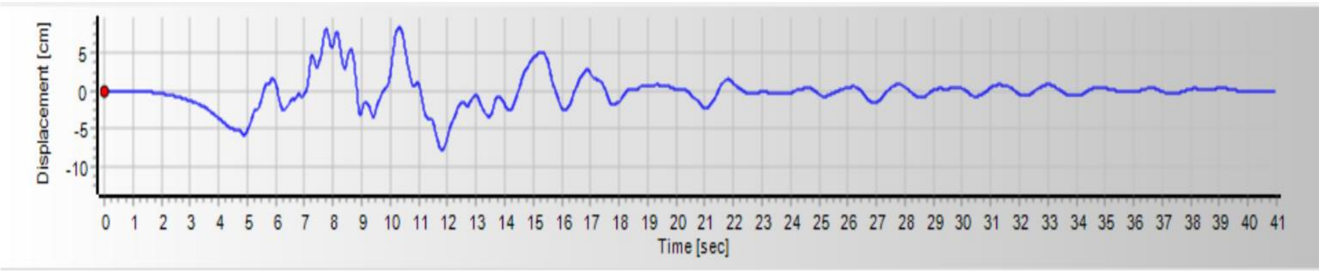

Figure 4.8: Nishi-Akashi Ground Displacement

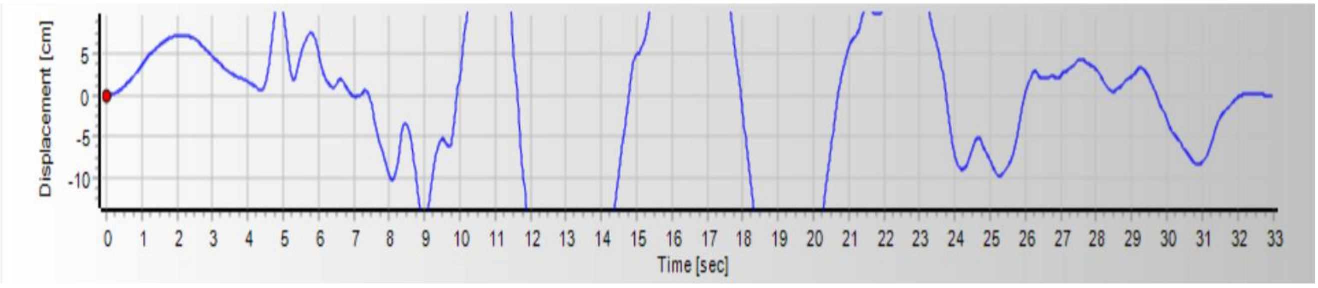

Figure 4.9: Tabas Ground Displacement

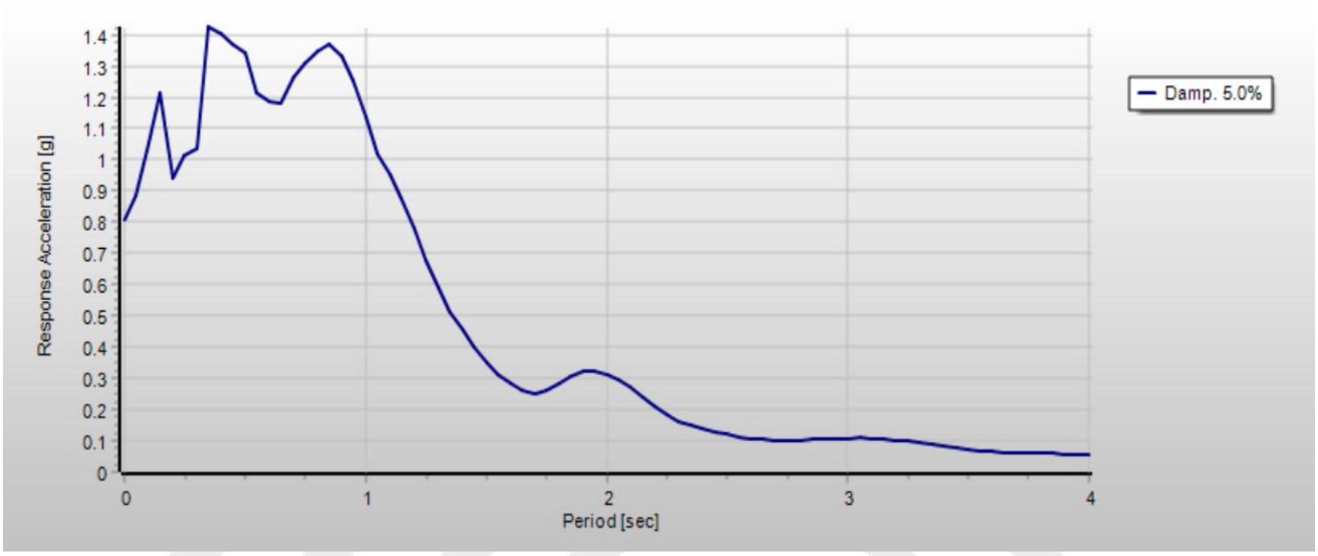

Figure 4.10: Bolu 5% Pseudo-Acceleration Spectrum

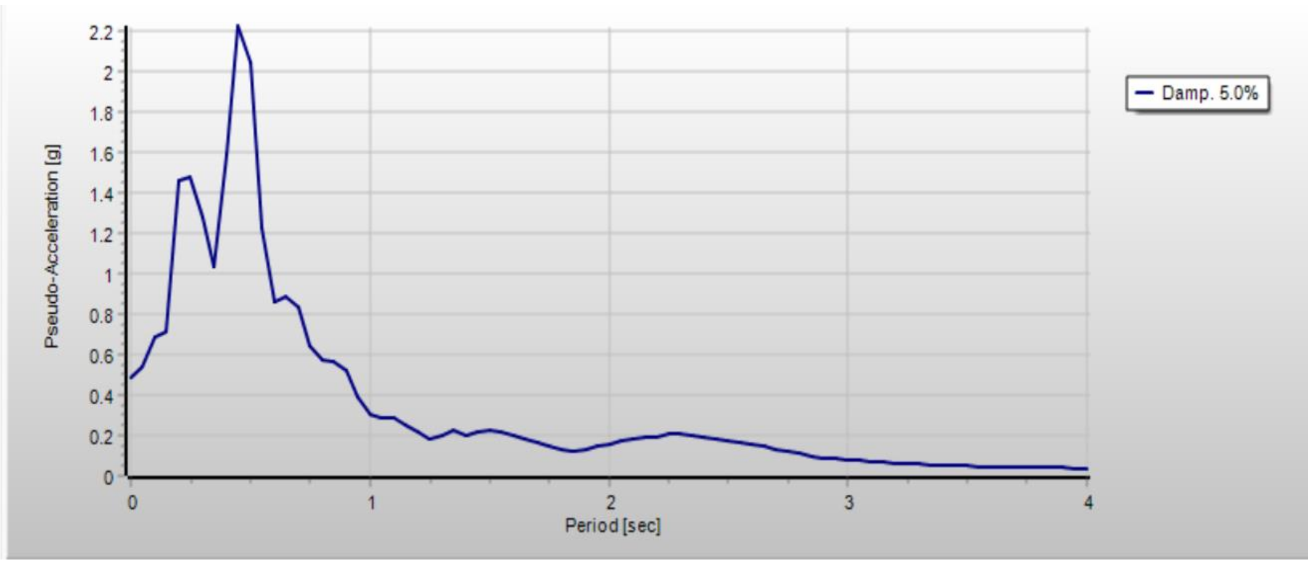

Figure 4.11: Nishi-Akashi 5% Pseudo-Acceleration Spectrum

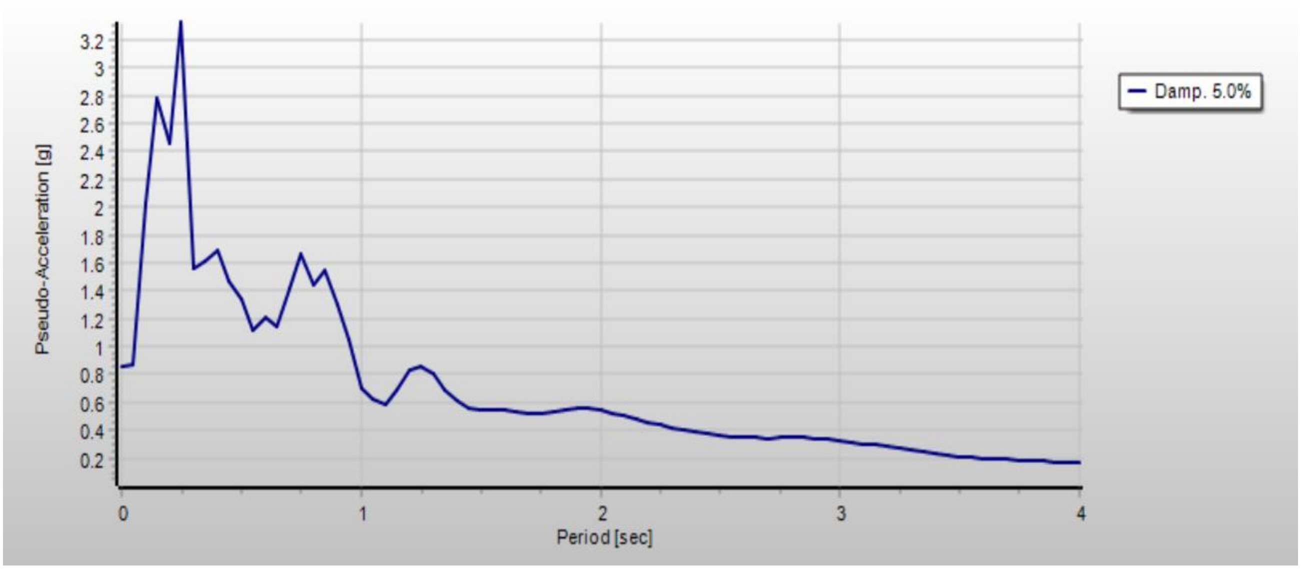

Figure 4.12: Tabas 5% Pseudo-Acceleration Spectrum

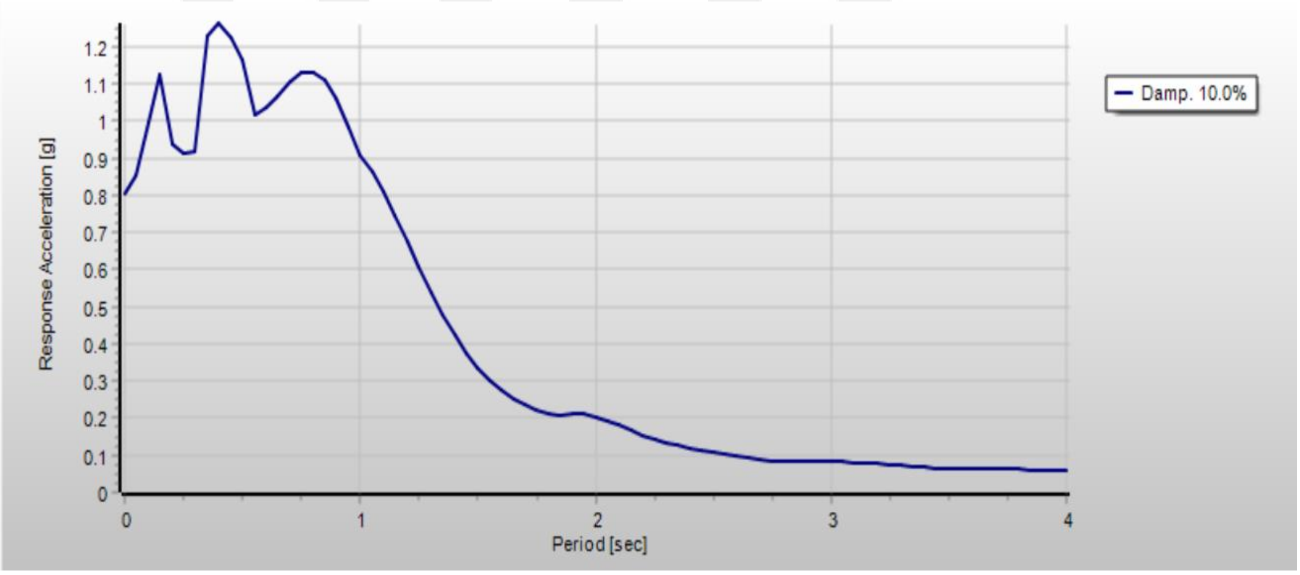

Figure 4.13: Bolu 10% Pseudo-Acceleration Spectrum

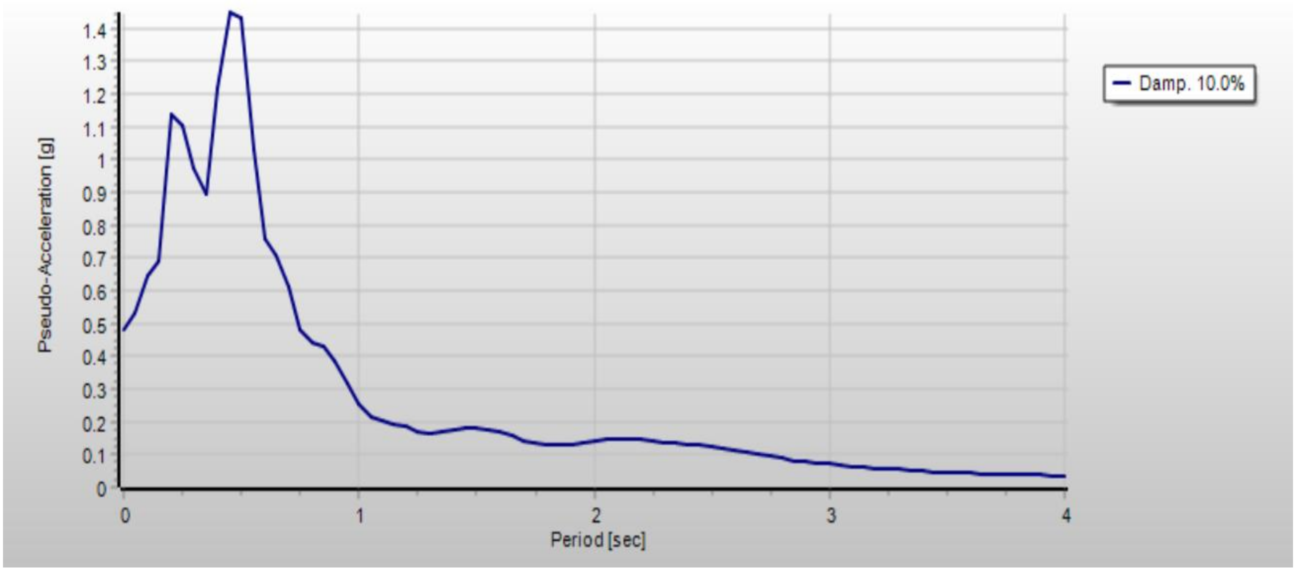

Figure 4.14: Nishi-Akashi 10% Pseudo-Acceleration Spectrum

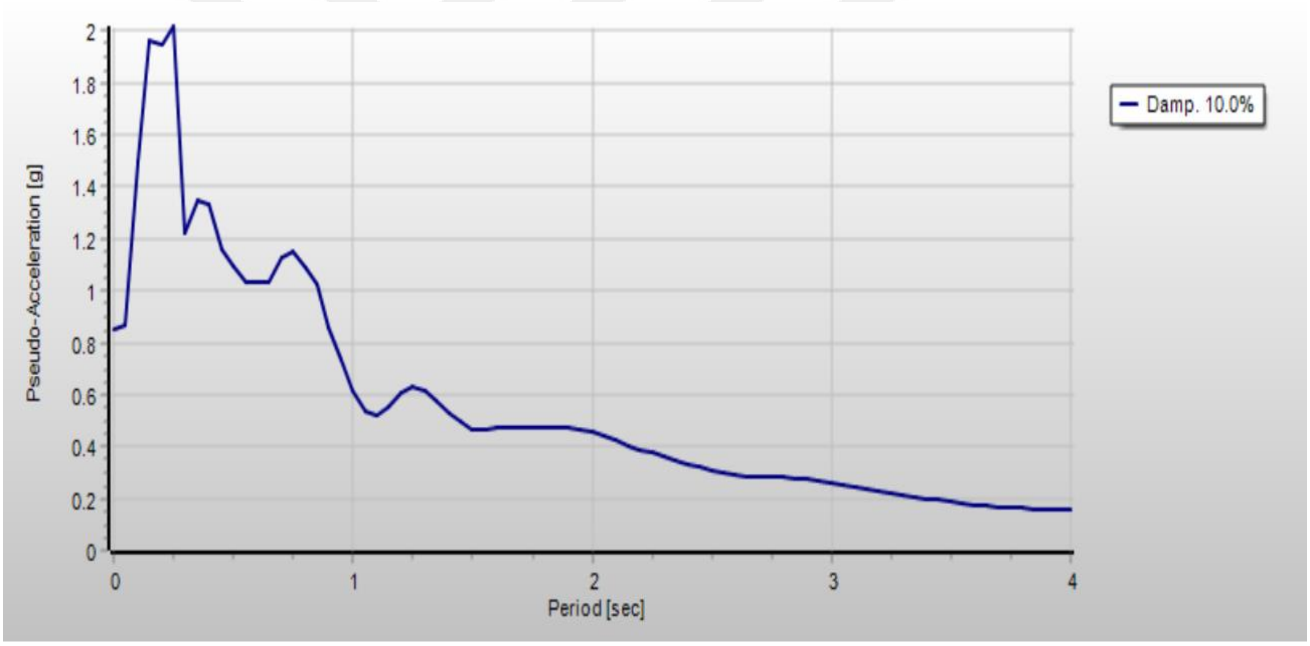

Figure 4.15: Tabas 10% Pseudo-Acceleration Spectrum

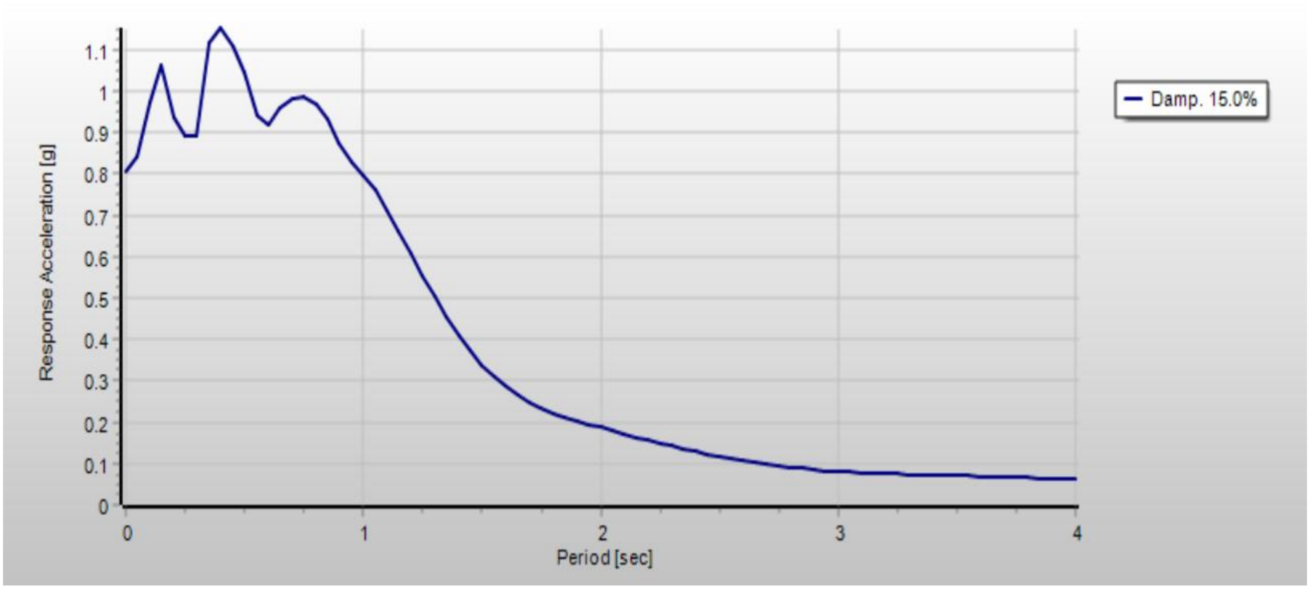

Figure 4.16: Bolu 15% Pseudo-Acceleration Spectrum

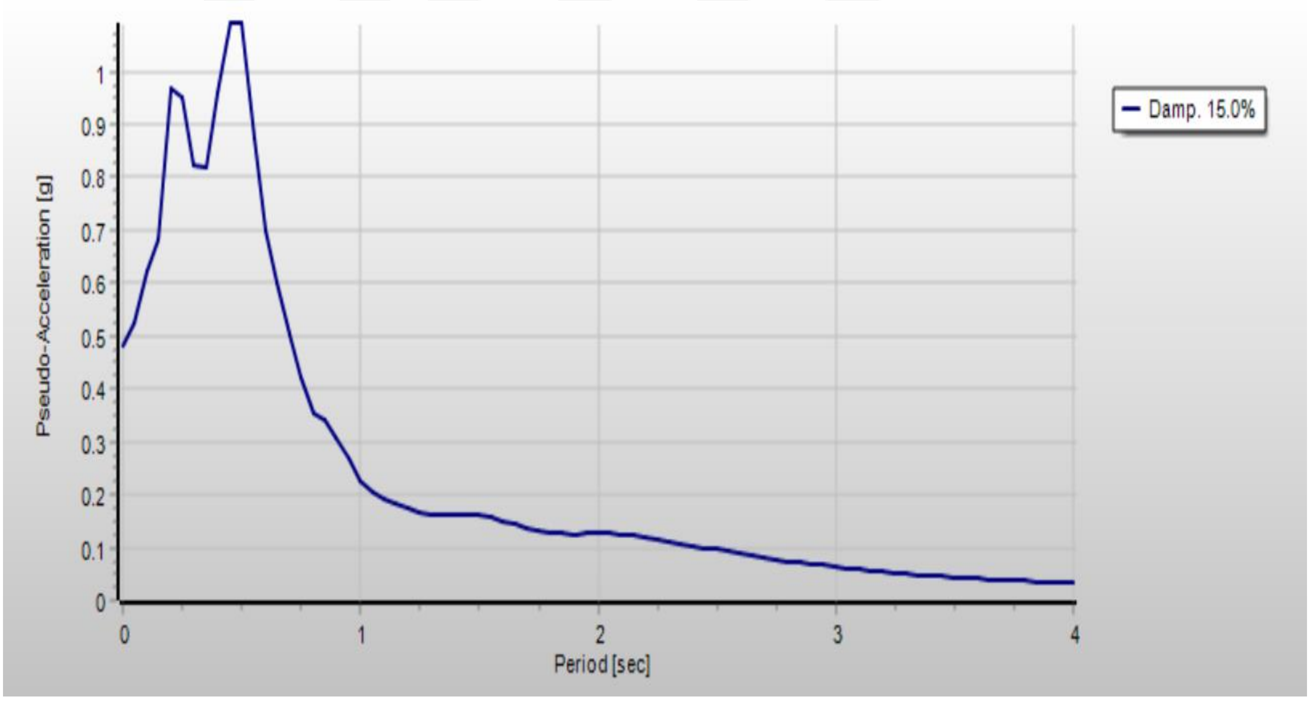

Figure 4.17: Nishi-Akashi 15% Pseudo-Acceleration Spectrum

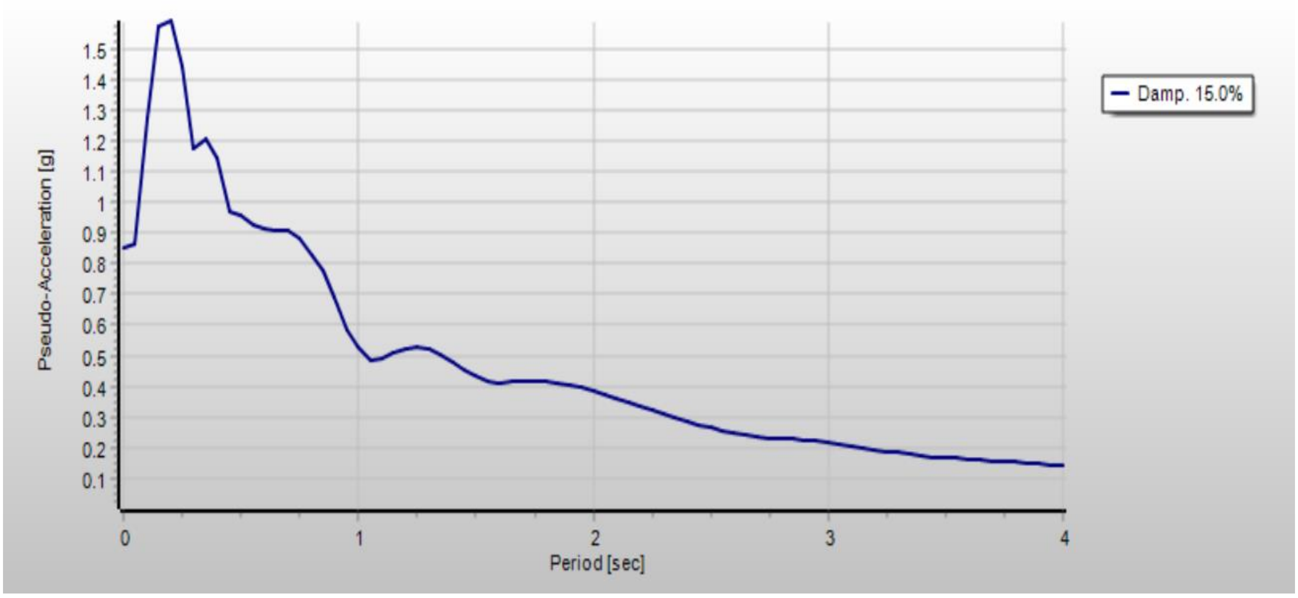

Figure 4.18: Tabas 15% Pseudo-Acceleration Spectrum

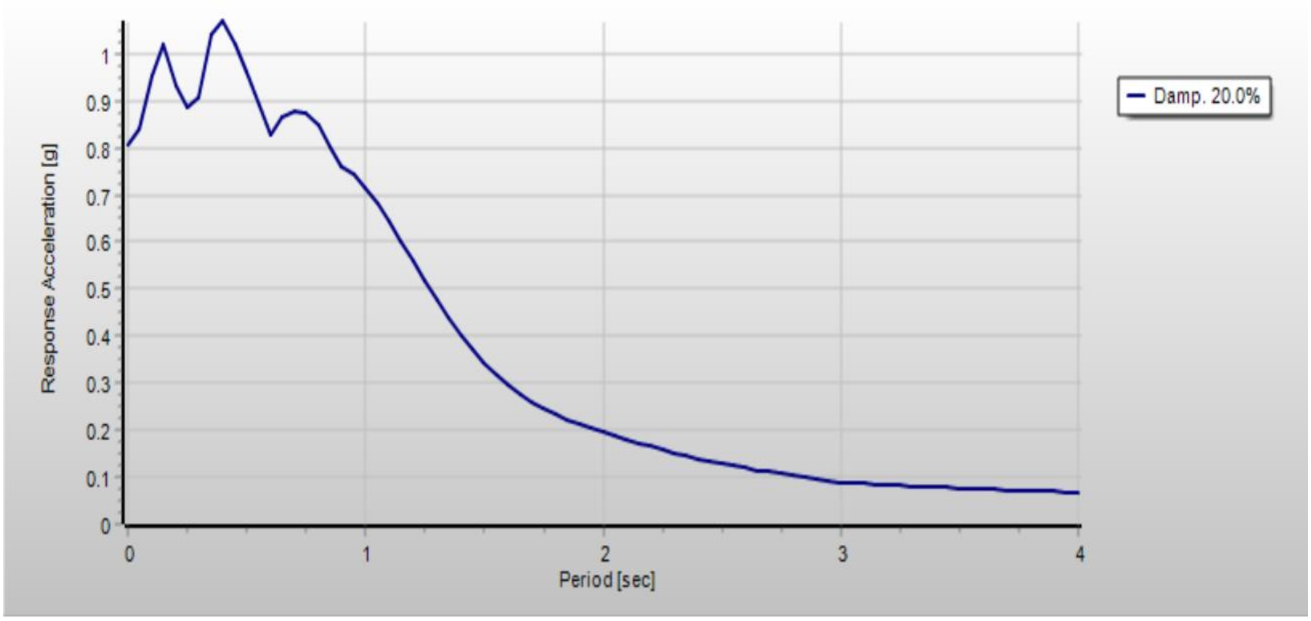

Figure 4.19: Bolu 20% Pseudo-Acceleration Spectrum

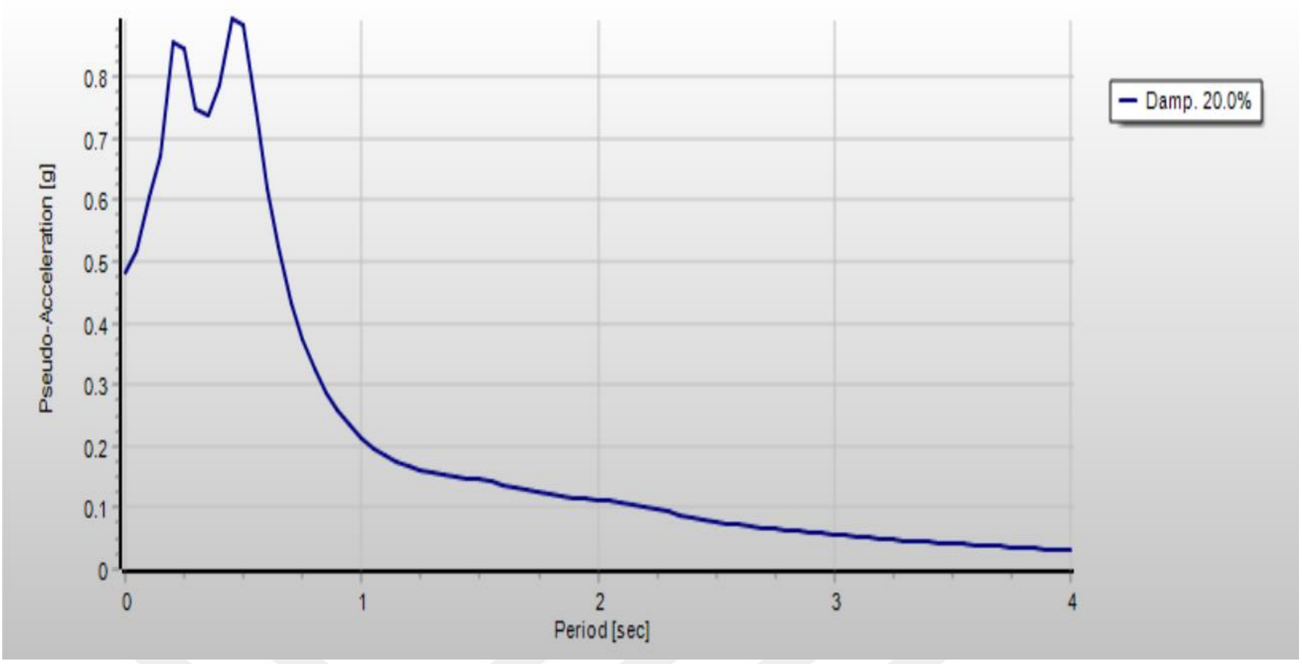

Figure 4.20: Nishi-Akashi 20% Pseudo-Acceleration Spectrum

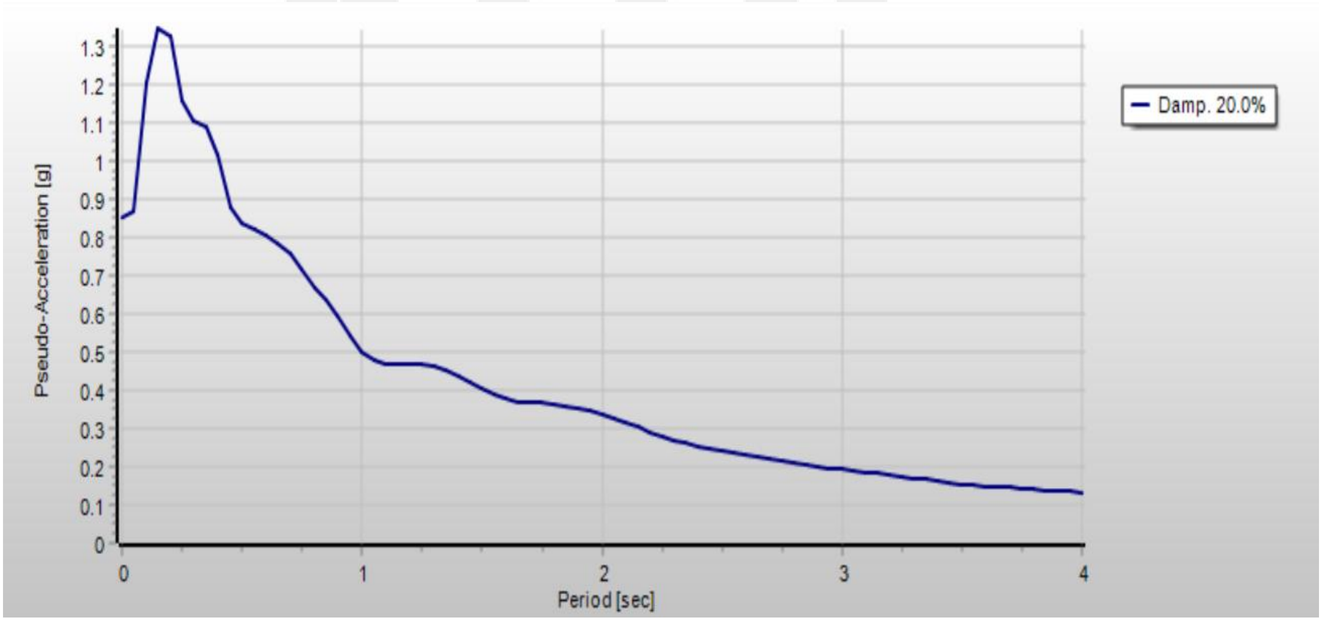

Figure 4.21: Tabas 20% Pseudo-Acceleration Spectrum

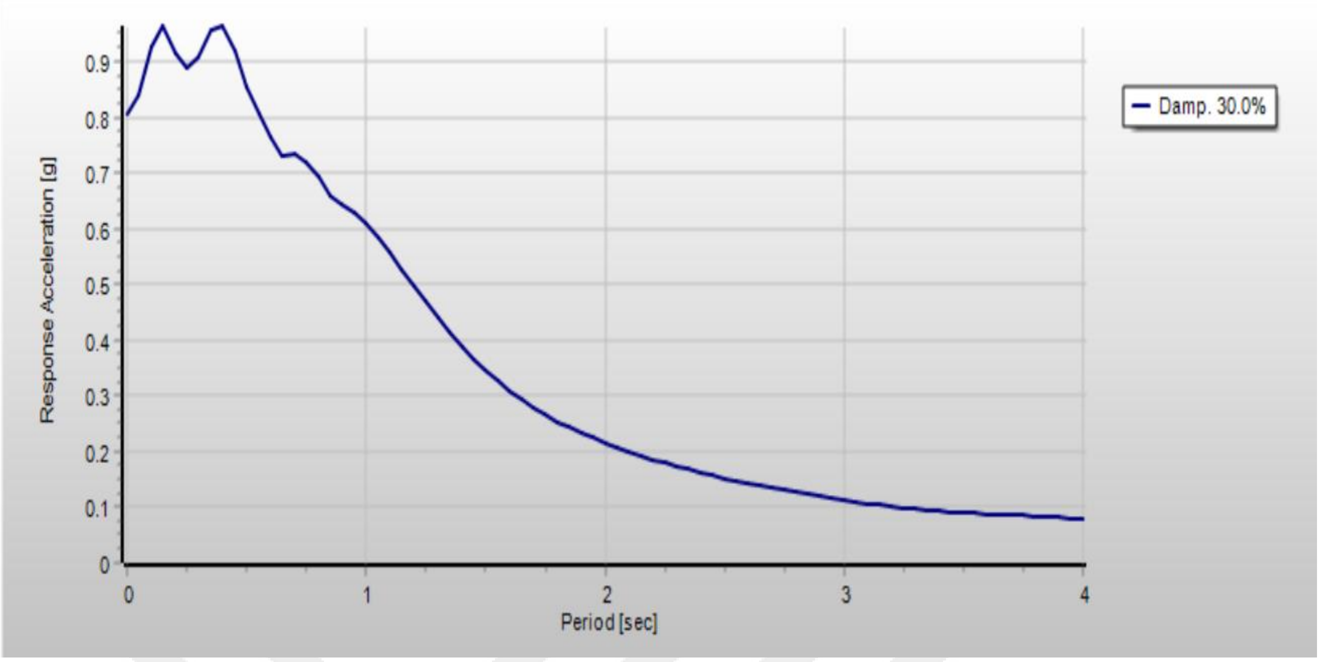

Figure 4.22: Bolu 30% Pseudo-Acceleration Spectrum

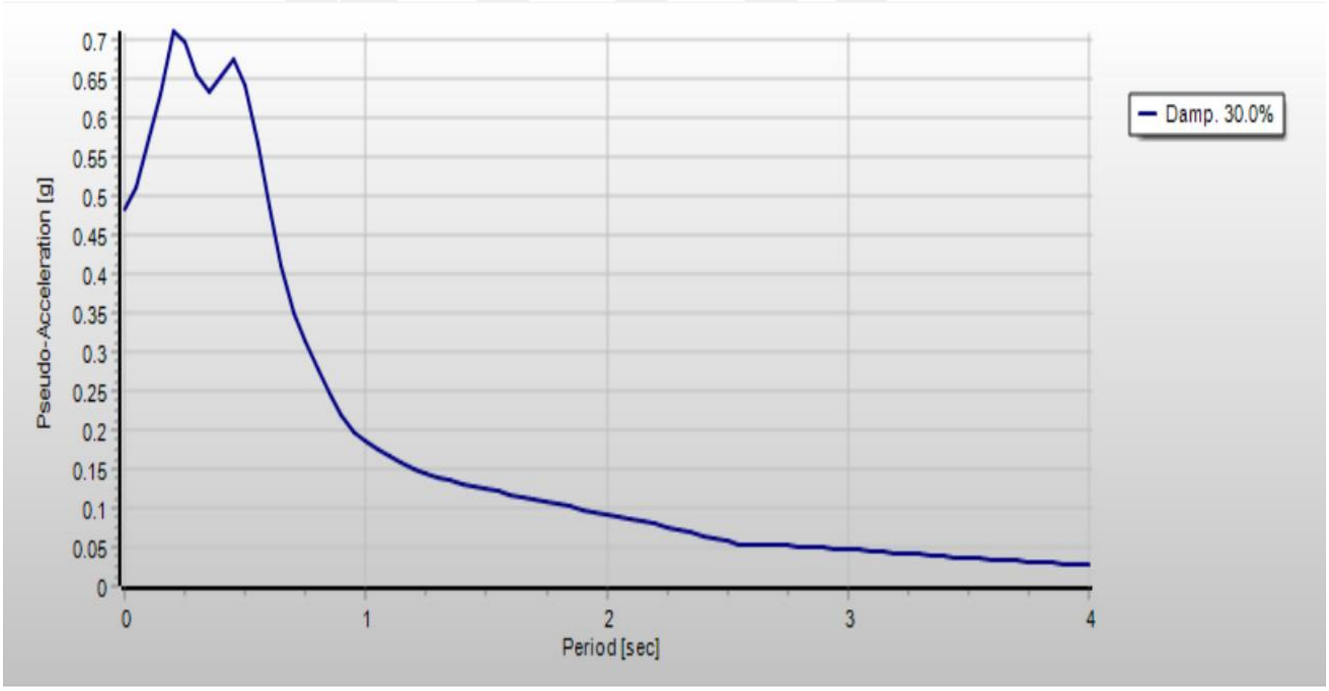

Figure 4.23: Nishi-Akashi 30% Pseudo-Acceleration Spectrum

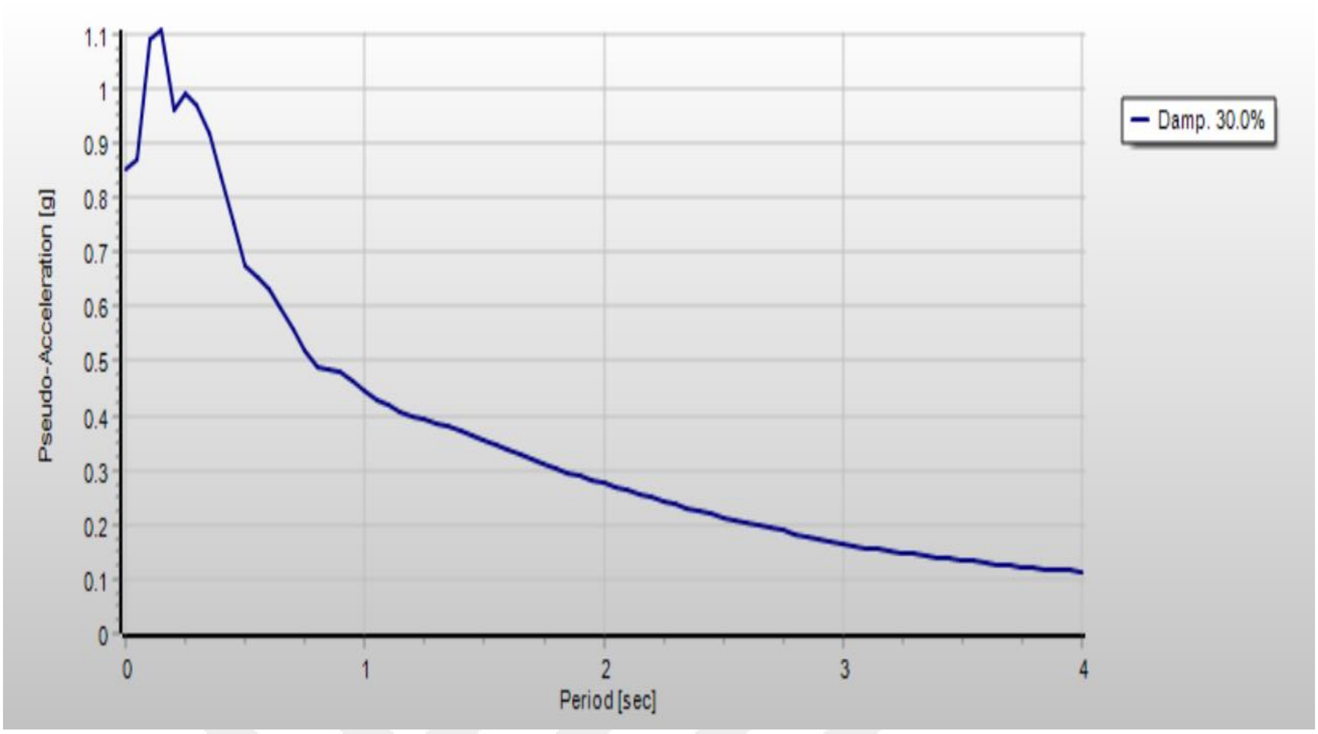

Figure 4.24: Tabas 30% Pseudo-Acceleration Spectrum

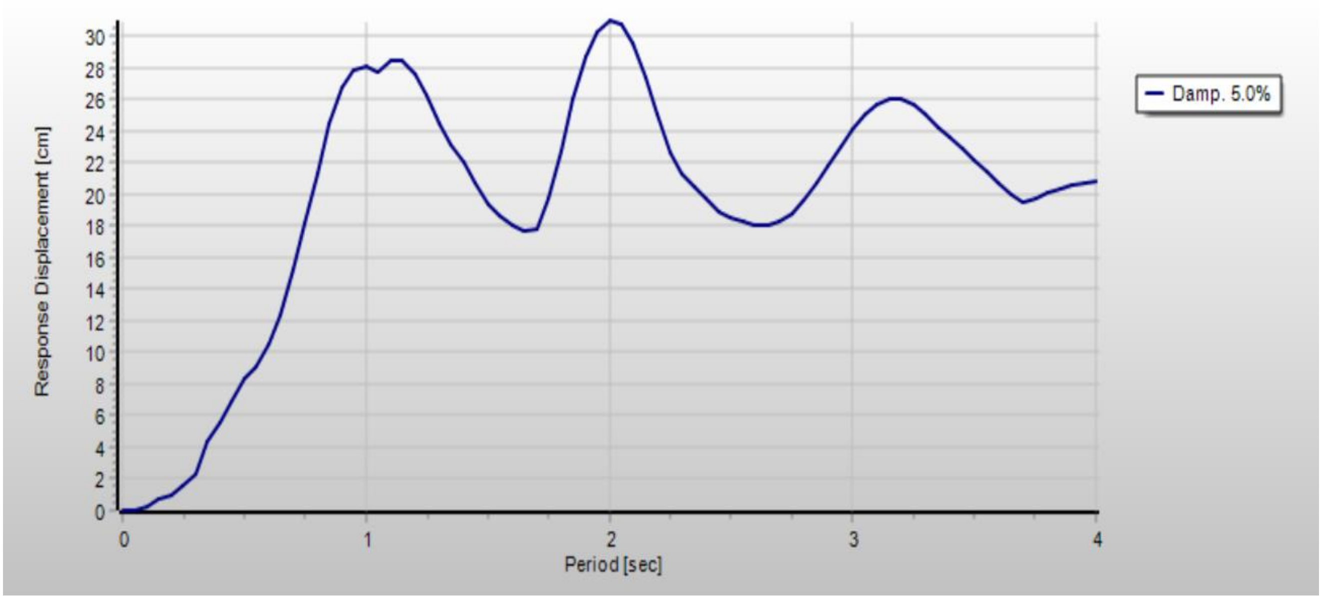

Figure 4.25: Bolu 5% Displacement Spectrum

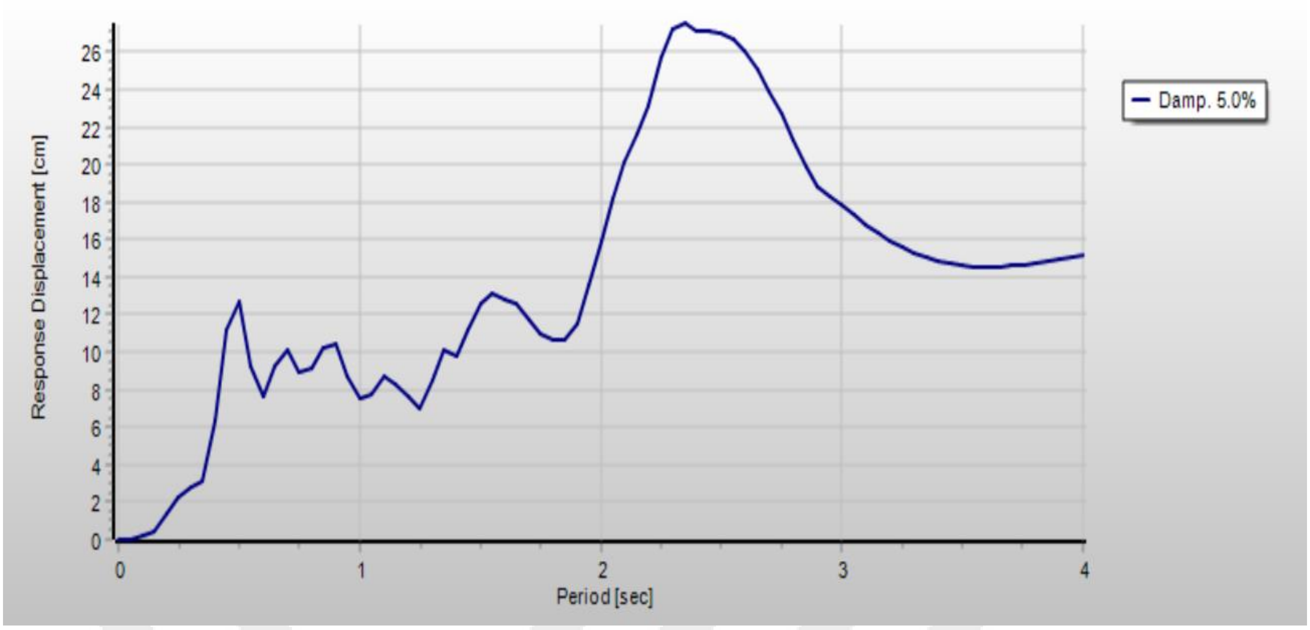

Figure 4.26: Nishi-Akashi 5% Displacement Spectrum

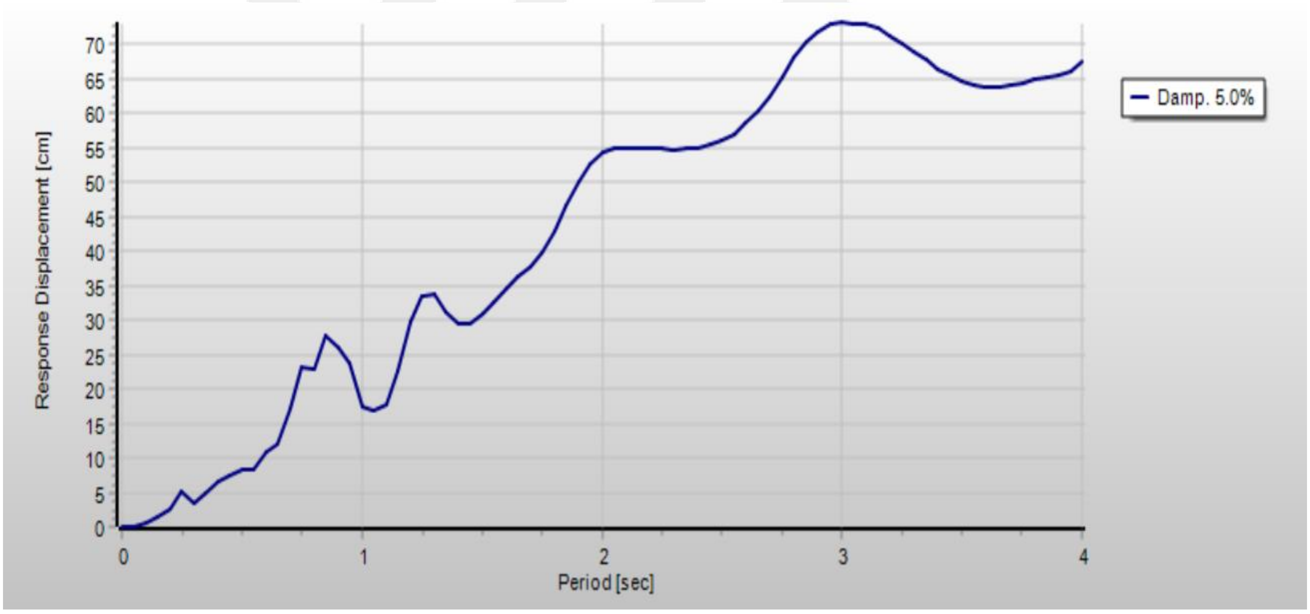

Figure 4.27: Tabas 5% Displacement Spectrum

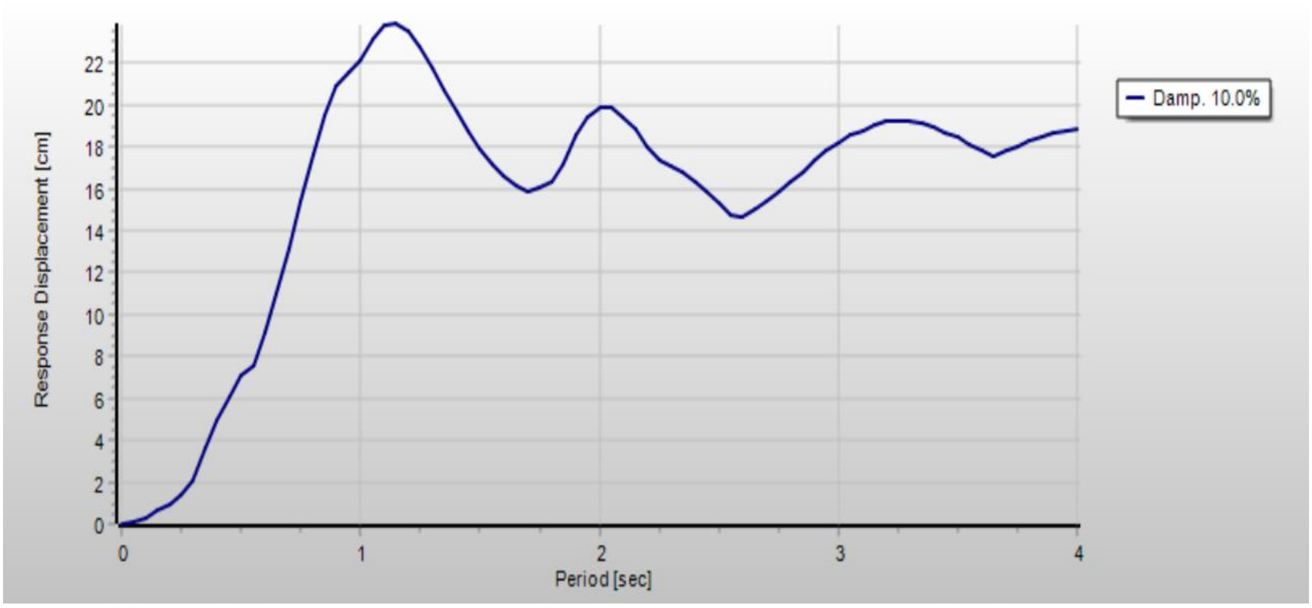

Figure 4.28: Bolu 10% Displacement Spectrum

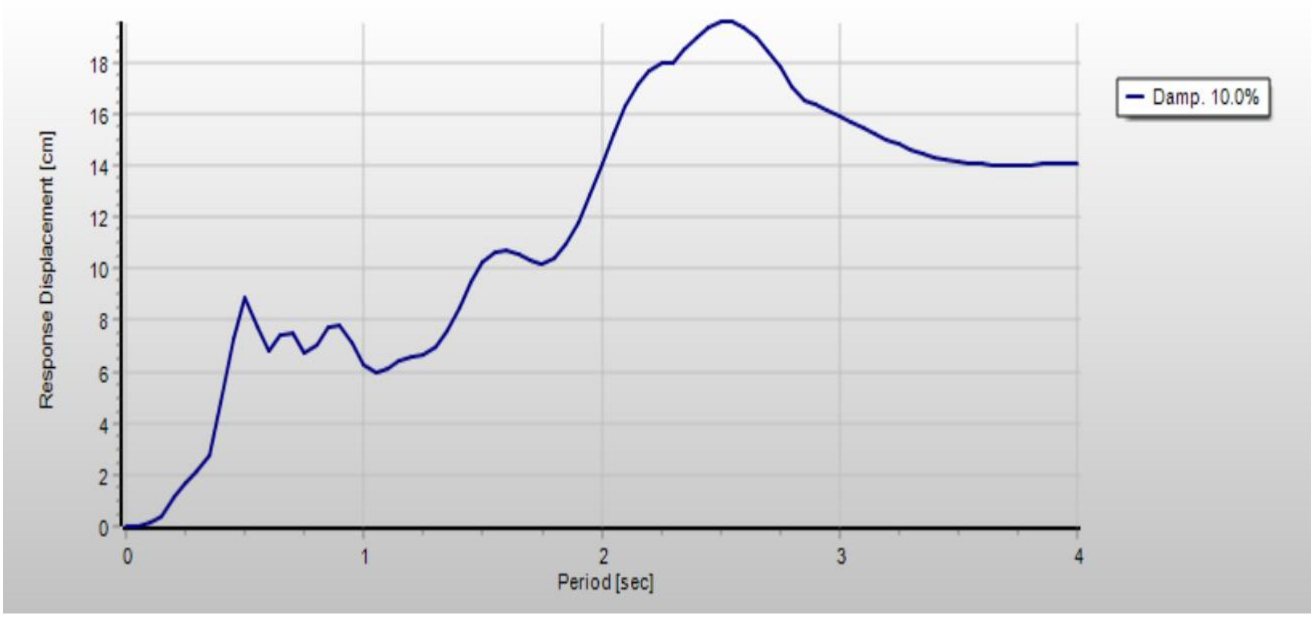

Figure 4.29: Nishi-Akashi 10% Displacement Spectrum

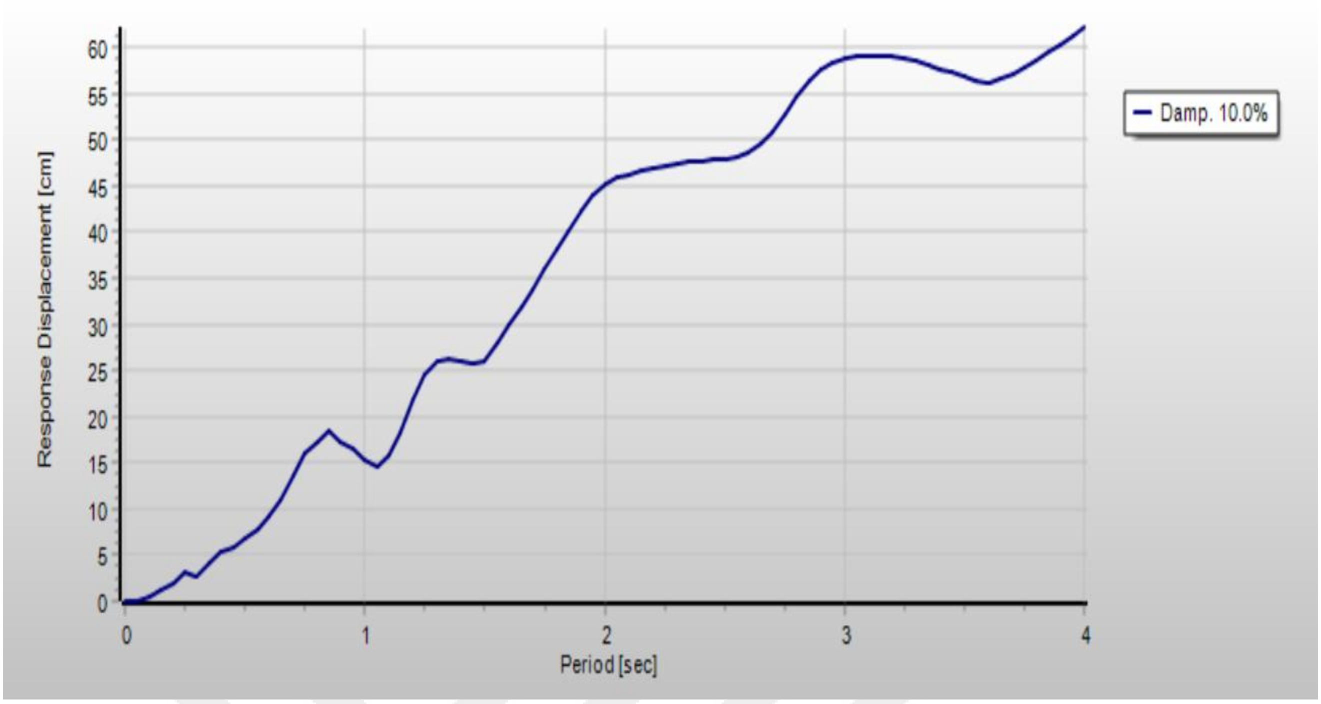

Figure 4.30: Tabas 10% Displacement Spectrum

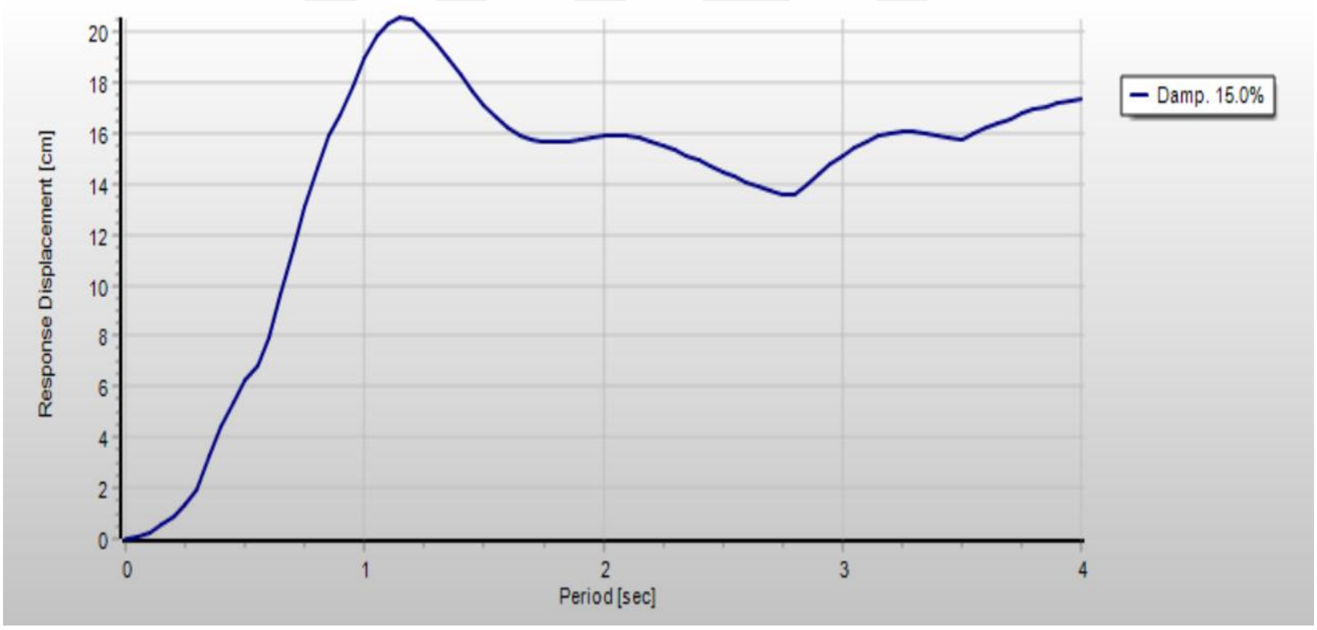

Figure 4.31: Bolu 15% Displacement Spectrum

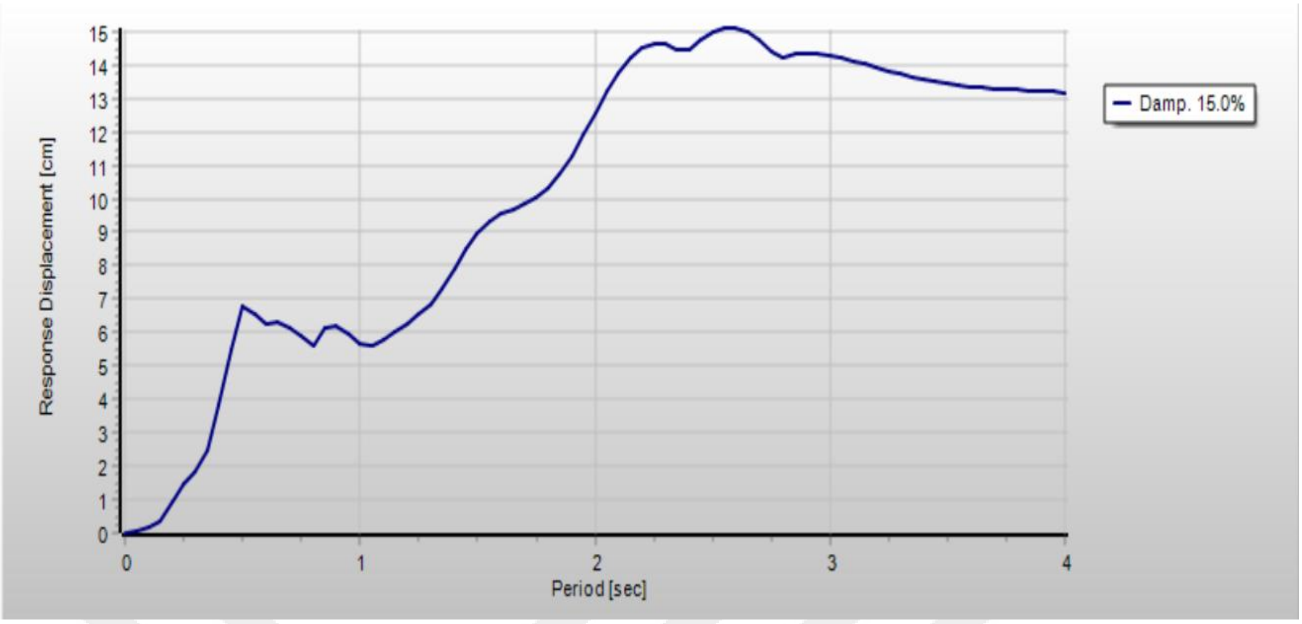

Figure 4.32: Nishi-Akashi 15% Displacement Spectrum

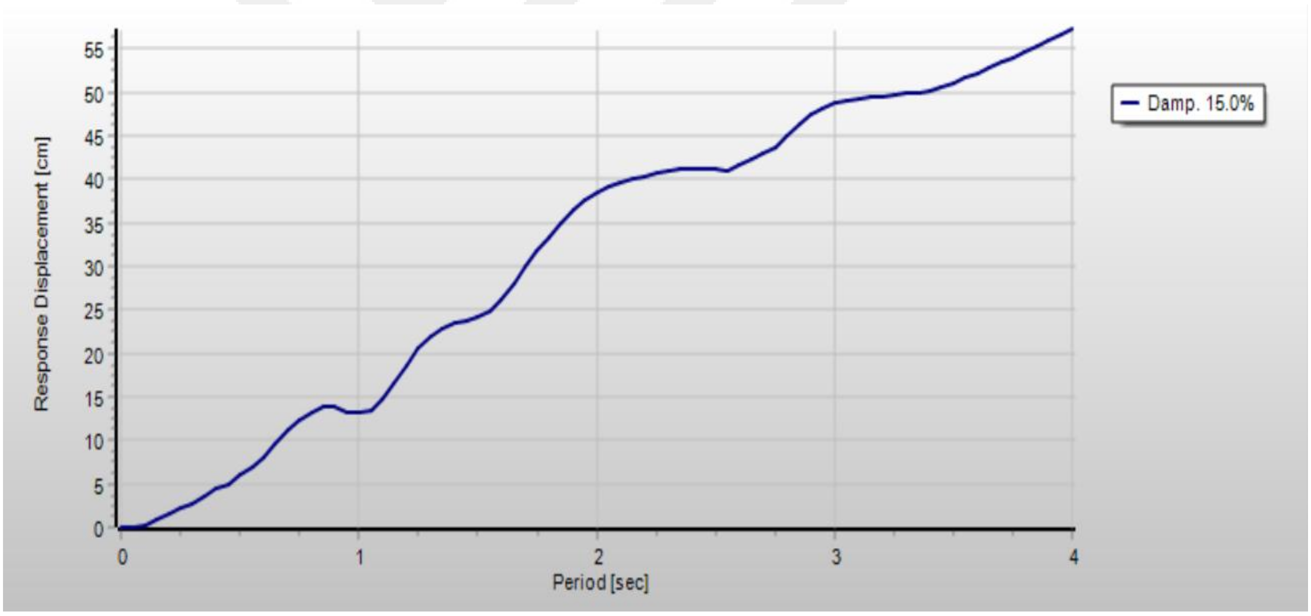

Figure 4.33: Tabas 15% Displacement Spectrum

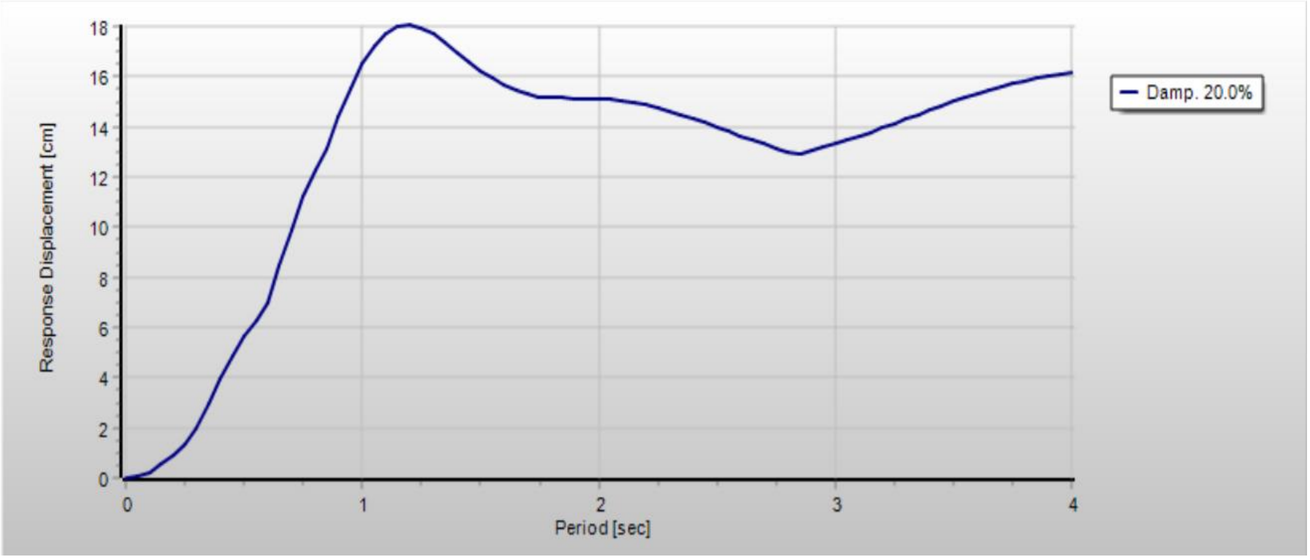

Figure 4.34: Bolu 20% Displacement Spectrum

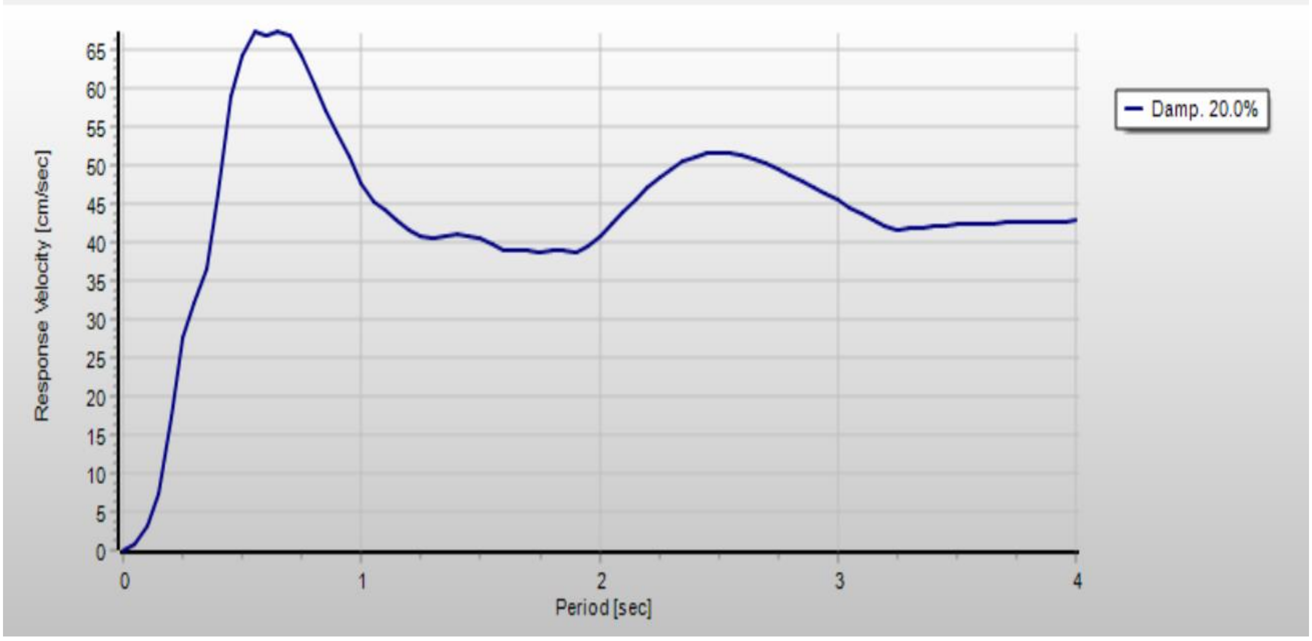

Figure 4.35: Nishi-Akashi 20% Displacement Spectrum

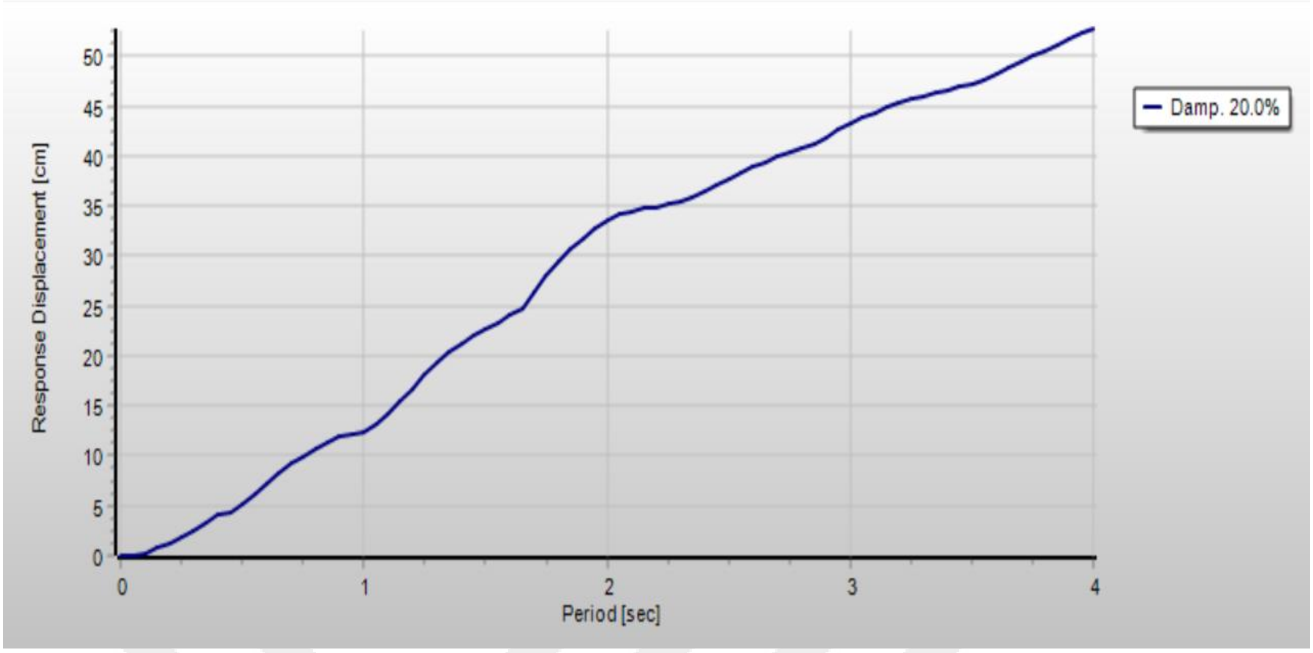

Figure 4.36: Tabas 20% Displacement Spectrum

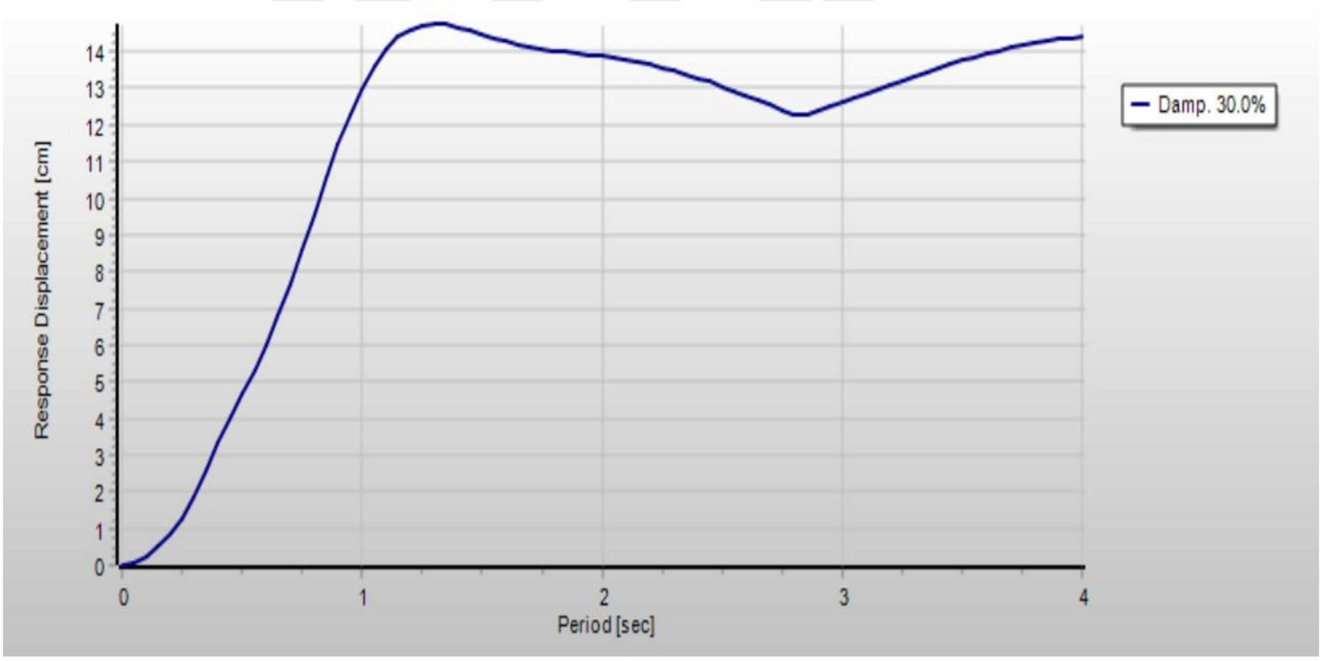

Figure 4.37: Bolu 30% Displacement Spectrum

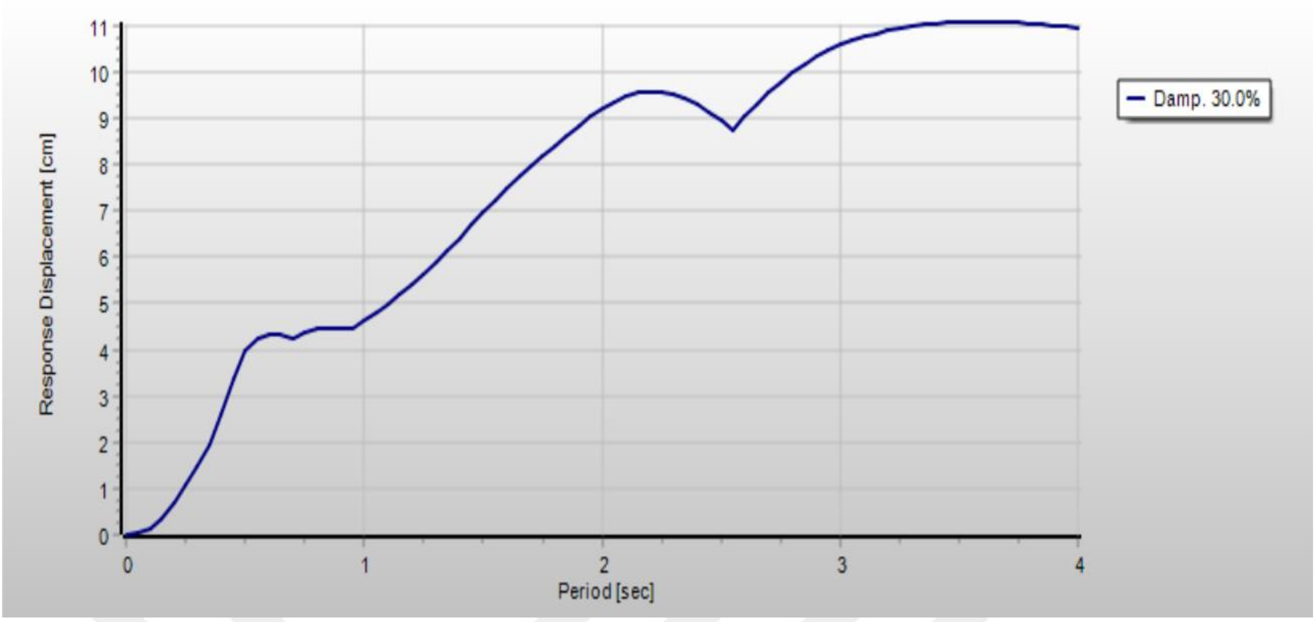

Figure 4.38: Nishi-Akashi 30% Displacement Spectrum

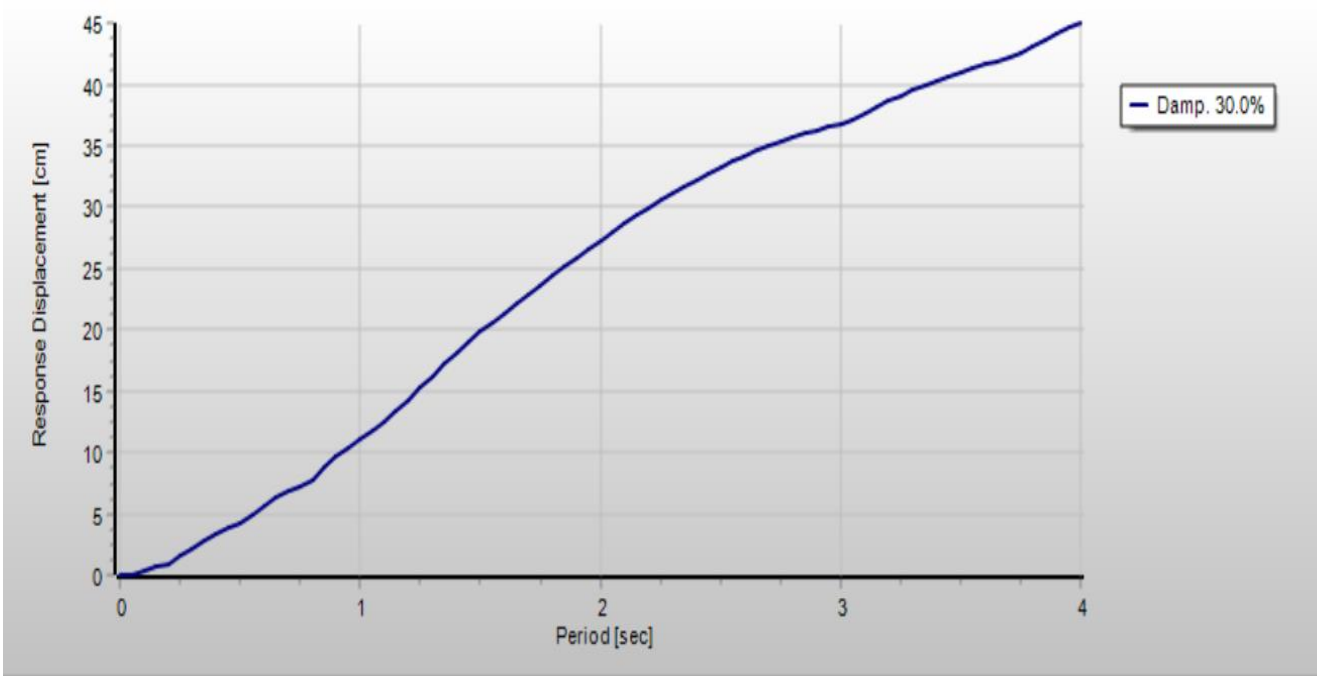

Figure 4.39: Tabas 30% Displacement Spectrum

4.2 Seismic Response of Bridge Structure (Fixed and Isolated model)

4.2.1 Maximum Nodal Displacement

Displacement values of the nodes located on the top of the bridge's ben-cap (5 and 6) for the two cases (fixed and isolated) of structure models were analyzed under three types of ground motions and illustrated in Figures 4.40 to 4.45. The analyzed outcomes show a notable decrease in the values of displacement for the TFP isolated condition at all the applied events; as the values of maximum displacement for both nodes (5 and 6) were decreased by 51% for the Bolu earthquake, 58% for Nishi-Akashi earthquake and by 73% for Tabas earthquake, which validates the efficiency of seismic isolation systems in reducing the displacement of the construction during the seismic events.

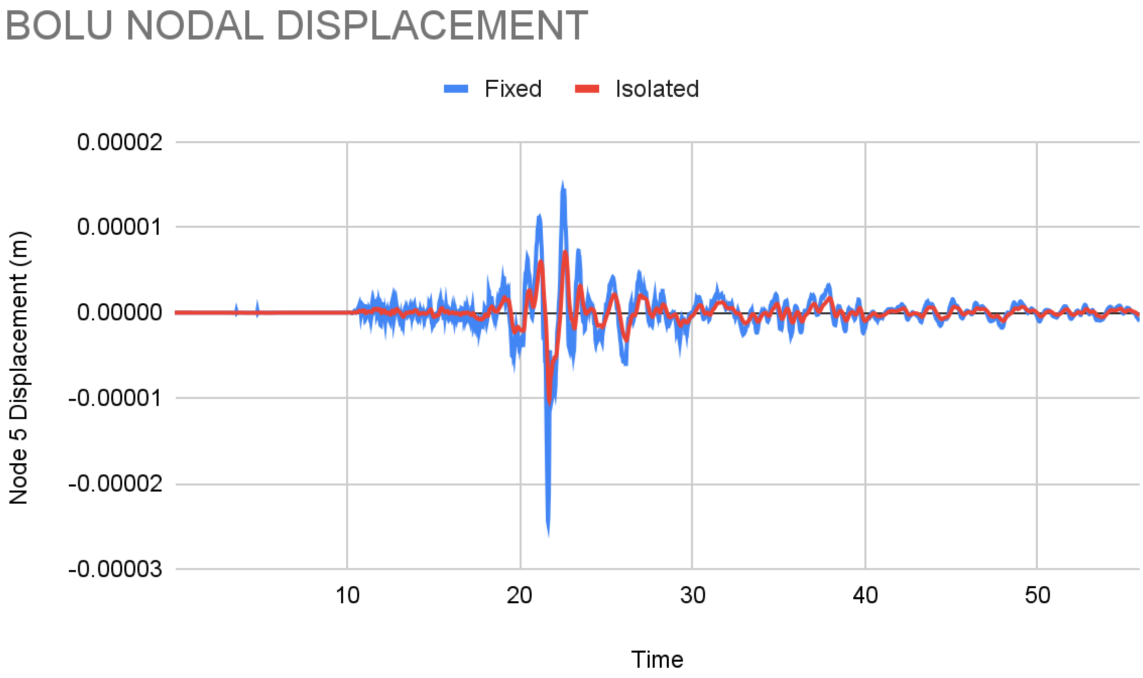

Figure 4.40: Node 5 Maximum Displacement Bolu – X direction

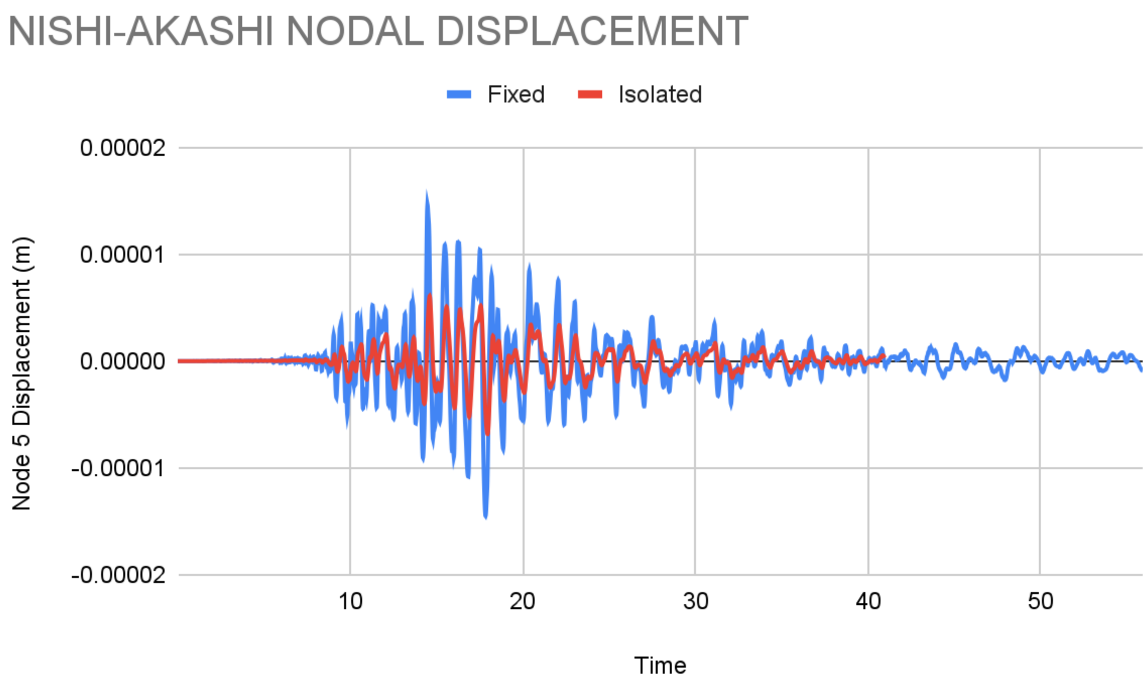

Figure 4.41: Node 5 Maximum Displacement Nishi-Akashi – X direction

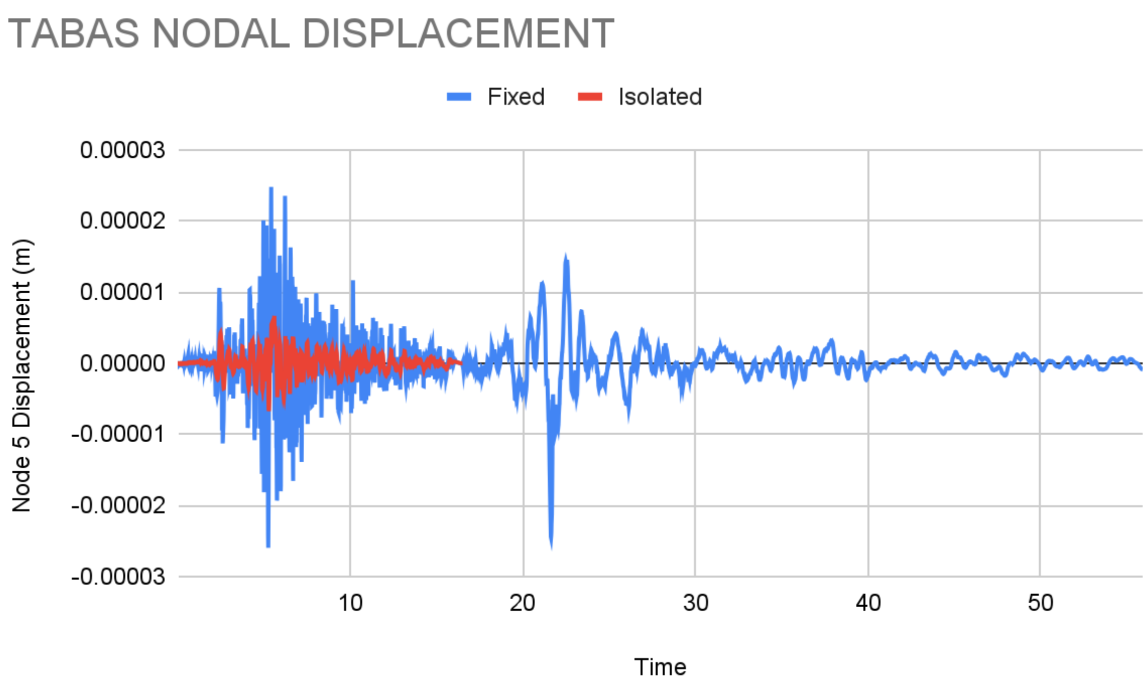

Figure 4.42: Node 5 Maximum Displacement Tabas – X direction

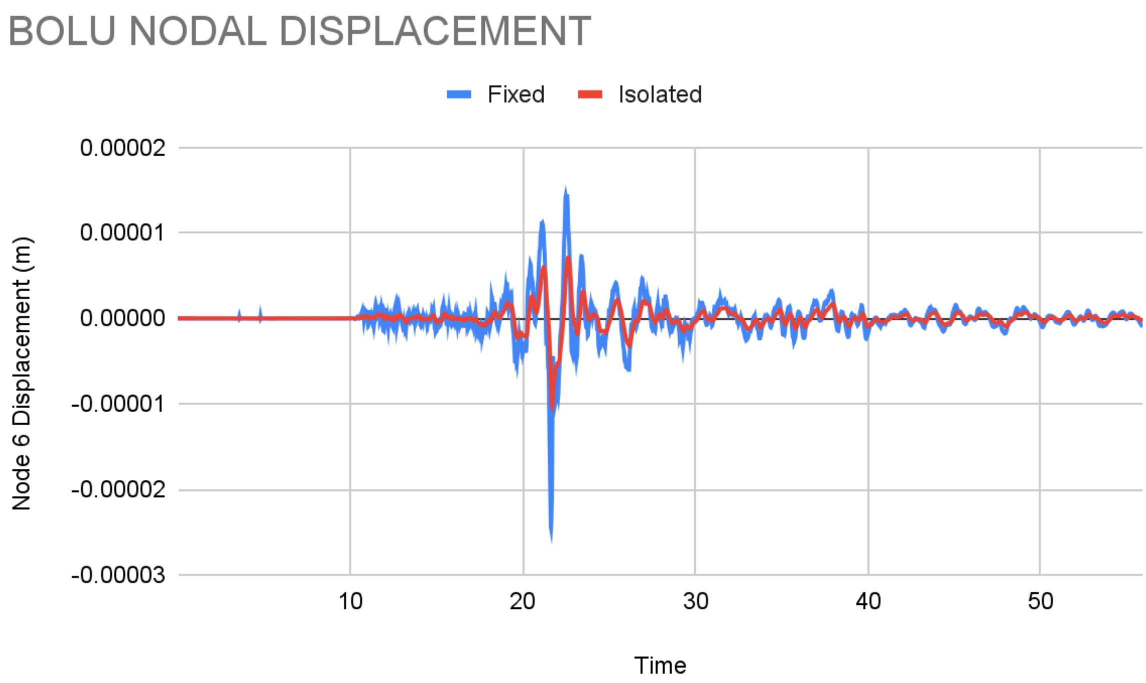

Figure 4.43: Node 6 Maximum Displacement Bolu – X direction

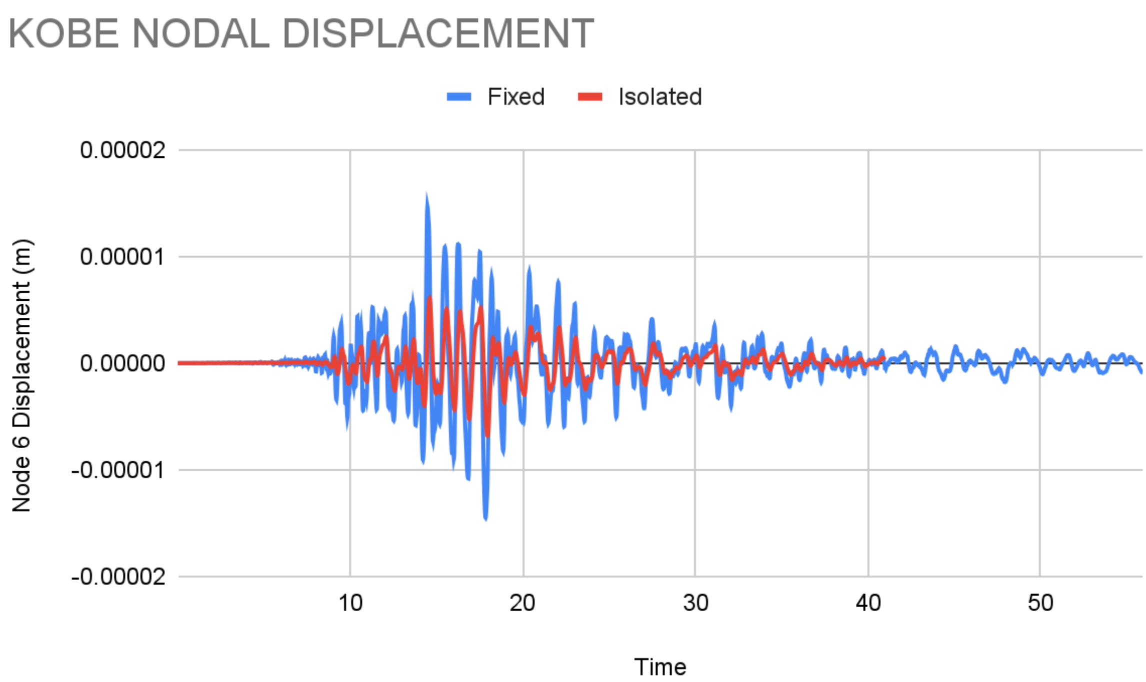

Figure 4.44: Node 6 Maximum Displacement Nishi Akashi – X direction

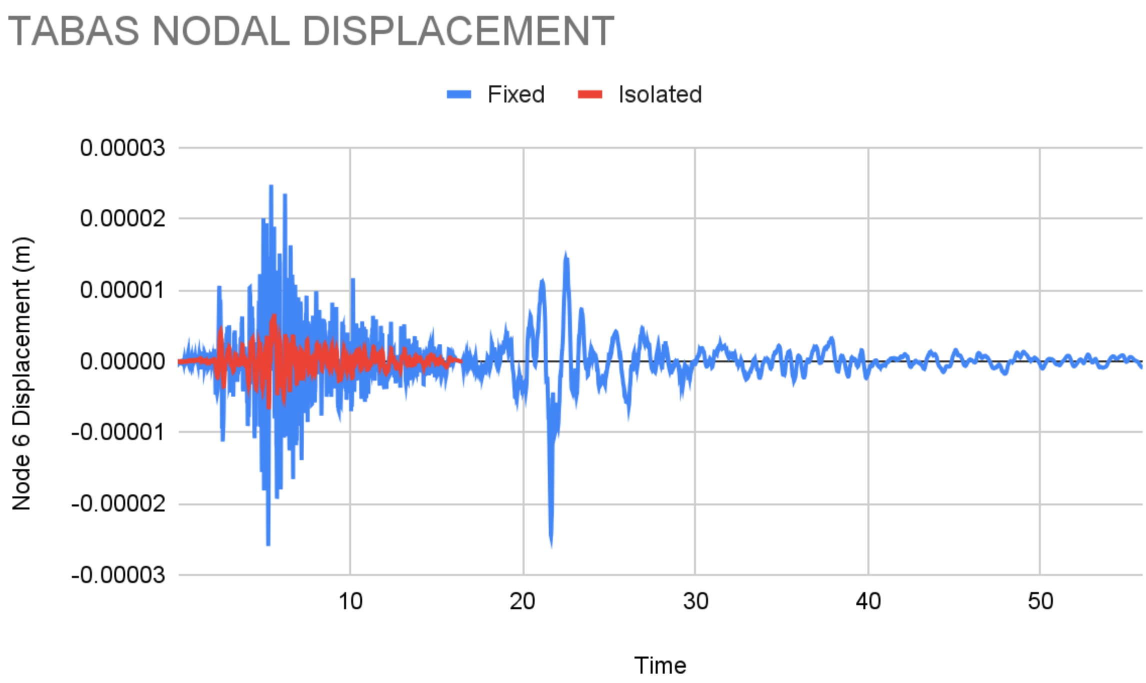

Figure 4.45: Node 6 Maximum Displacement Tabas – X direction

4.2.2 Base Shear Reaction

The base shear reaction is an estimation that refers to the maximum expected lateral force affecting a structure's base due to seismic events. The base shear reaction values of the nodes located at the bottom of the bridge's columns (1 and 2) for the two cases (fixed and isolated) of structure models were analyzed under three types of ground motions and illustrated in Figures 4.46 to 4.51. The analyzed outcomes show a notable decrease in the values of base shear reaction for the TFP isolated condition at all the applied events; as the values of maximum base shear reaction for both nodes (1 and 2) were decreased by 67% for the Bolu earthquake, 62% for Nishi-Akashi earthquake and by 79% for Tabas earthquake, which also proves the efficiency of seismic isolation systems in reducing base shear reactions of the constructions during the seismic events.

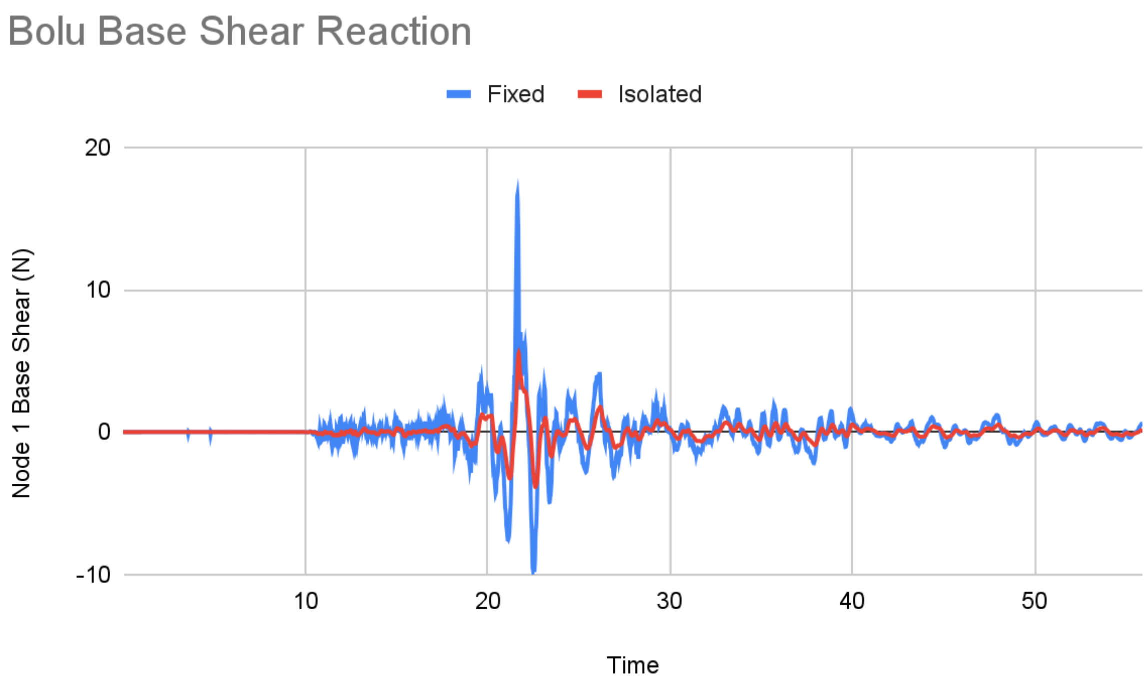

Figure 4.46: Node 1 Base Shear Reaction Bolu – X direction

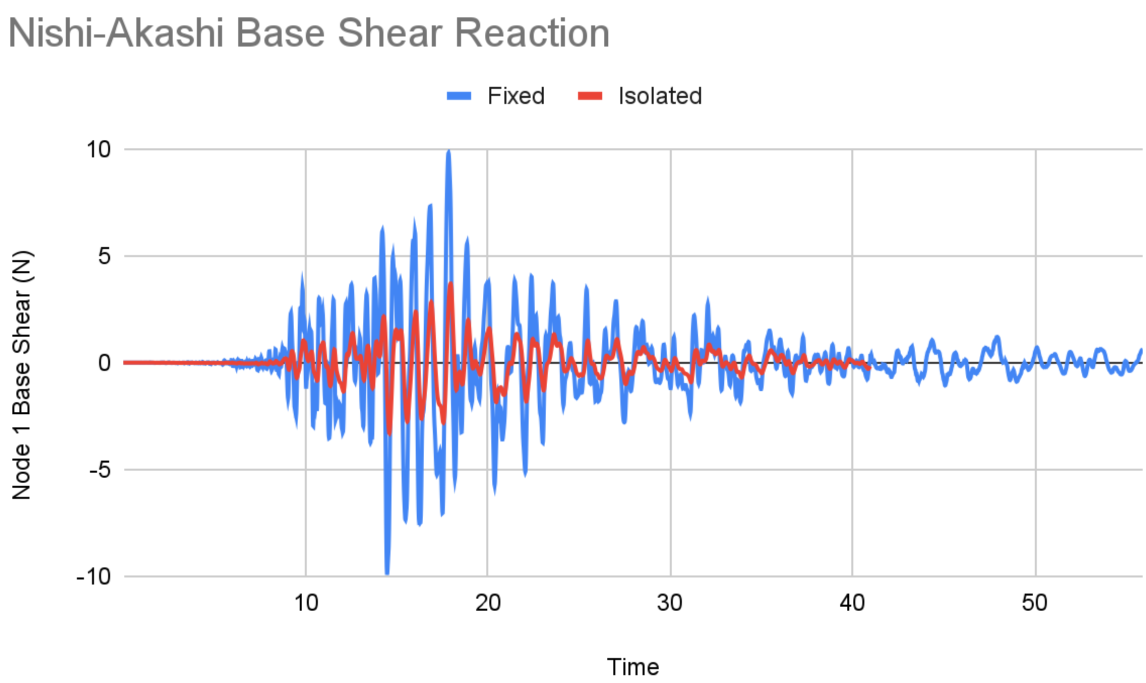

Figure 4.47: Node 1 Base Shear Reaction Nishi-Akashi – X direction

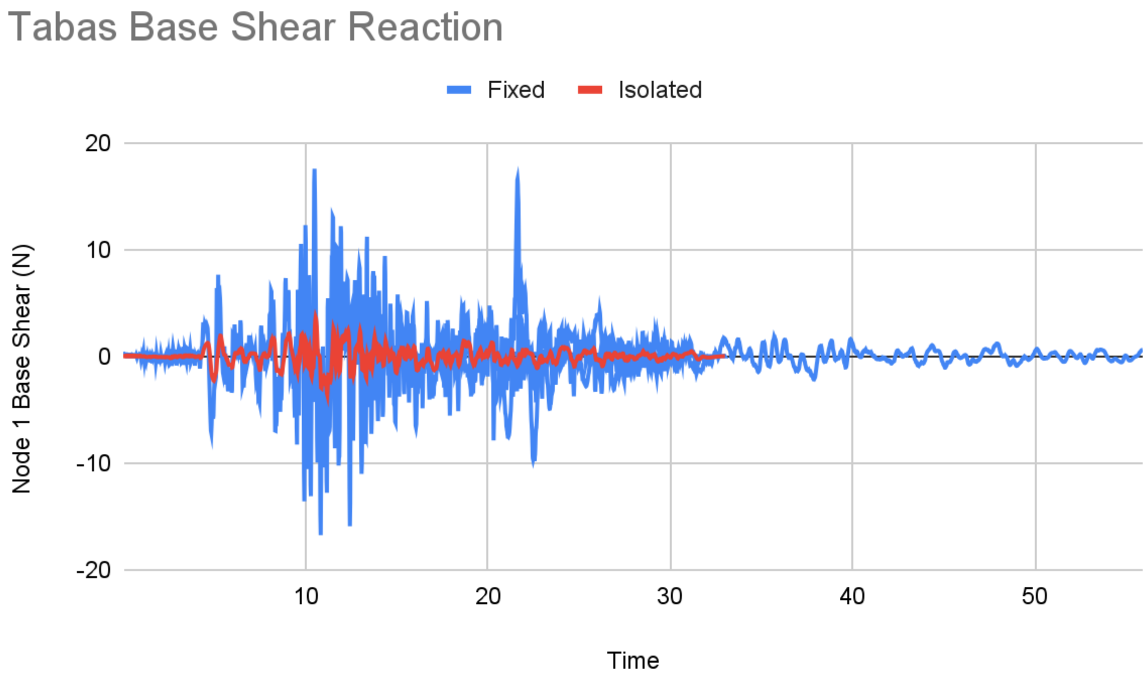

Figure 4.48: Node 1 Base Shear Reaction Tabas – X direction

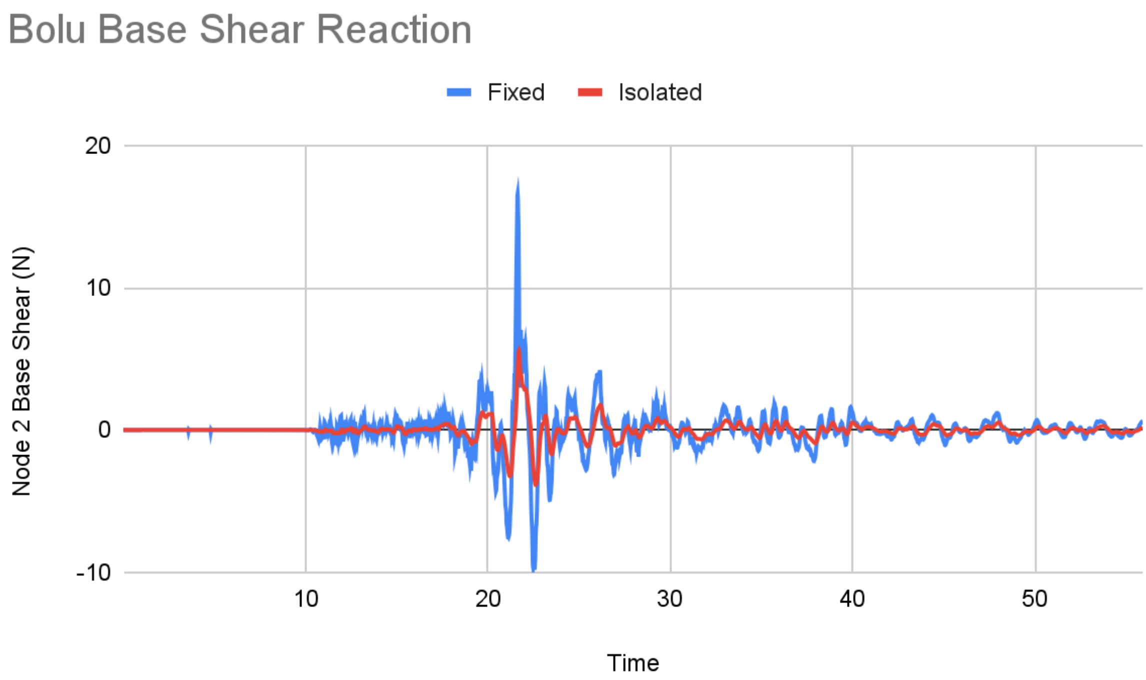

Figure 4.49: Node 2 Base Shear Reaction Bolu - X direction

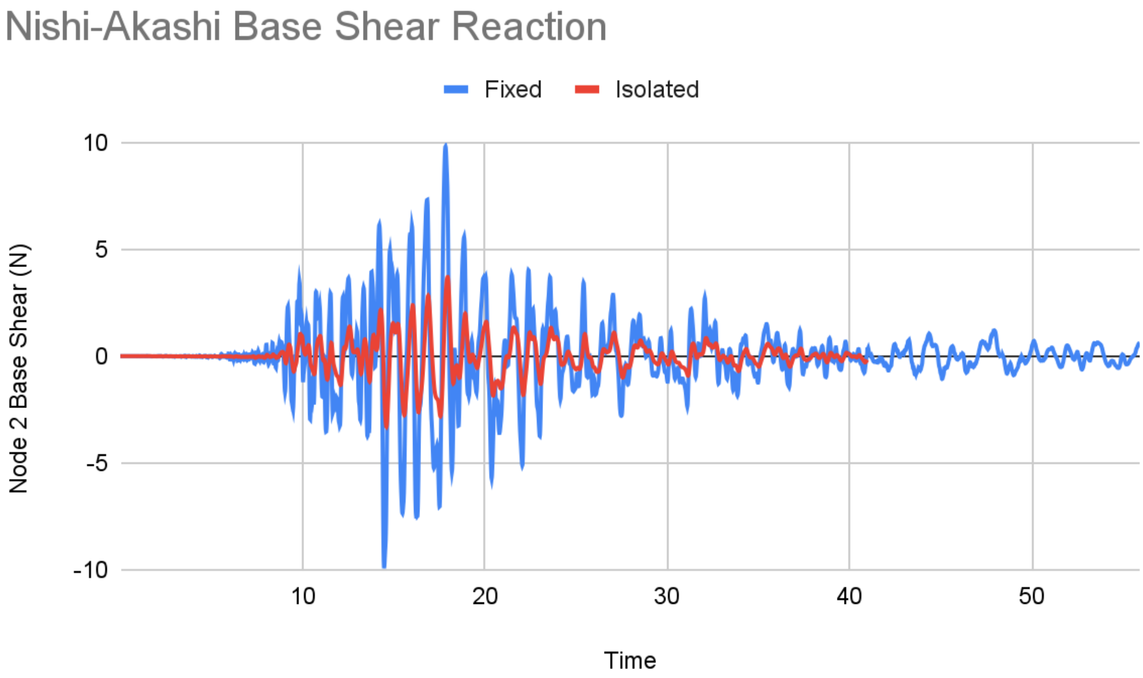

Figure 4.50: Node 2 Base Shear Reaction Nishi-Akashi – X direction

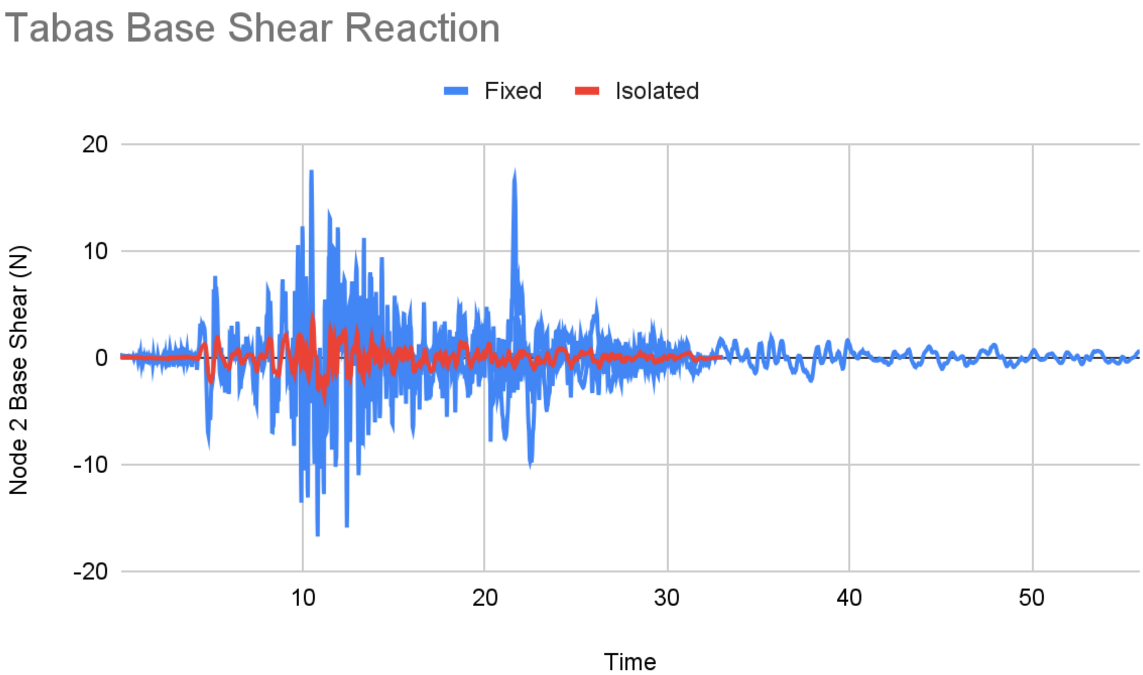

Figure 4.51: Node 2 Base Shear Reaction Tabas – X direction

4.2.3 Nodal Displacement & Base Shear Reaction Comparison

Absolute maximum and minimum values of nodal displacement and base shear reaction were defined and presented in Figures 4.52 and 4.53 comparatively for both conditions of bridge structure models (Fixed and Isolated) for the three applied types of ground motions (Bolu, Nishi-Akashi, and Tabas earthquakes) in the horizontal X direction. The Figures show the notable decrease in values for the TFP isolated condition at all the seismic events. Table 4.2 shows the decrease in maximum and minimum values of nodal displacement and base shear reaction as a percentage after the use of triple friction isolator for the bridge's structure.

Table 4.2: Reduction in Maximum and Minimum Values after the use of TFP for the bridge's structure.

Seismic Response	Nodal Displacement		Base Shear Reaction	
	Max	Min	Max	Min
Bolu, Duzce earthquake	51%	58%	67%	61%
Nishi-Akashi, Kobe earthquake	58%	53%	62%	67%
Tabas, Iran earthquake	73%	74%	79%	79%

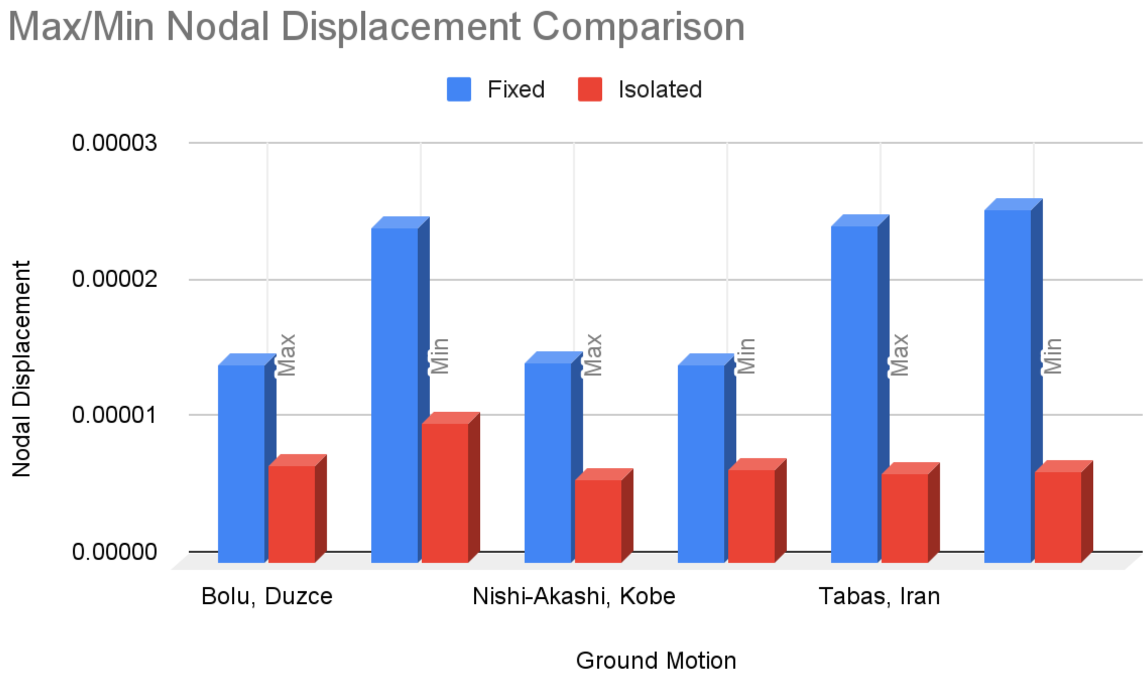

Figure 4.52: Absolute Maximum/Minimum Nodal Displacement Values – X direction

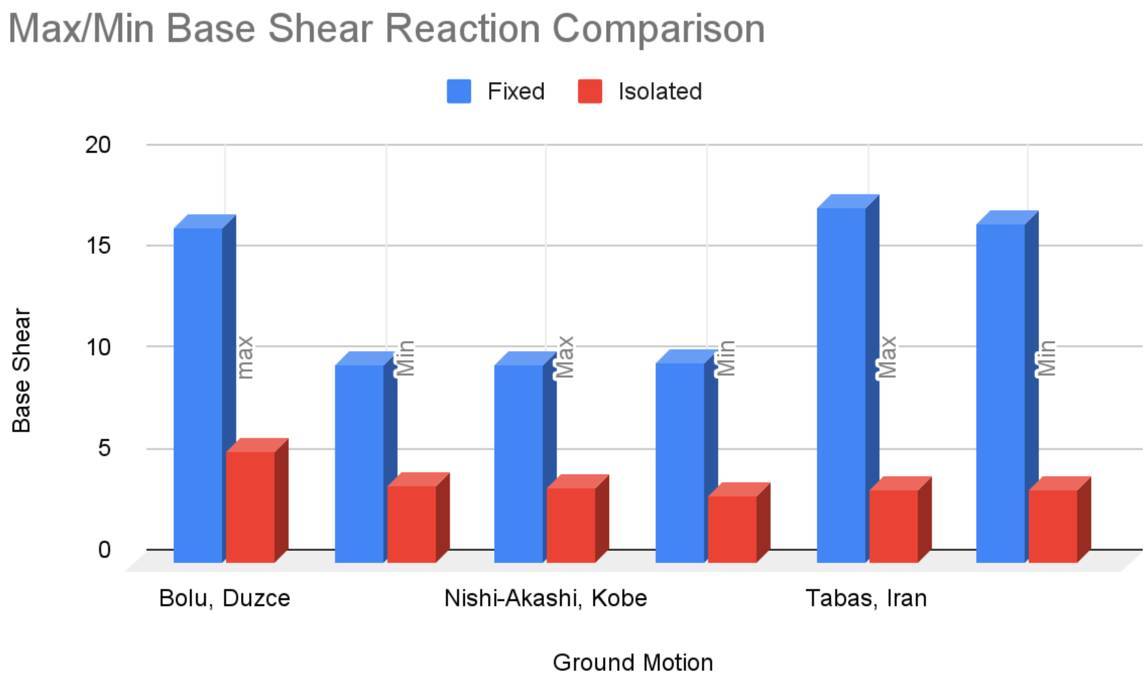

Figure 4.53: Absolute Maximum/Minimum Base Shear Reaction Comparison – X direction

4.3 Force – Displacement Curves of the Isolators (Hysteresis Loops)

Isolator hysteretic loops clarify the relationship between the displacement and force of the TFP isolator. The hysteretic loops could be also utilized to define the effective damping obtained from the isolation system, in addition to defining the amount of power dissipated in each cycle. The displacement values obtained for the applied TFP Isolators were 544.581 mm,169.676 mm, and 329.664mm for Bolu, Nishi-Akashi, and Tabas ground motions respectively, these values are considered low values which allow movement only at the internal sliding interfaces and lead to low energy dissipation. The maximum value observed for the displacement of the TFP bearing was at Bolu ground motion.

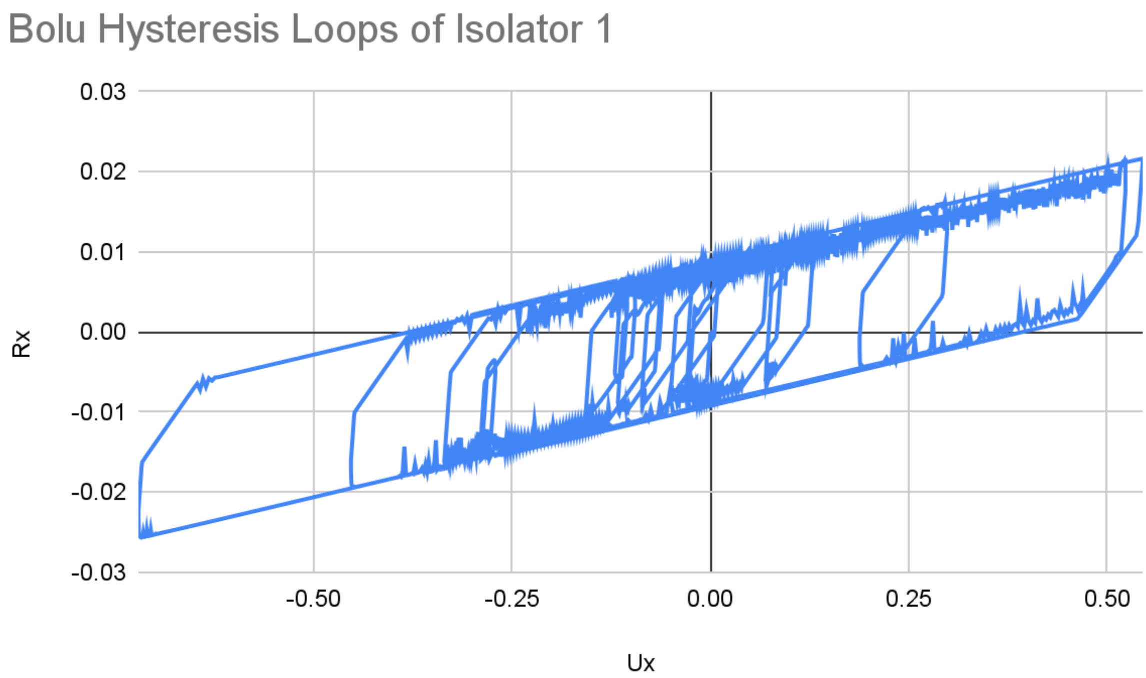

Figure 4.54: Bolu Hysteresis Loop of Isolator 1 – X direction

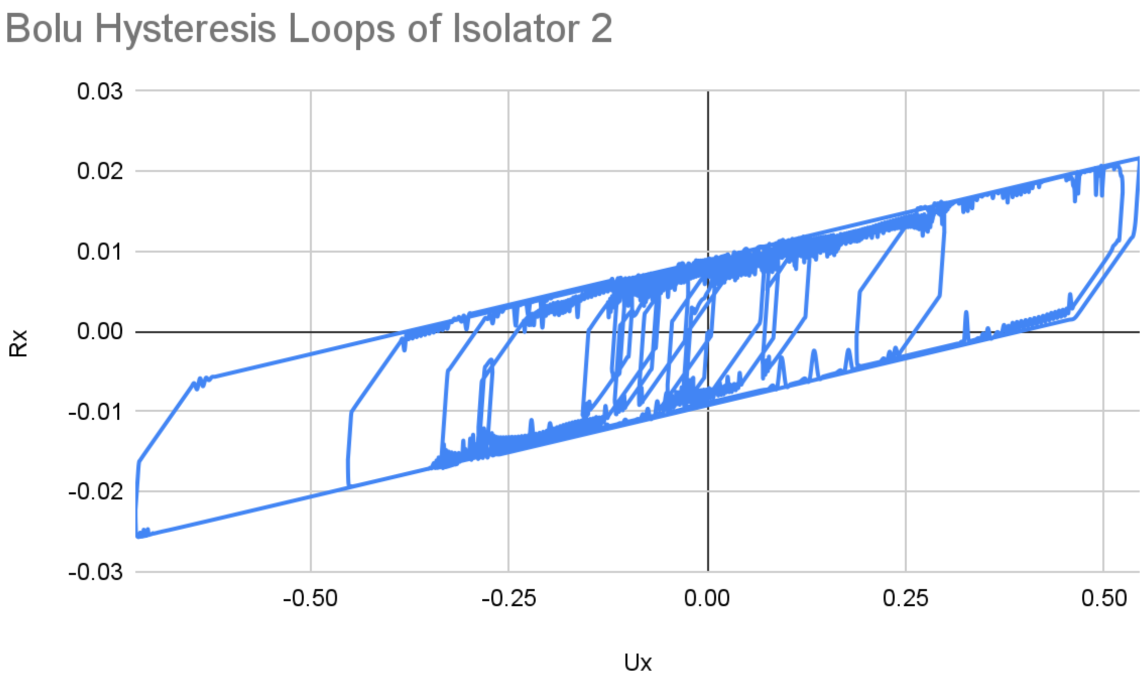

Figure 4.55: Bolu Hysteresis Loop of Isolator 2 – X direction

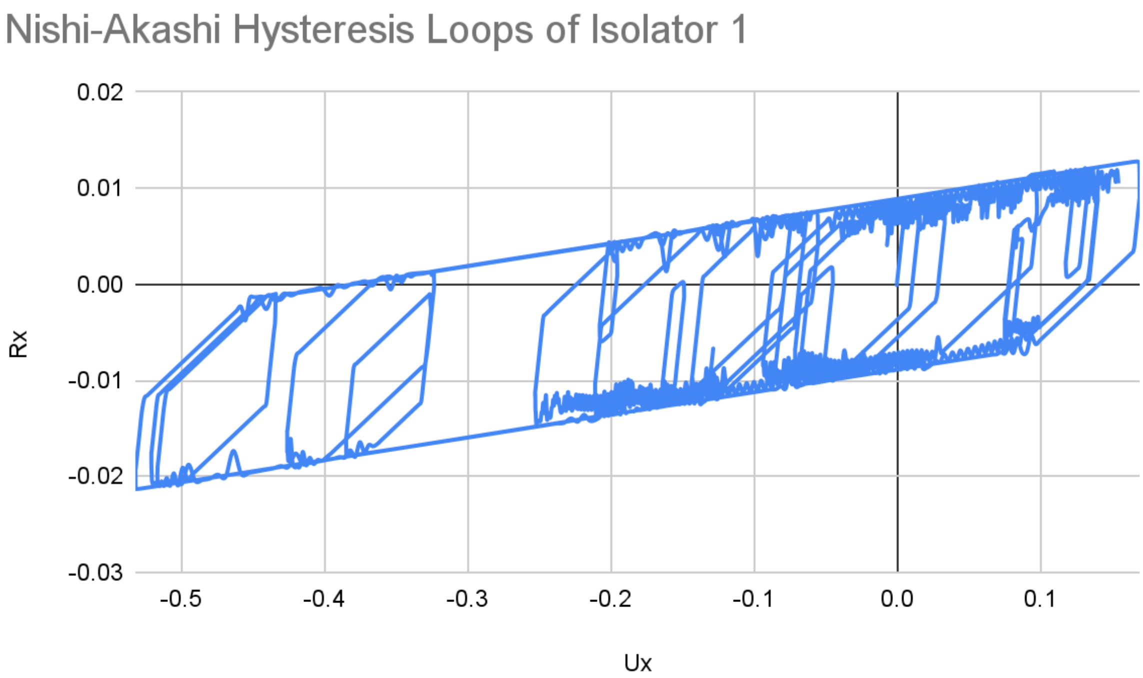

Figure 4.56: Nishi Akashi Hysteresis Loop of Isolator 1– X direction

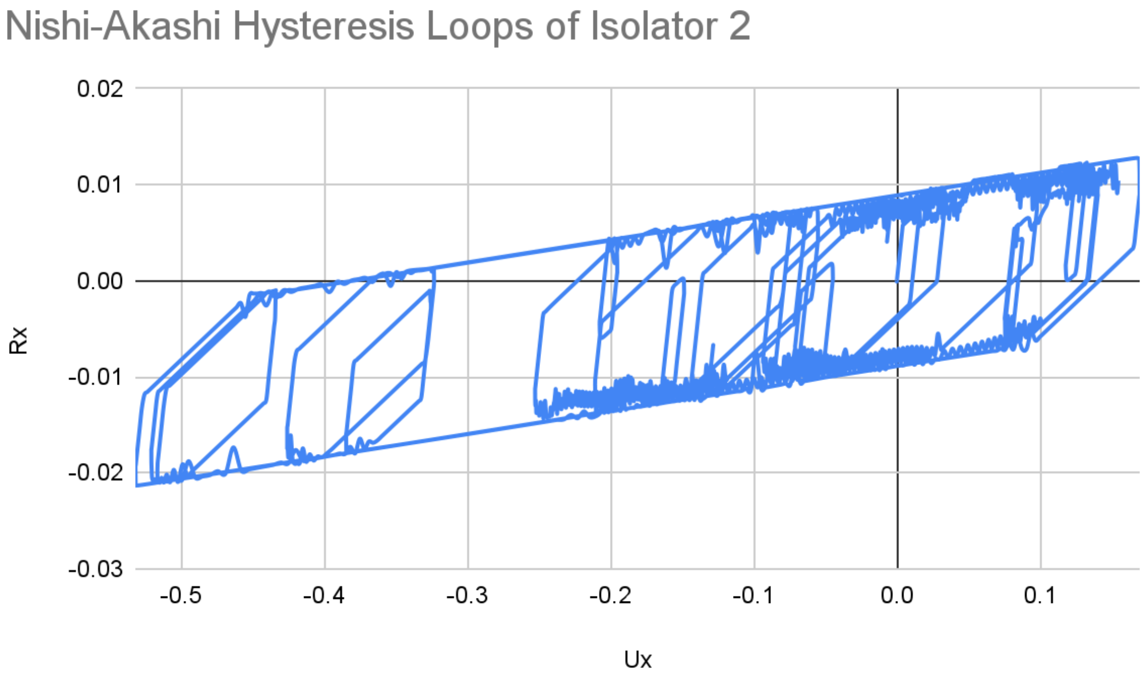

Figure 4.57: Nishi Akashi Hysteresis Loop of Isolator 2 – X direction

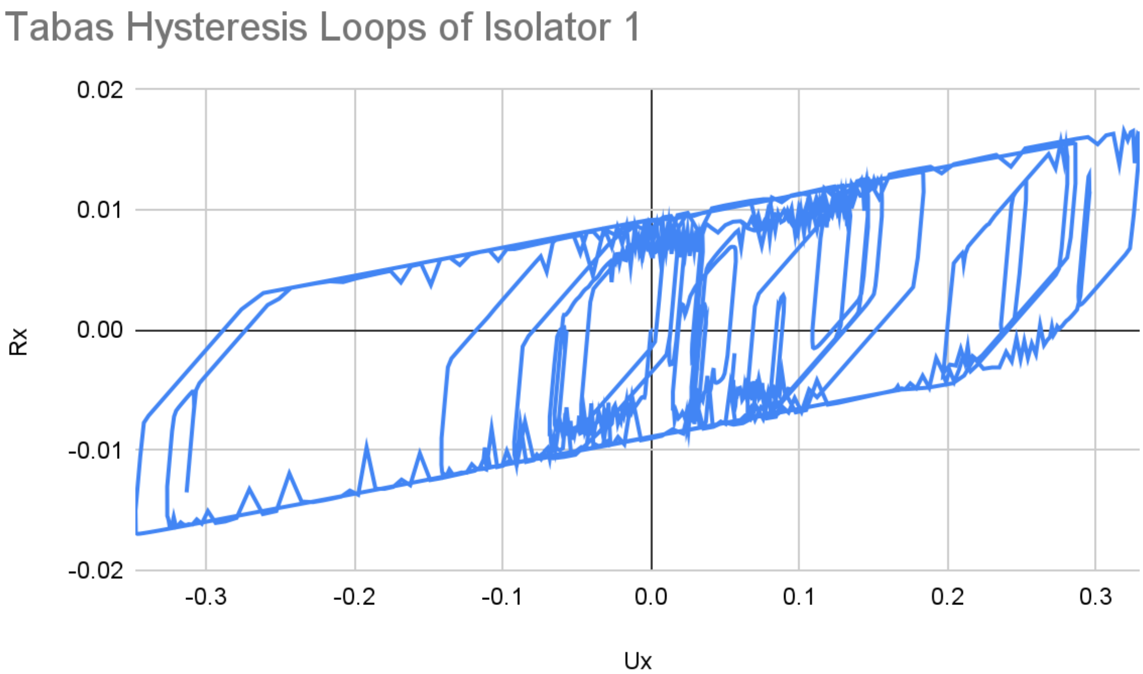

Figure 4.58: Tabas Hysteresis Loop of Isolator 1 – X direction

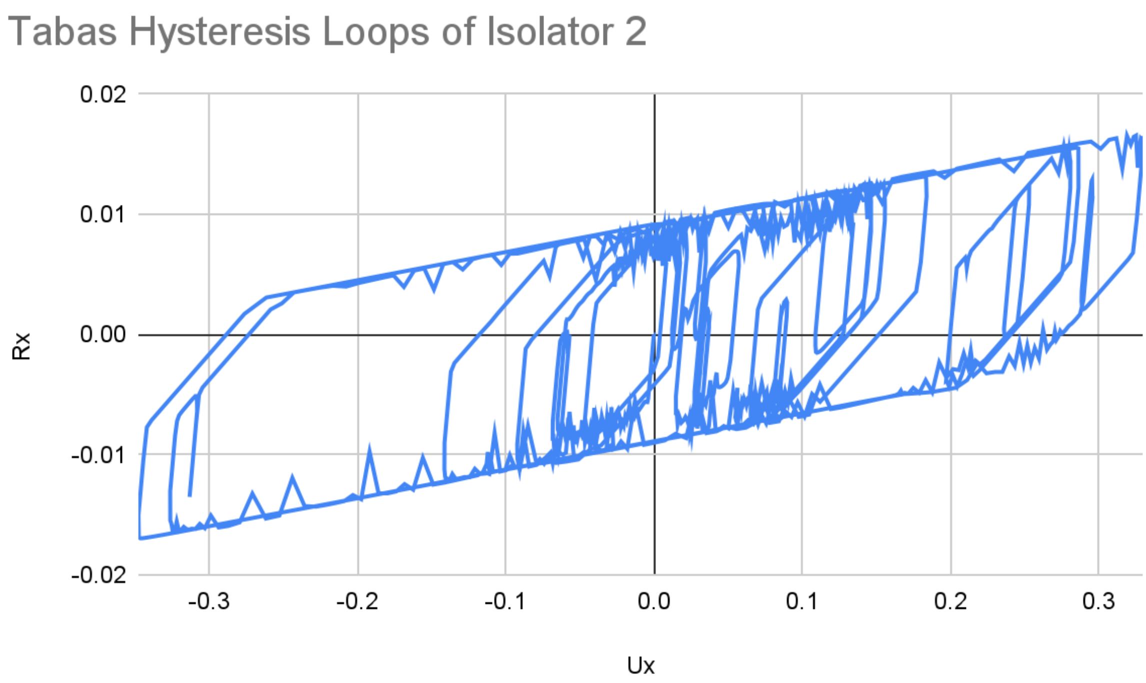

Figure 4.59: Tabas Hysteresis Loop of Isolator 2 – X direction

CHAPTER 5

CONCLUSION SUMMARY AND RECOMMENDATIONS

5.1 Conclusions Summary

In this paper, the concept of seismic isolation systems and their benefits for the structures is introduced. Also, the design principles and types of the seismic isolators and their mechanism are reviewed and summarized in addition to their mathematical equations. Moreover, the response of the seismically isolated bridges with triple friction pendulum bearings is studied and compared with the traditional fixed-based bridges. The structure of the bridge is modeled and analyzed with the non-linear time history analyses (THA) in both cases of the base, under three types of seismic events (Bolu, Nishi-Akashi, and Tabas ground motions). based on the analyses carried out for the considered bridge model the following results can be deduced:

- The response of the TFP isolated bridge structure during seismic events is better than the response of the fixed-based structure; as the isolation system leads to an approximate reduction of around 61% in displacement values and around 69% in base shear values for all the applied earthquakes.

- The behavior of the structures supported by triple friction pendulum isolators can be directly affected by the radii and the friction coefficient of these systems under a moderate period, while the displacement amplitude doesn't have a direct effect on the demeanor of these structures.

- The use of the isolation system decreased the nodal displacement of the nodes on the top of the bridge's bent cap, which will subsequently be transferred to the superstructure. Consequently, the superstructure will experience a slight imperceptible displacement; where the isolation system dissipates earthquake energy transmitted from the substructure.

- The values of displacement and base shear reaction of the isolated bridge structure can be controlled effectively unlike the fixed-based structure bridges.

5.2 Suggestions for further research

This simple case study investigated the seismic isolation effects on displacement and base shear of bridge structures, and it can be expanded by assessing the execution of any current bridge structure. Moreover, an evaluation for base isolated constructions could be employed by applying linear and non-linear static assessment procedures according to different seismic codes. However, for the generalization of any obtained results, the analysis should be done for a number of structures.

References

[1] Gonzalez, Arturo. Schorr, Michael. Valdez, Benjamin and Alejandro Mungaray. "Bridges: Structures and Materials, Ancient and Modern". DOI: 10.5772/intechopen.90718. (2020). 8 Dec 2020.

[2] "*Seismic Base Isolation*". 18 January 2021. Wikipedia, the free encyclopedia. 08 Dec 2020. [Online]. Available: <https://en.wikipedia.org/wiki/Seismic_base_isolation>.

[3] Pressler, Margaret Webb. "More earthquakes than usual? Not really". KidsPost. Washington Post: Washington Post. pp. C10. (2010). 8 Dec 2020.

[4] M. Efiloglu, "Understanding the concept of base isolation," 2013.

[5] N. Torunbalci and G. Ozpalanlar, "Earthquake Response Analysis of Mid-Story Buildings Isolated with Various Seismic Isolation Techniques Abstract," 2008.

[6] Llunji, Mentor (2016). Seismic Architecture - The architecture of earthquake resistant structures. Msproject. ISBN 9789940979409.

[7] Robinson Research Institute, https://www.victoria.ac.nz/robinson/about/bill-robinson

[8] Masoumi, Mohammad Mehdi (2016-03-31). "Ancient Base Isolation System in Mausoleum of Cyrus the Great". International Journal of Earthquake Engineering and Hazard Mitigation (IREHM). 4 (1). ISSN 2282-6912. Archived from the original on 2018-03-29. Retrieved 2017-06-11.

[9] "*Tomb of Cyrus*". 23 April 2022. Wikipedia, the free encyclopedia. 1 April 2022. [Online]. Available: https://en.wikipedia.org/wiki/Tomb_of_Cyrus.

[10] Seda Özdemir, "Investigation of Seismic Isolation Efficiency for Building Structures (2016)," 2016.

[11] Constantinou M.C, I. Kalpakidis, A. Filiatrault and R.A. Ecker Lay. *"LRFD-Based Analysis and Design Procedures for Bridge Bearings and Seismic Isolators"- Technical Report MCEER-11-0004*. Published: (September 26, 2011).

[12] FEMA/MBDSI 2003, Seismic Protective Systems: *SEISMIC ISOLATION, Design Examples, Instructional Material Complementing FEMA 451.*

[13] Buckle. Ian G, Micheal C. Constantinou, Murat Dicleli and Hamid Ghasemi. *"Seismic Isolation of Highway Bridges" - Special Report MCEER-06-SP07. 2006.* Published: (August 21, 2006).

[14] M. C. Constantinou, A. S. Whittaker, Y. Kalpakidis, D. M. Fenz, and G. Apostolakis, *Seismic Isolation of Bridges - Technical Report MCEER-07-0012*. 2007. Buffalo, New York: Report Submitted to the State of California Department of Transportation version 2. 2007.

[15] Ryan, Keri L, and Richins, Brian. "*Design, Analysis, and Seismic Performance of A Hypothetical Seismically Isolated Bridge on Legacy Highway"- Technical Report No. UT-11-01*. Published: (January 2011). Utah Department of Transportation Research Division. Report.

[16] Seismic component devices, Agrawal A.K., Amjadian M. Department of Civil and Environmental Engineering, The City College of the City University of New York, 160 Convent Ave.,New York, NY 10031.

[17] Chapter 14 "Design of Structures with Seismic Isolation" Ronald L Mayes, Ph.D. Consulting Engineer, Berkeley, California. Farzad Naeim, Ph.D., S.E. Vice President and Director of Research and Development, John A. Martin and Associates, Inc., Los Angeles, California.

[18] Becker, Tracy Celeste. "Advanced Modelling of the Performance of Structures Supported on Triple Friction Pendulum Bearings". UC Berkeley Electronic Theses and Dissertations, 2011: 137pp.

[19] Fenz, Daniel M., and Micheal C. Constantinou. (2008a). *Spherical sliding isolation bearings with adaptive behavior: Theory. 2nd edition*. 37 vols. pp.163-183. Buffalo, New York: Wiley InterScience. 2007.

[20] M. Malekzadeh and T. Taghikhany, "Multi-Stage Performance of Seismically Isolated

Bridge Using Triple Pendulum Bearings". *Advances in Structural Engineering., vol* 15, no. 7, (2012): 1181-1196 pp. 8 January 2021.

[21] F. Weber, J. Distl, and C. Braun, "Isolation Performance Assessment of Adaptive Behaviour of Triple Friction Pendulum," *J. Civ. Eng. Res.*, vol. 7, no. 1, pp. 17–33, 2017.

[22] D. M. Fenz and M. C. Constantinou, *Mechanical Behavior of Multi-Spherical by*. 2008

[23] G. P. Warn and K. L. Ryan, "A Review of Seismic Isolation for Buildings: Historical Development and Research Needs," *Buildings*, vol. 2, no. 4, pp. 300–325, 2012.

[24] Rajan Wankhade, "Performance Analysis of RC Moment Resisting Frames Using Different Rubber Bearing Base Isolation Techniques". *International Conference on Innovations in Concrete for Infrastructure Challenges At Nagpur, India October 6/7,* (2017).

[25] H. H. N. and J. L. Tassoulas., "Directional Effects of Shear Combined with Compression on Bridge Elastomeric Bearings.," 2009.

[26] Romo, Marcelo. Morales, Enrique. O'Connor, Jeromi. Mosquera, Pedro. Nicolaou, Sissy and Guillermo Diaz-Fanas. "LOS CARAS ISOLATED BRIDGE IN THE 2016, MUISNE ECUADOR EARTHQUAKE: PERFORMANCE OF SYNCHRONIZING DEVICES". *Conference paper: 16 European Conference on Earthquake Engineering*, (2018): 12pp.

[27] Earthquake Protection System EPS. "Seismic Isolation Engineering Experts Protect Against Earthquake Damage". 8 Dec 2020. [Online]. Available: < https://www.earthquakeprotection.com/>.

[28] Historic and notable bridges of the U.S. "Lake Natoma Crossing". 20 November 2016. BRIDGEHUNTER.COM. 8 Dec 2020. [Online]. Available: < https://bridgehunter.com/ca/sacramento/bh37310/>.

[29] International Database and Gallery of Structures. "Antioch Bridge". 8 Dec 2020. [Online]. Available: <https://structurae.net/en/structures/antioch-bridge-1978>.

[30] "Benicia – Martinez Bridge". 25 December 2020. Wikipedia, the free encyclopedia. 08

Dec 2020. [Online]. Available: <https://en.wikipedia.org/wiki/Benicia%E2%80%93Martinez_Bridge_>.

[31] Metropolitan Transportation Commission. “Dumbarton Bridge”. 8 Dec 2020. [Online]. Available: <https://mtc.ca.gov/about-mtc/what-mtc/bay-area-toll-authority/dumbarton-bridge>.

[32] Scastro, Civil. “*HELICOIDAL BRIDGE SANTA ROSA*”. 2012. 10 January 2021. [Online]. Available: <https://scastro- civil.blogspot.com/2012/05/puente-helicoidal-santa-rosa.html>.

[33] “Tappan Zee Bridge (1955–2017)”. 23 April 2022. Wikipedia, the free encyclopedia. 27 Mar 2022. [Online]. Available: <https://en.wikipedia.org/wiki/Tappan_Zee_Bridge_(1955%E2%80%932017>.

[34] J. Wen, Q. Han, and X. Du, “Shaking Table Tests of Bridge Model with Friction Sliding Bearings Under Bi-Directional Earthquake Excitations”. *Structure and Infrastructure Engineering*, vols 15, ed 9, May (2019): 164-1278 pp. 10 April 2022.

[35] Fenz, Daniel M., and Micheal C. Constantinou. (2008c). *Modeling Triple Friction Pendulum Bearings for Response - History Analysis*.4th edition. 24 vols. pp.1011-1028. Buffalo, New York: Earthquake Engineering Research Institute, 2008.

[36] OpenSees, “Time History Analysis of a 2D Elastic Cantilever Column.” [Online]. Available: https://opensees.berkeley.edu/wiki/index.php/Time_History_Analysis_of_a_2D_Elastic_Cantilever_Column.

[37] “OpenSees". 18 April 2022. Wikipedia, the free encyclopedia. 10 Mar 2022. [Online]. Available: https://en.wikipedia.org/wiki/OpenSees.

[38] “MSBridge Multi-Span Bridge Analysis.” 20 December 2021. [Online]. Available: http://www.soilquake.net/msbridge/index.html.

[39] “Peer Ground Motion Database”, Pacific Earthquake Engineering Research Centre.

[40] Constantinou. M.C, A.S. Whittaker, Y. Kalpakidis, D.M. Fenz, and G.P. Warn. *"Performance of Seismic Isolation Hardware Under Service and Seismic Loading"- Technical Report MCEER-07-0012*. Published: (August 27, 2007).

[41] D. Fenz and M. C. Constantinou, *Development, implementation and verification of dynamic analysis models for multi-spherical sliding bearings: Technical Report MCEER-08-0018*. 2008.

[42] MICROSOFT EXCEL, Commercial computer program.

[43] Amaral. Frederico and Guerreiro. Luis, *Effect of Vertical Component of Earthquake on the Response of a Friction Pendulum Bearing Base Isolation System: Second European Conference on Earthquake Engineering and Seismology, ISTANBUL AUG. 25-29, 2014*.

[44] SEISMOSIGNAL, Earthquake Engineering Software Solutions.

APPENDIX A

PRELIMINARY DESIGN CALCULATION OF A TRIPLE FRICTION PENDULUM BEARING

This effective radius of TFP surfaces is based on the guidelines presented in [11] Appendix C.

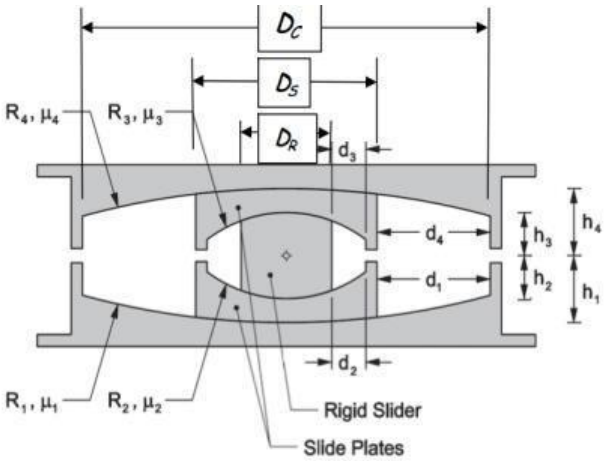

Figure A.1: Triple Friction Pendulum Parameters [11]

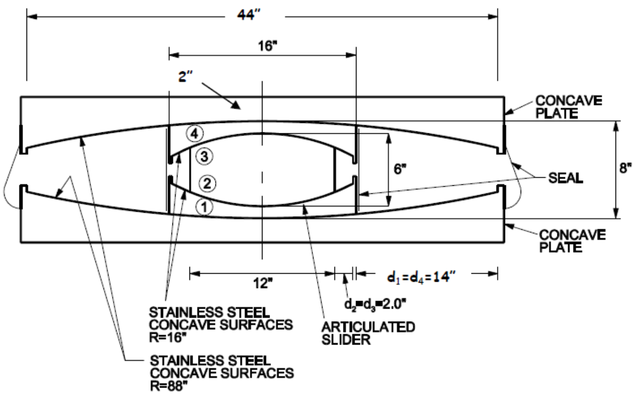

Figure A.2: Triple Friction Pendulum Numerical Parameters [11]

The design of triple friction bearing is mainly characterized by the effective outer radius R_{eff1} and R_{eff4} . The calculation of radii is shown as following:

R_1= R_4= 88 inch, R_2= R_3= 16 inch.

$h_1 = h_4 = 4$ inch, $h_2 = h_3 = 3$ inch.

$R_{eff1} = R_{eff4} = R_1 - h_1 = 88 - 4 = 84$ inch.

$R_{eff2} = R_{eff3} = R_2 - h_2 = 16 - 3 = 13$ inch.

APPENDIX B

ANALYSIS RESULTS GRAPHS FOR FIXED BASE AND TFP ISOLATED BRIDGE STRUCTURE MODEL

In This section, OpenSees' analysis results for the considered three ground motions (Bolu, Nishi-Akashi and Tabas) will be presented as graphical charts using EXCEL software, for both cases; isolated and non-isolated bridge structure model. The graphical outcomes will be presented for:

- The nodal displacement of the nodes (5 and 6) on the top of bridge's bent-cap for the fixed base and the isolated structure at the same time, and for the nodes (7 and 8) on the top of the TFP bearings in the isolated structure at the horizontal direction X.
- The base shear reaction of the nodes (1 and 2) at the bottom of bridge's columns; as the maximum lateral force value concentrates at the base level, for both cases isolated and non-isolated structure at the horizontal direction X.

I. Nodal Displacement U_X

Based on Analyses outcomes the nodal displacement for the fixed and TFP isolated base at the horizontal direction will be illustrated in Figures B.1 to B.18 for the three considered ground motions.

Fixed base structure

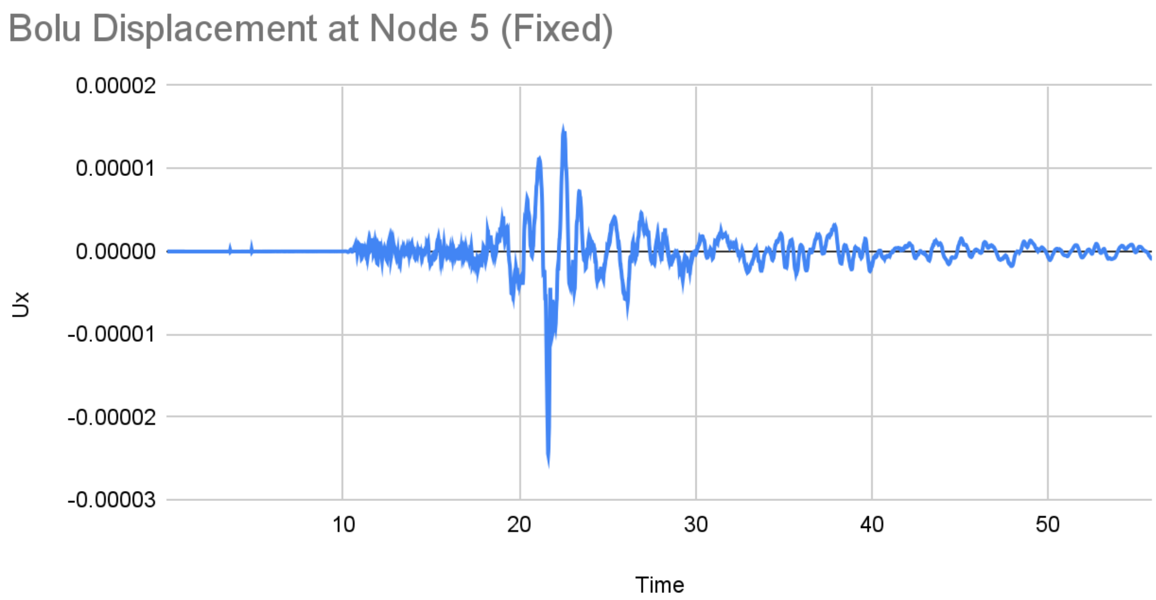

Figure B.1: Fixed Base Node 5 Bolu Displacement – X Direction

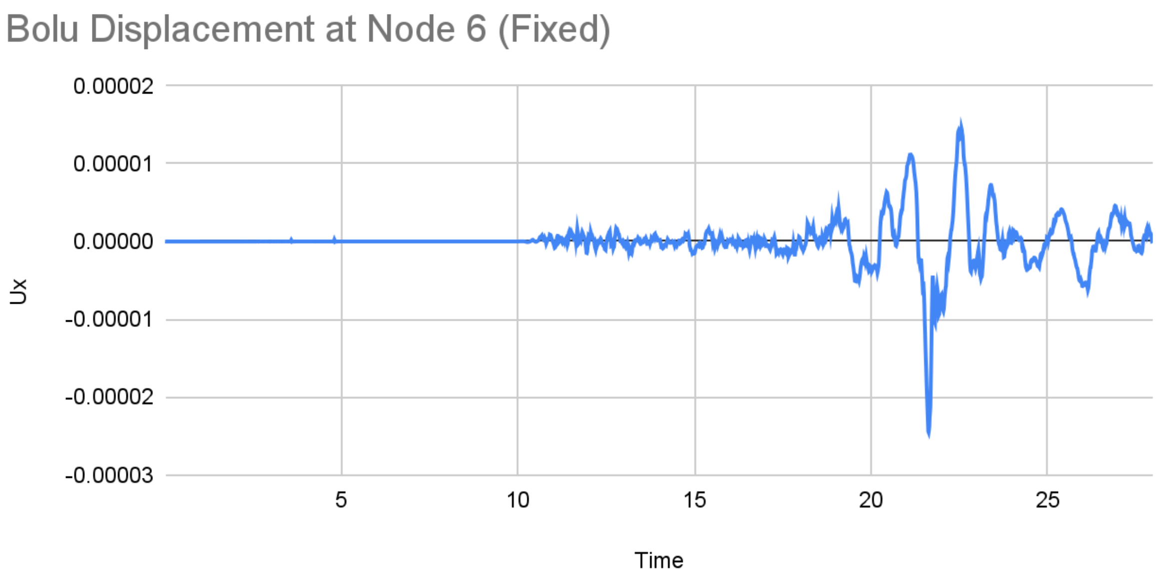

Figure B.2: Fixed Base Node 6 Bolu Displacement – X Direction

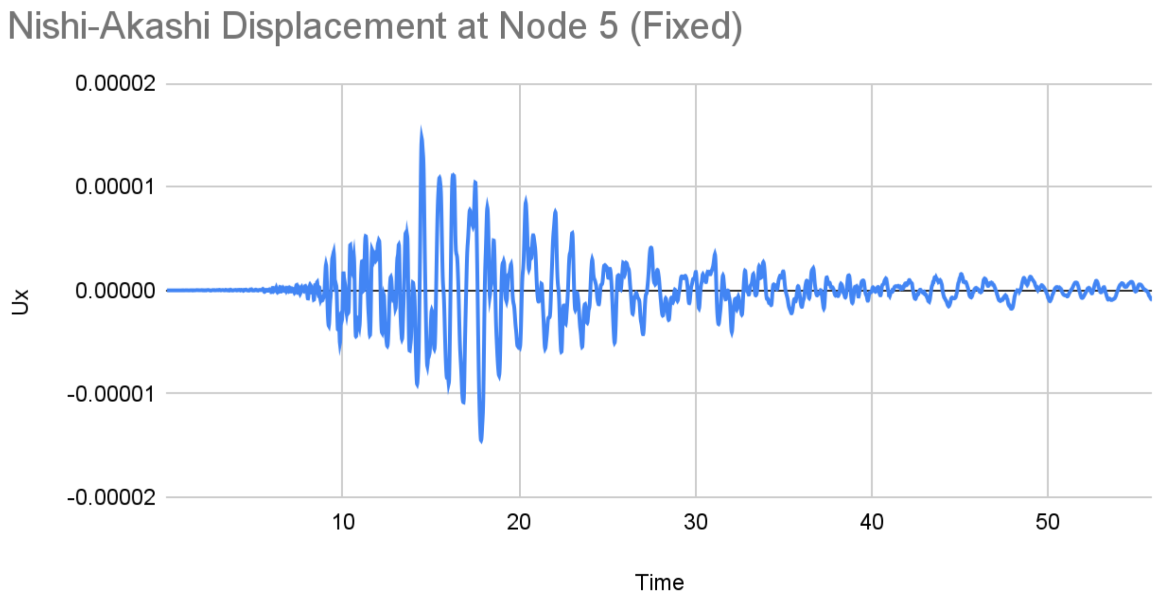

Figure B.3: Fixed Base Node 5 Nishi-Akashi Displacement – X Direction

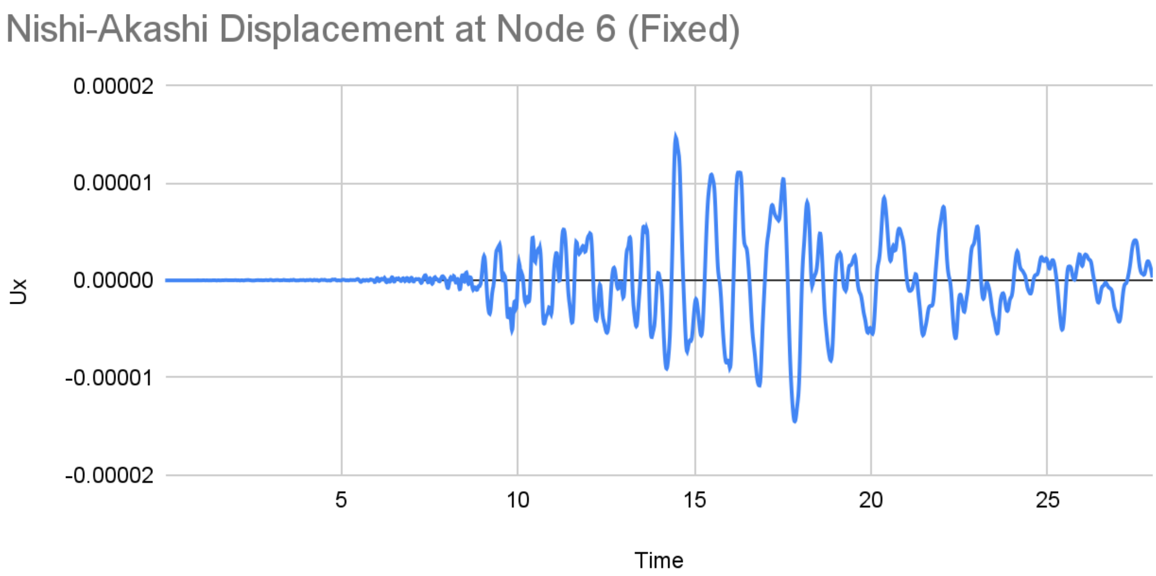

Figure B.4: Fixed Base Node 6 Nishi-Akashi Displacement – X Direction

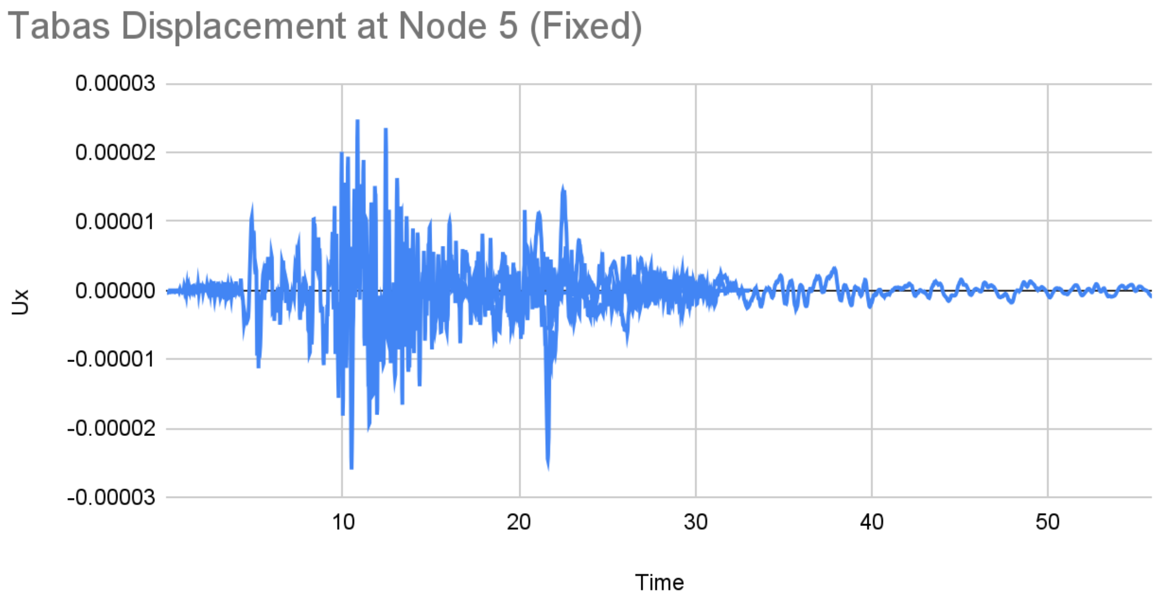

Figure B.5: Fixed Base Node 5 Tabas Displacement – X Direction

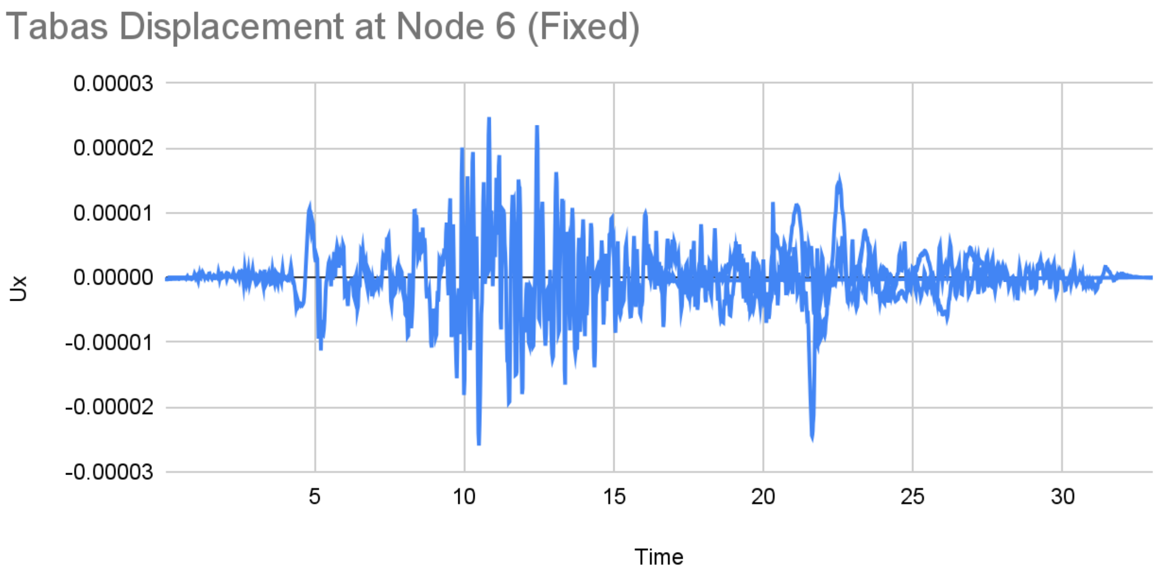

Figure B.6: Fixed Base Node 6 Tabas Displacement – X Direction

Triple Friction Pendulum isolated structure

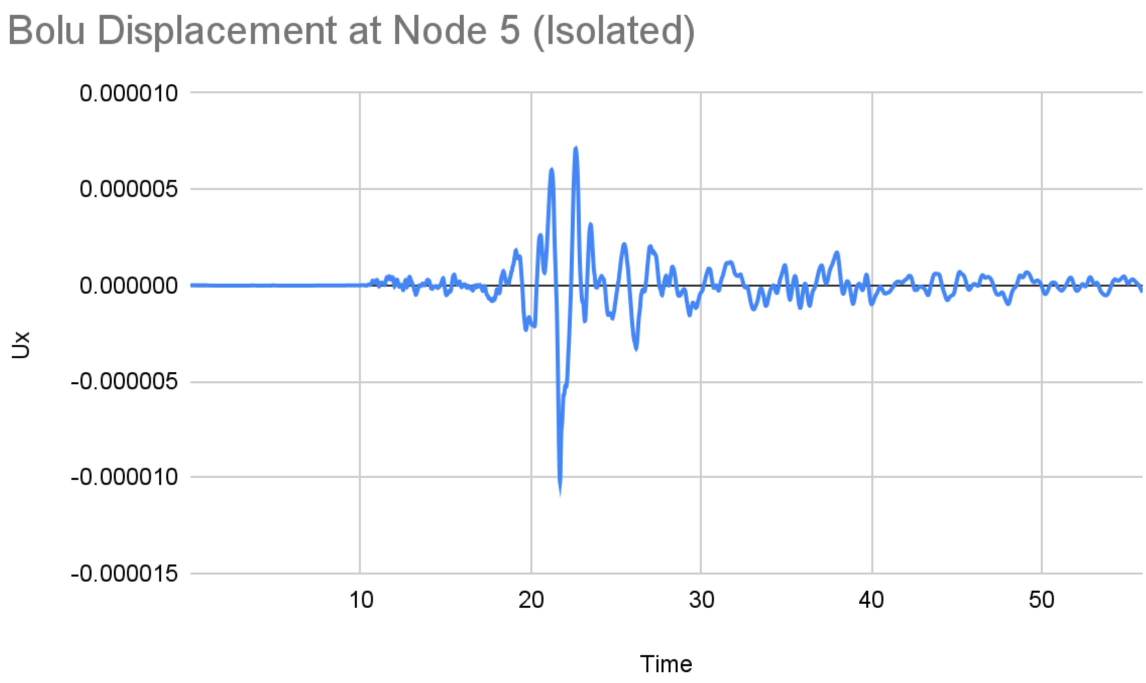

Figure B.7: Isolated Base Node 5 Bolu Displacement – X Direction

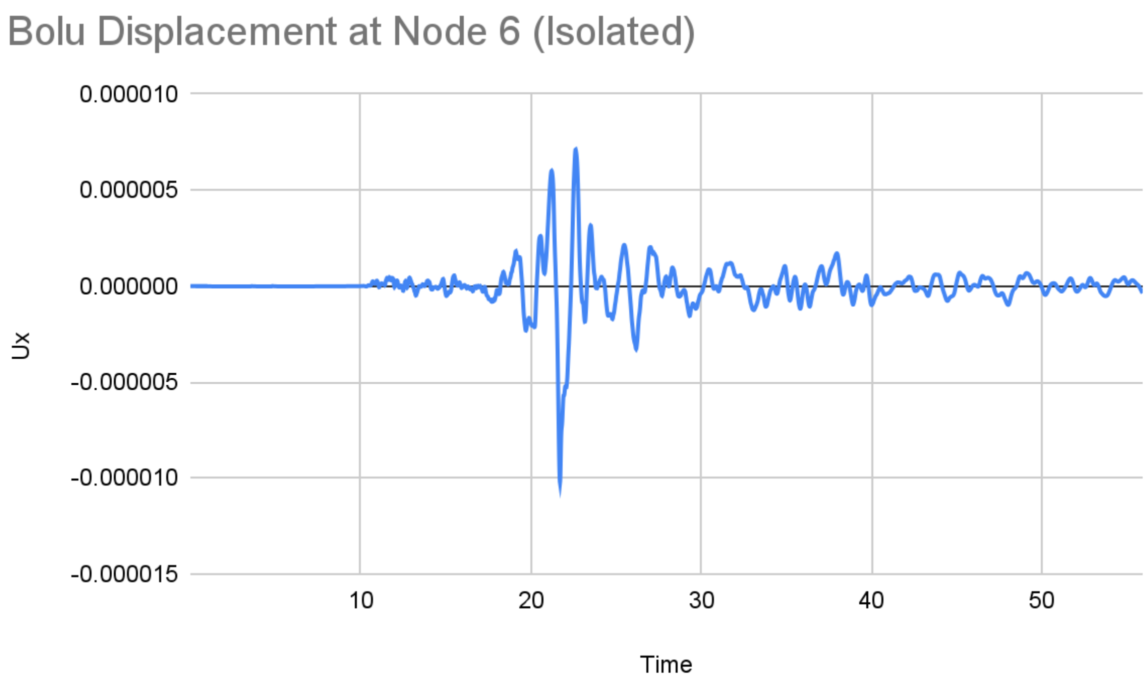

Figure B.8: Isolated Base Node 6 Bolu Displacement – X Direction

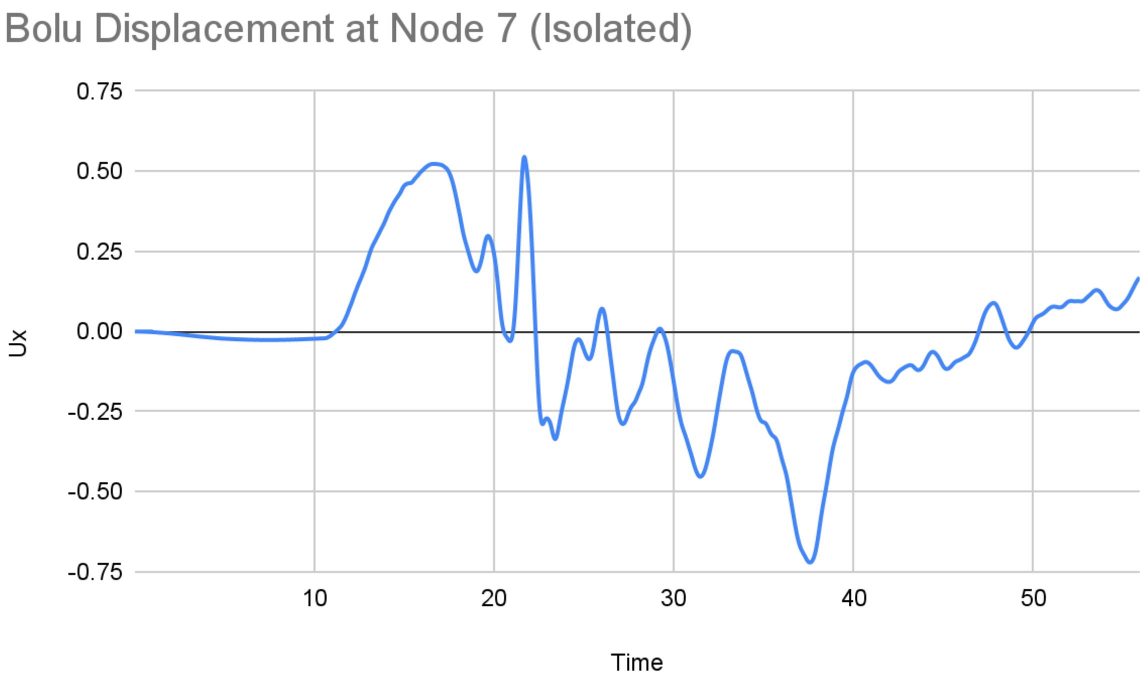

Figure B.9: Isolated Base Node 7 Bolu Displacement – X Direction

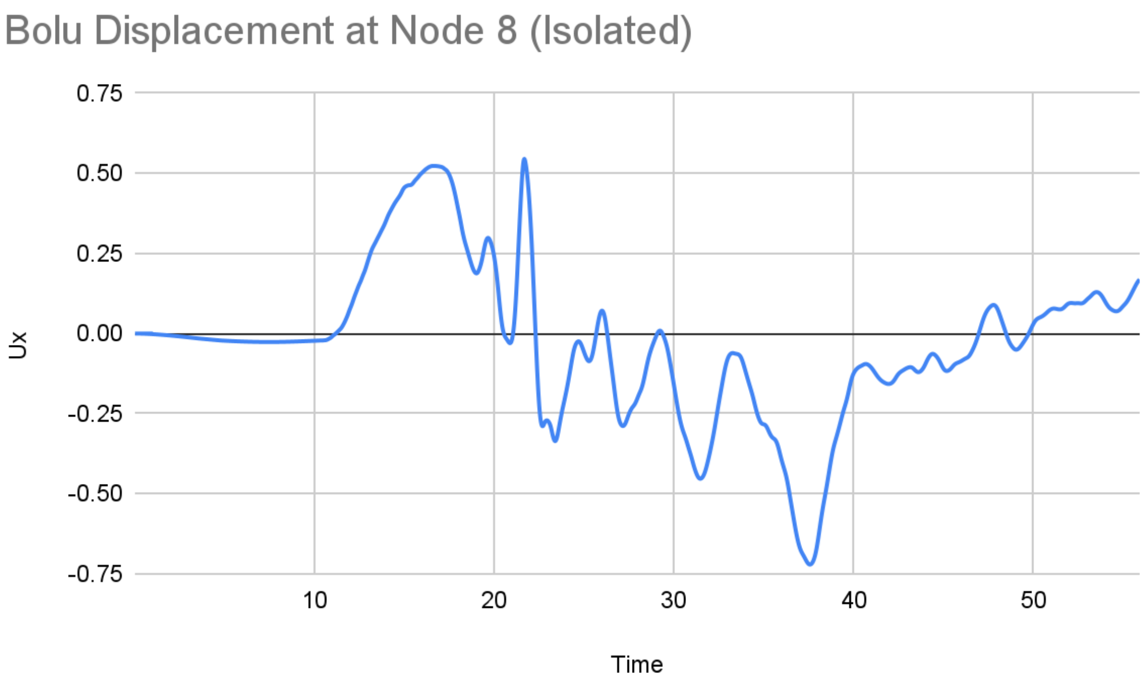

Figure B.10: Isolated Base Node 8 Bolu Displacement – X Direction

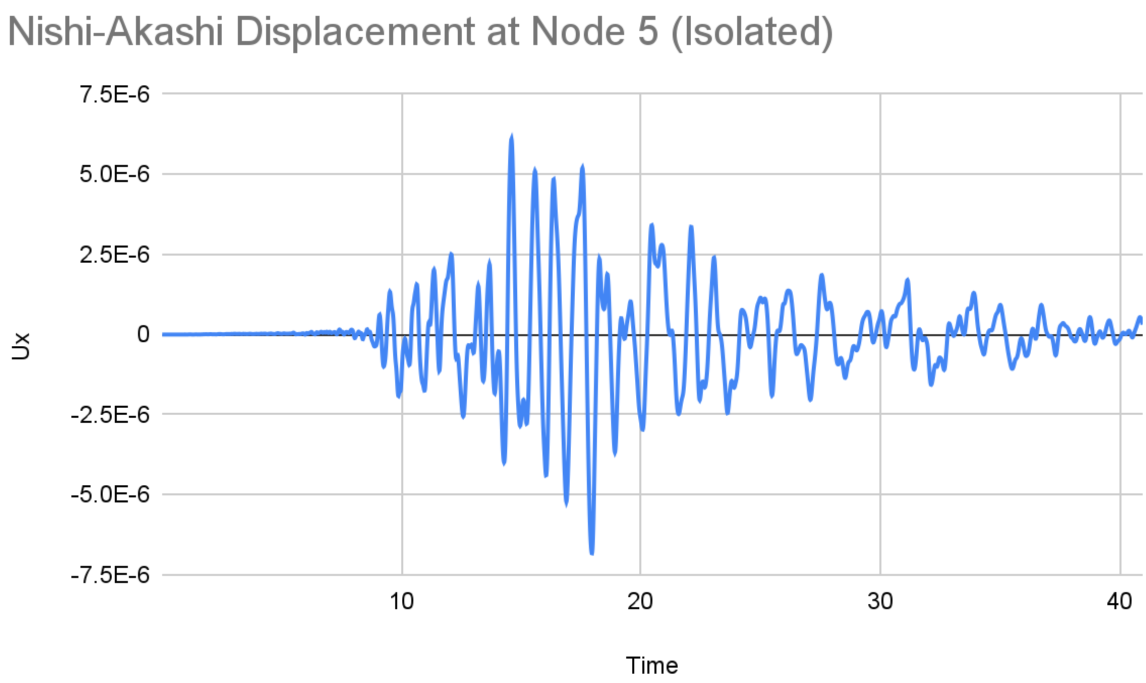

Figure B.11: Isolated Base Node 5 Nishi-Akashi Displacement – X Direction

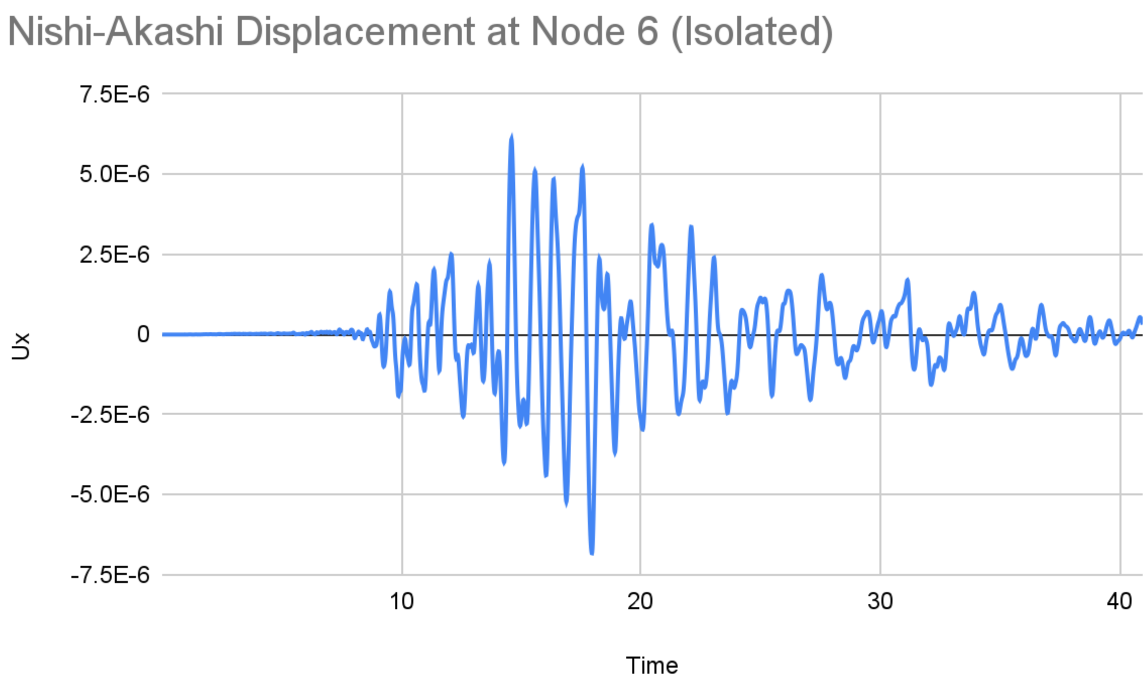

Figure B.12: Isolated Base Node 6 Nishi-Akashi Displacement – X Direction

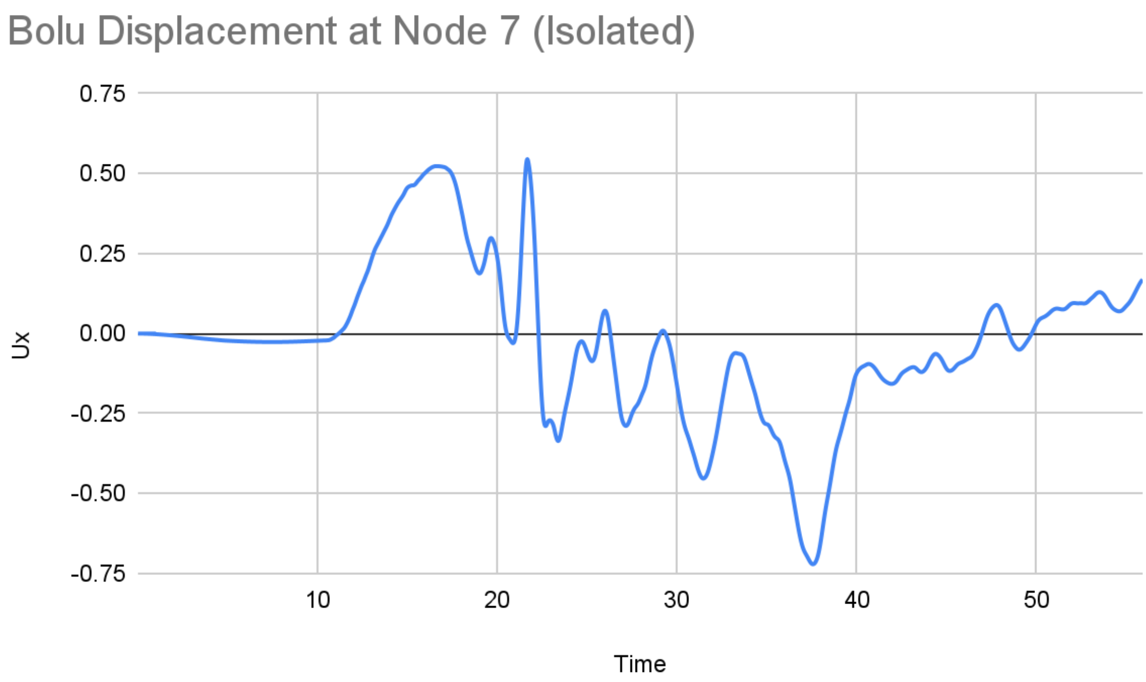

Figure B.13: Isolated Base Node 7 Nishi-Akashi Displacement – X Direction

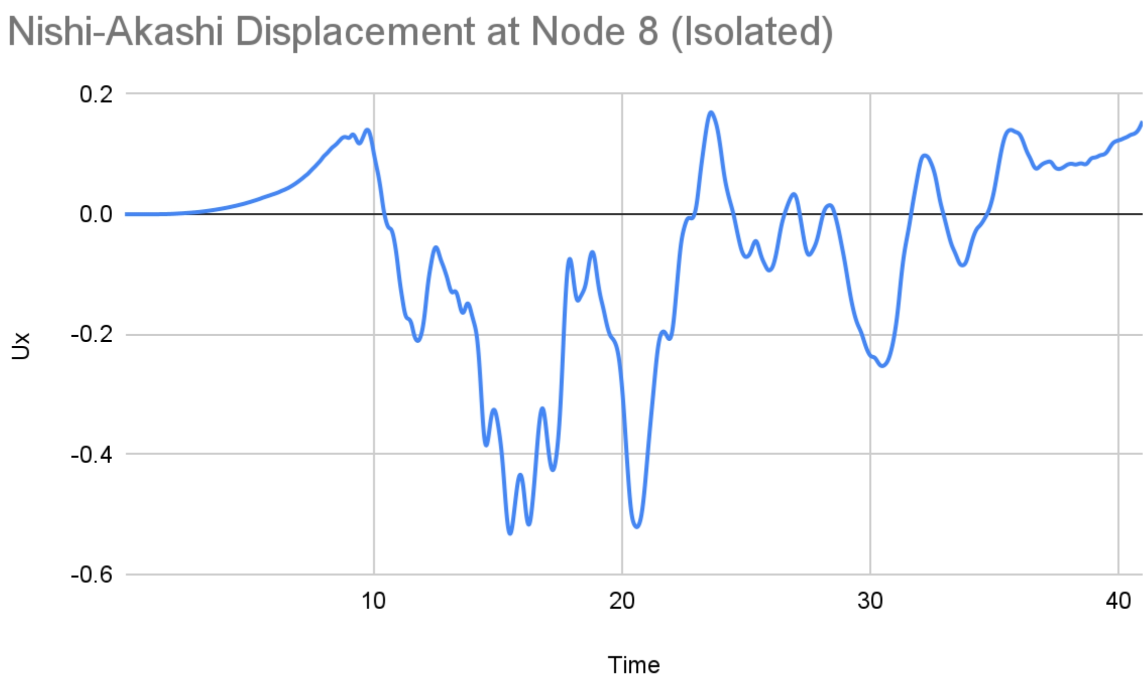

Figure B.14: Isolated Base Node 8 Nishi-Akashi Displacement – X Direction

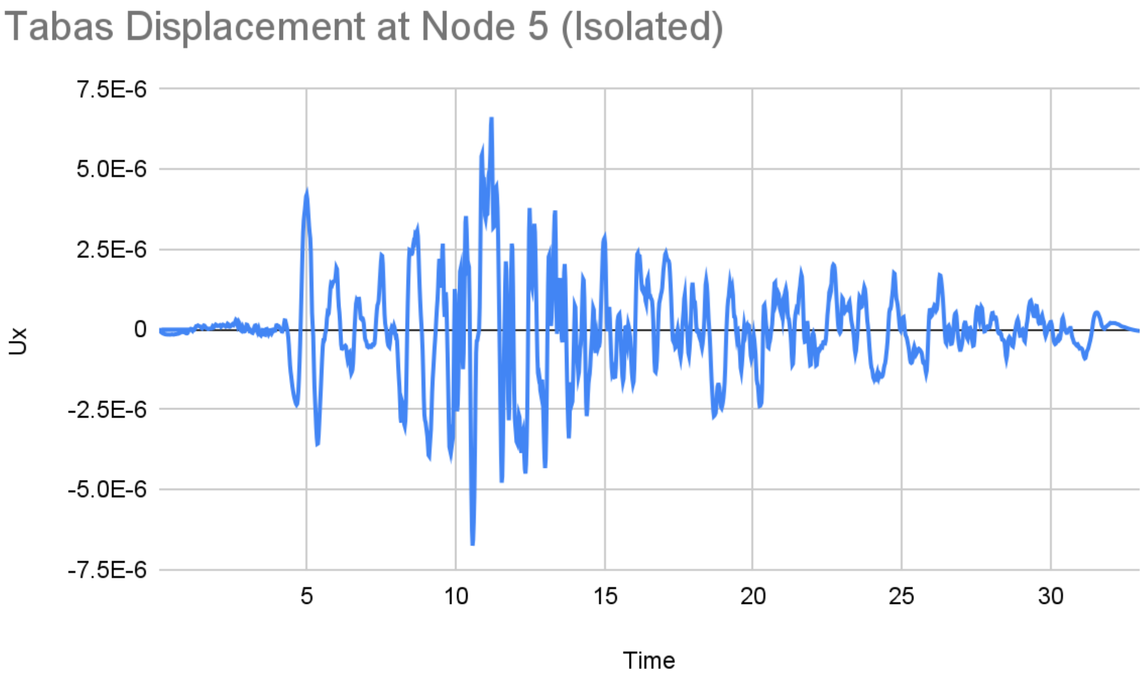

Figure B.15: Isolated Base Node 5 Tabas Displacement – X Direction

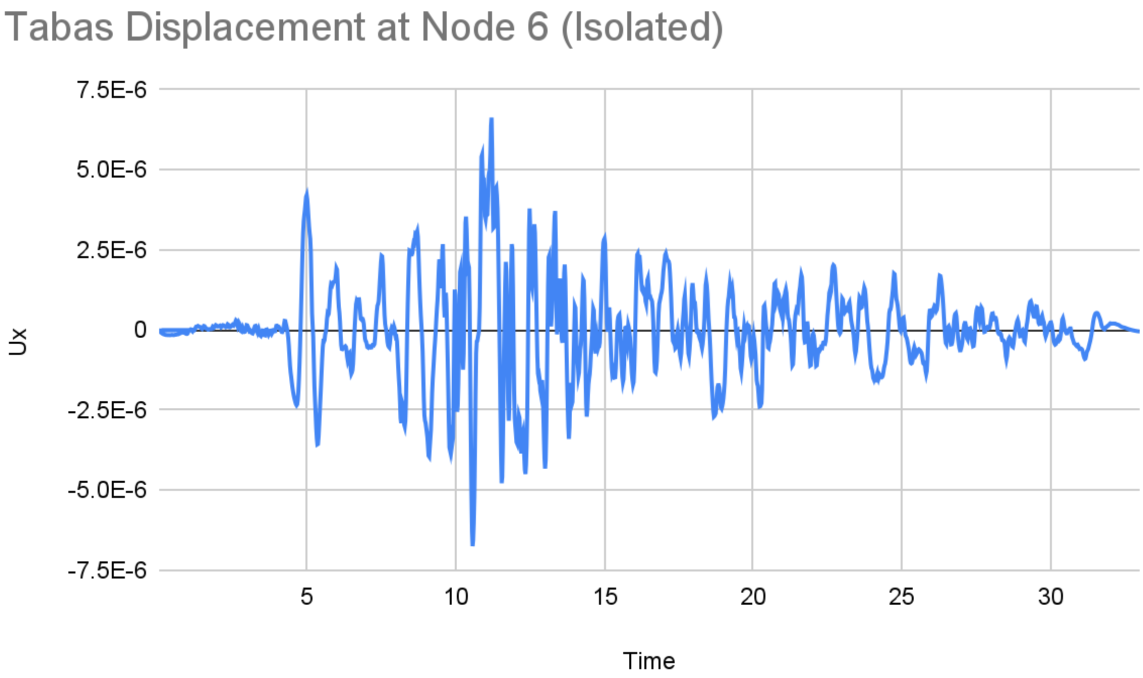

Figure B.16: Isolated Base Node 6 Tabas Displacement – X Direction

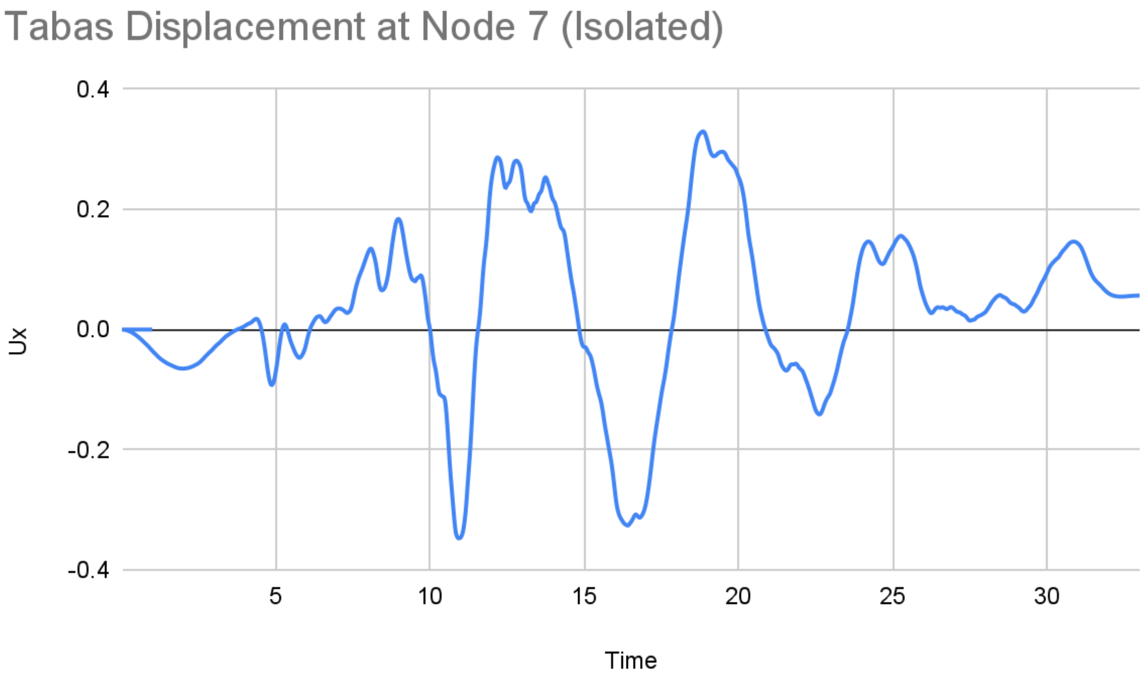

Figure B.17: Isolated Base Node 7 Tabas Displacement – X Direction

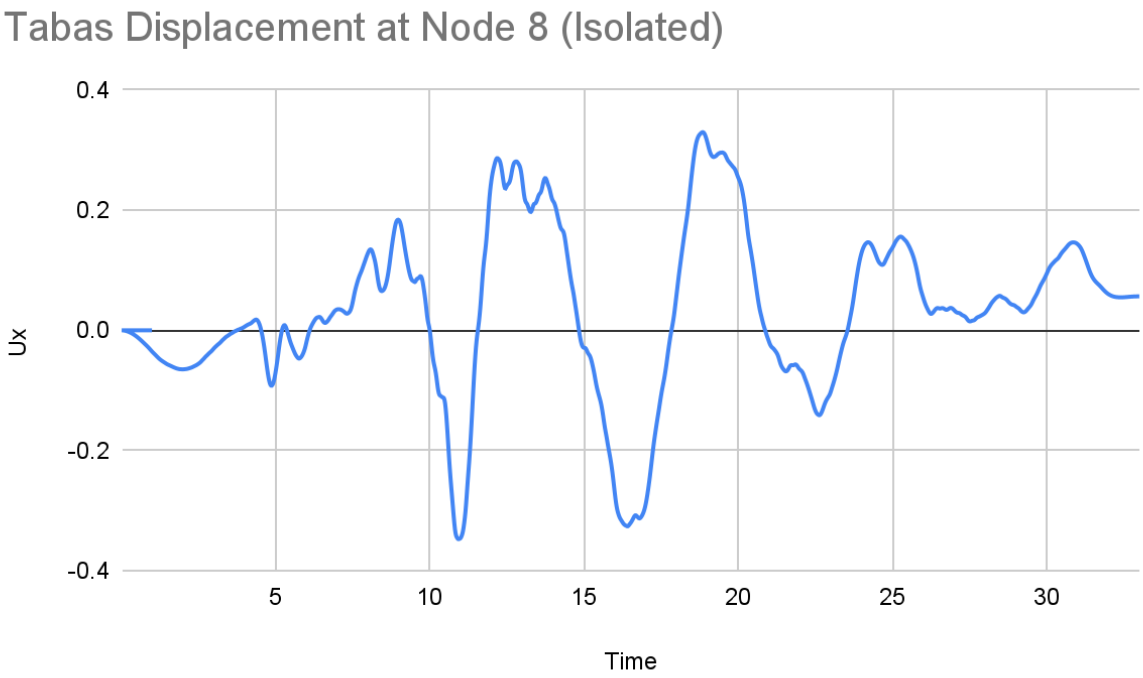

Figure B.18: Isolated Base Node 8 Tabas Displacement – X Direction

II. Base Shear Reaction

Based on Analyses outcomes the base shear reaction for the fixed and TFP isolated base at the horizontal direction will be illustrated in Figures B.19 to B.30 for the three considered ground motions.

Fixed base structure

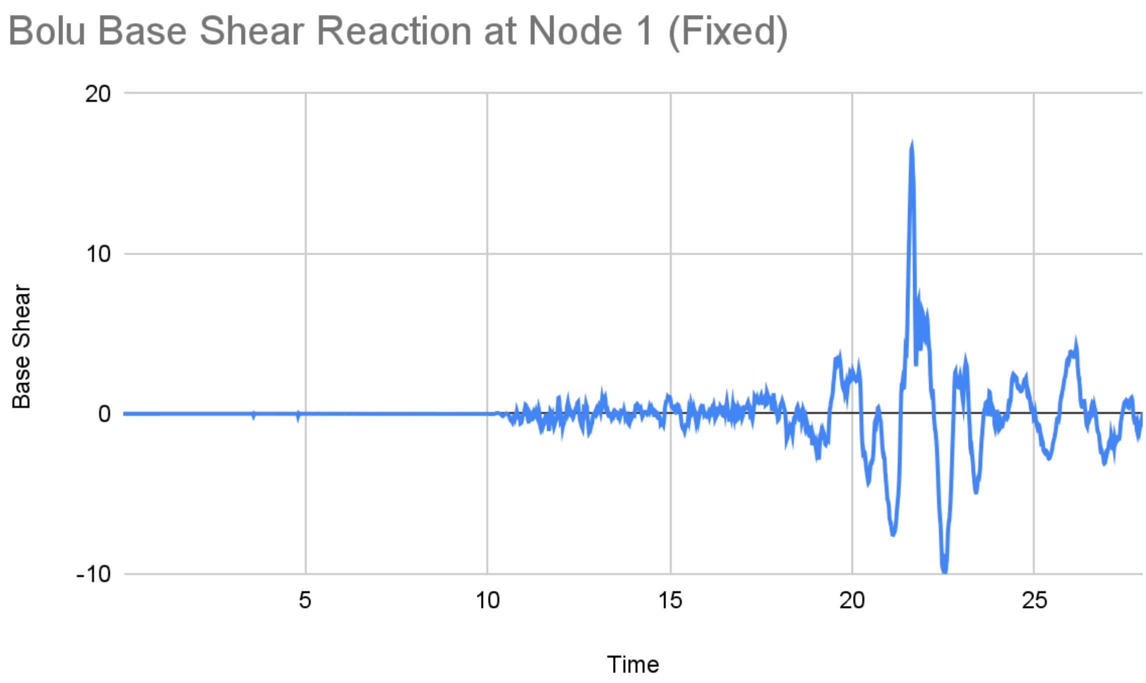

Figure B.19: Fixed Base Node 1 Bolu Base Shear Reaction – X Direction

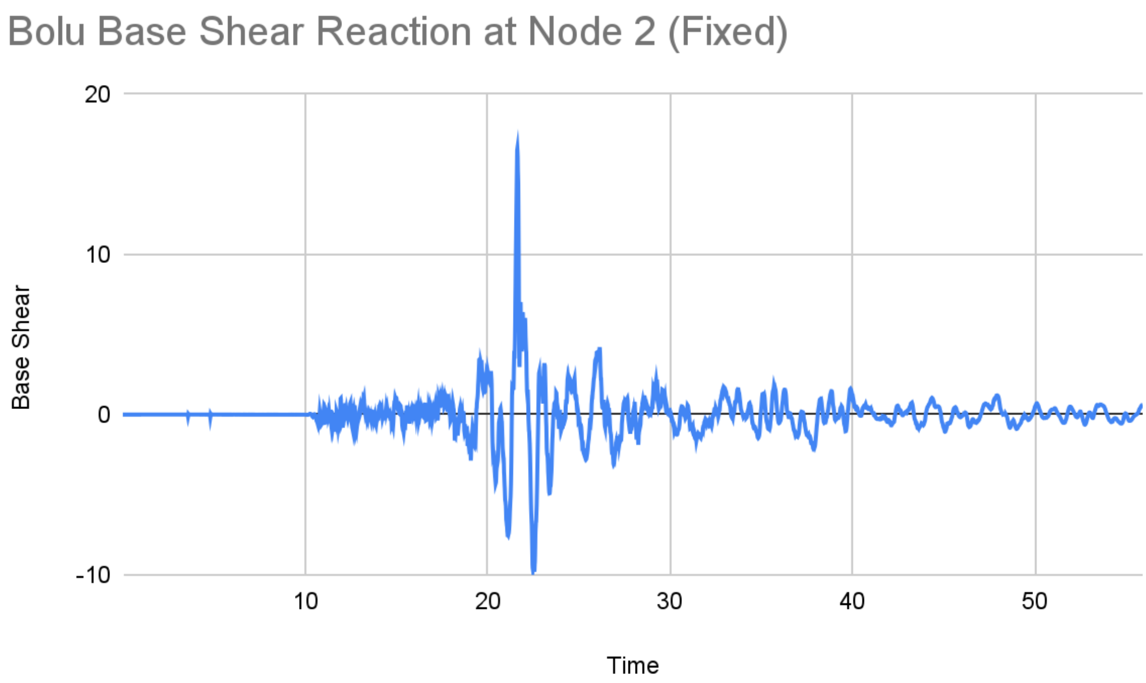

Figure B.20: Fixed Base Node 2 Bolu Base Shear Reaction – X Direction

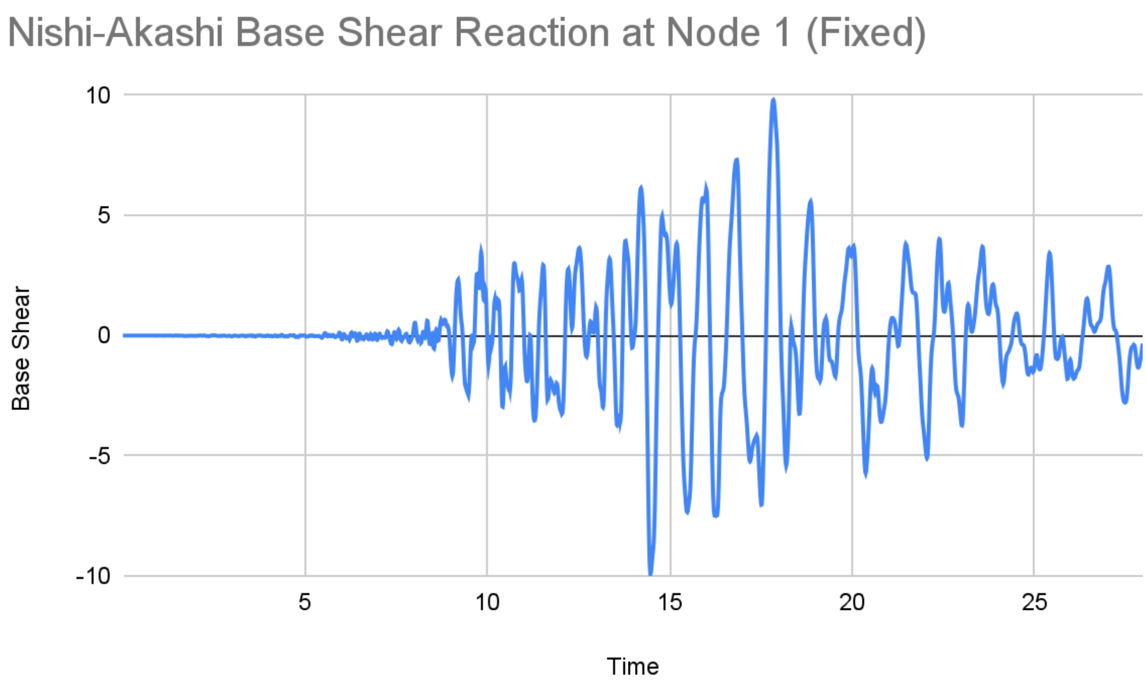

Figure B.21: Fixed Base Node 1 Nishi-Akashi Base Shear Reaction – X Direction

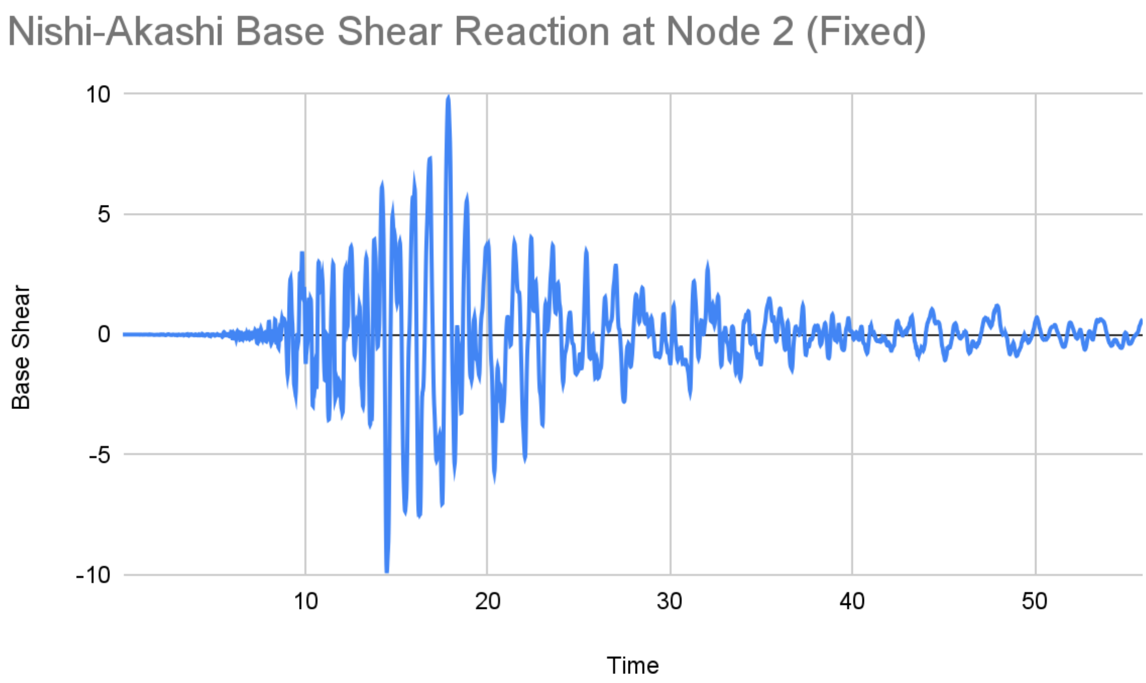

Figure B.22: Fixed Base Node 2 Nishi-Akashi Base Shear Reaction – X Direction

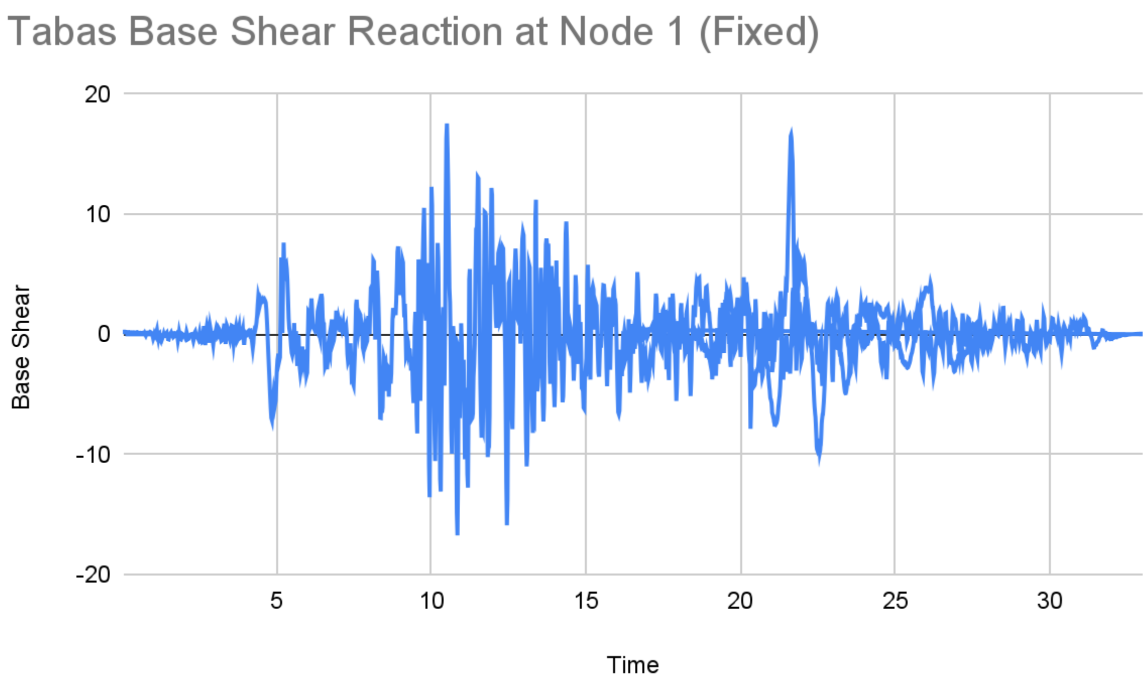

Figure B.23: Fixed Base Node 1 Tabas Base Shear Reaction – X Direction

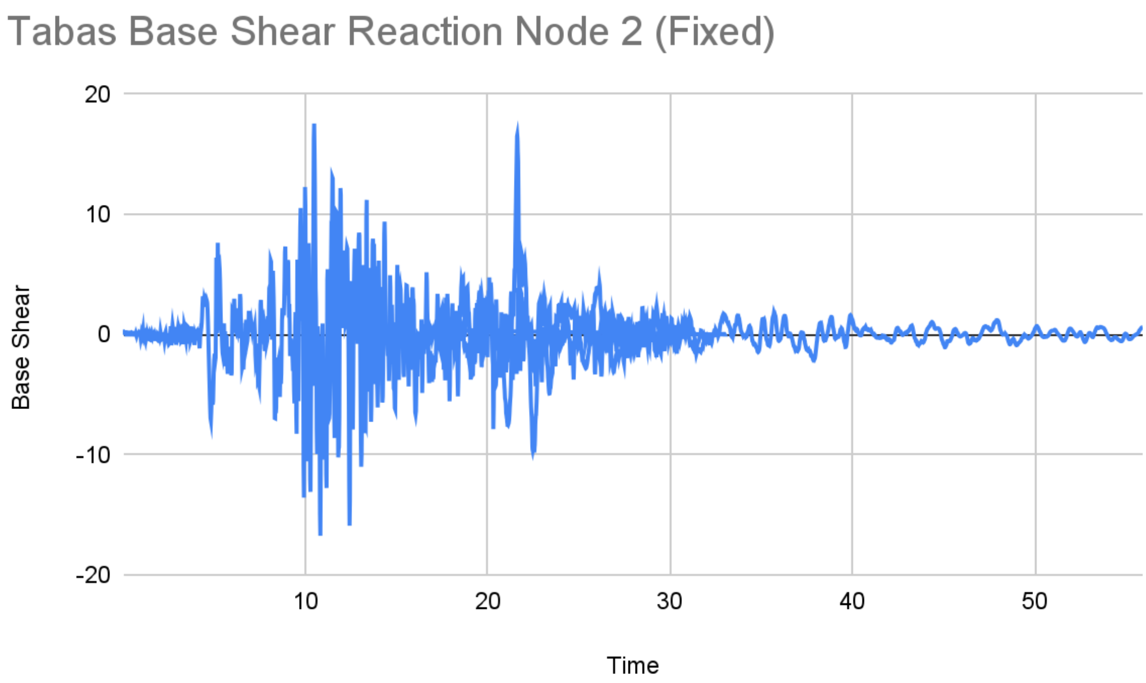

Figure B.24: Fixed Base Node 2 Tabas Base Shear Reaction – X Direction

Triple Friction Pendulum isolated structure

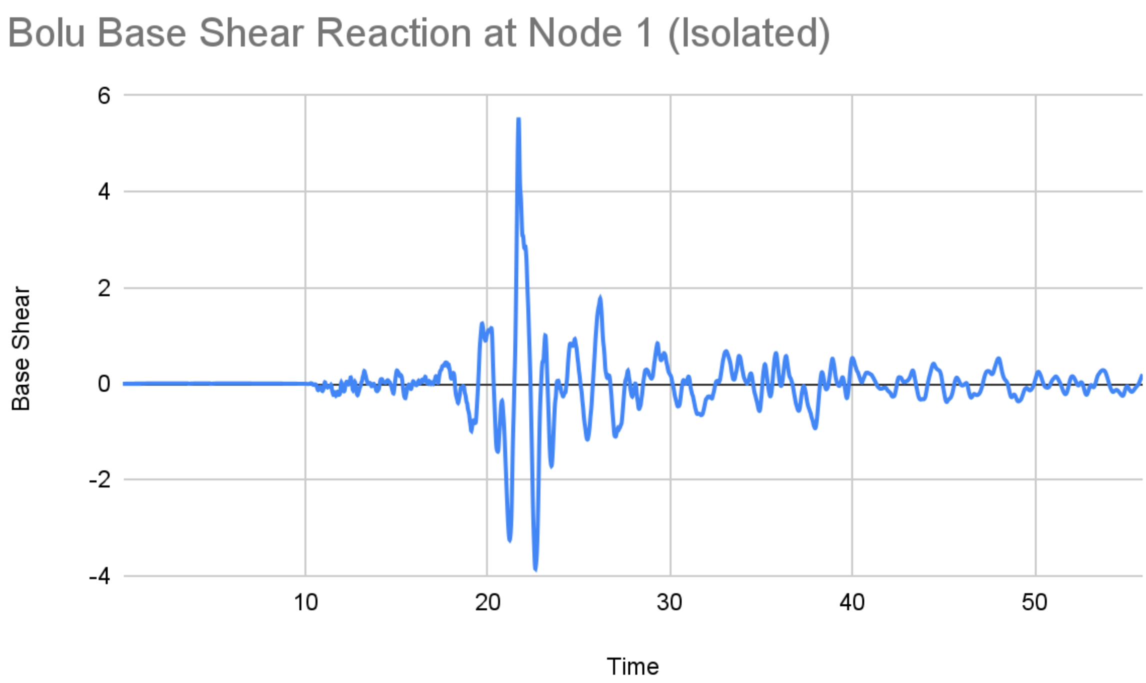

Figure B.25: Isolated Base Node 1 Bolu Base Shear Reaction – X Direction

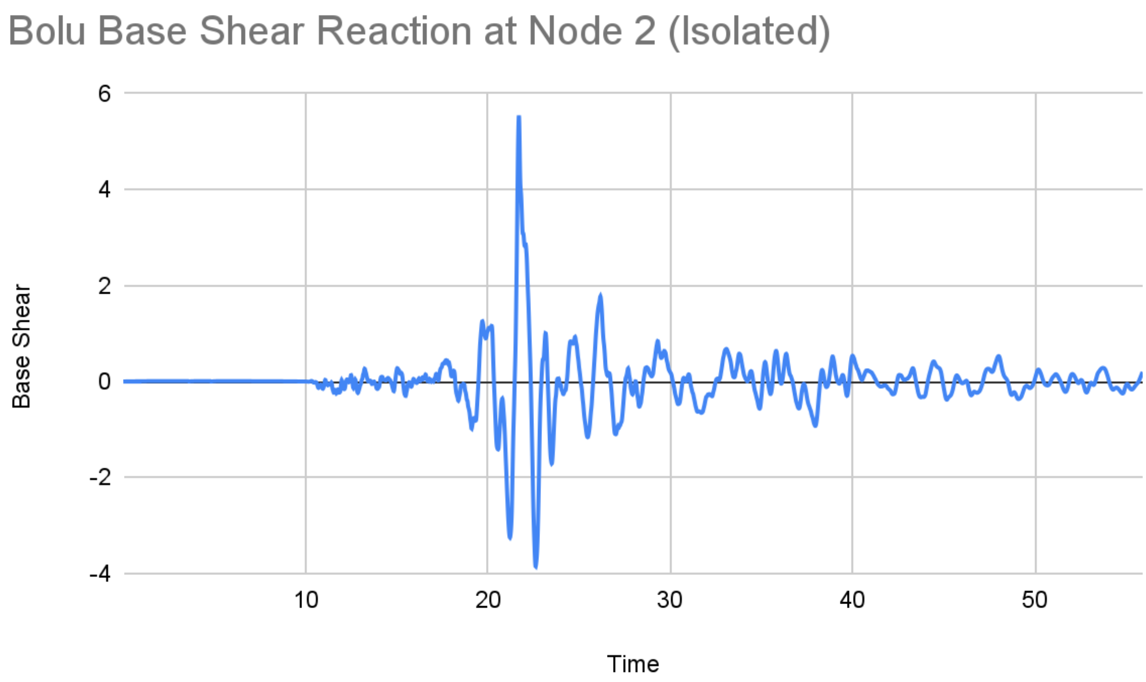

Figure B.26: Isolated Base Node 2 Bolu Base Shear Reaction – X Direction

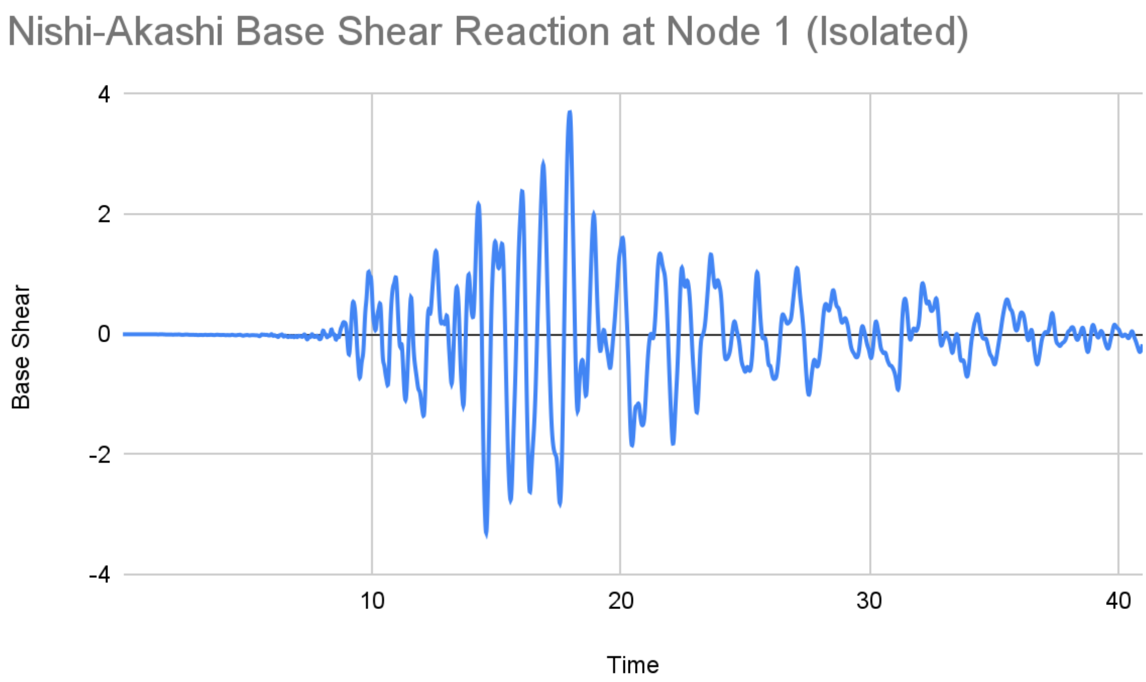

Figure B.27: Isolated Base Node 1 Nishi-Akashi Base Shear Reaction – X Direction

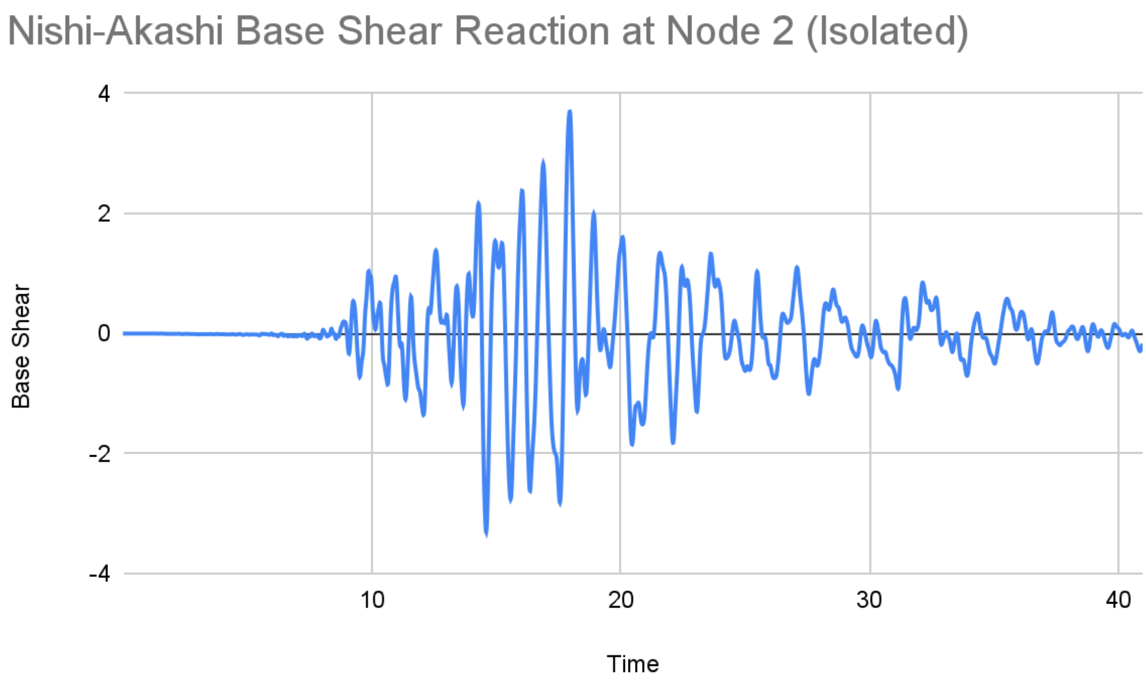

Figure B.28: Isolated Base Node 2 Nishi-Akashi Base Shear Reaction – X Direction

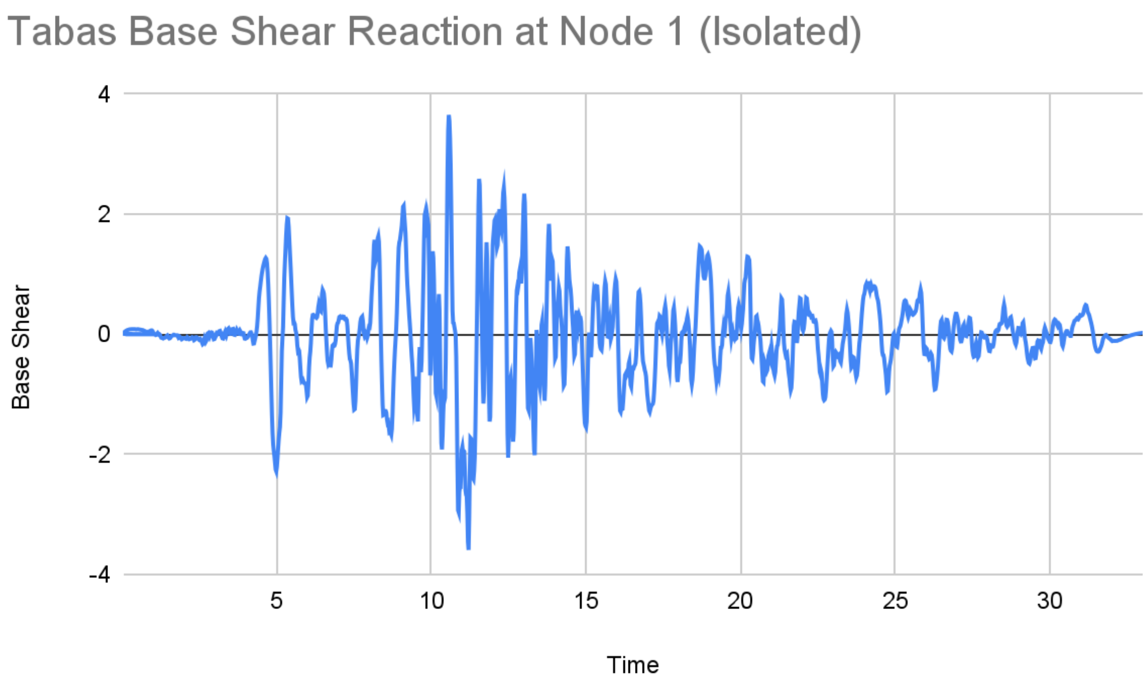

Figure B.29: Isolated Base Node 1 Tabas Base Shear Reaction – X Direction

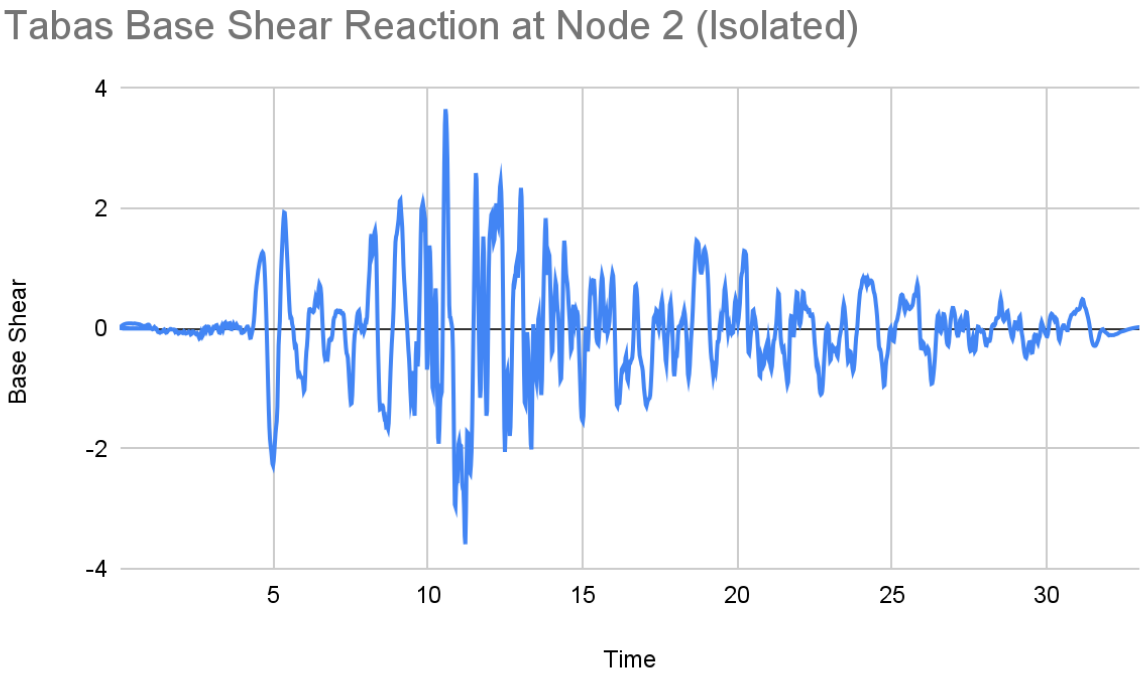

Figure B.30: Isolated Base Node 2 Tabas Base Shear Reaction – X Direction